Signal Concentration and Related Concepts in Time-Frequency and on the Unit Sphere

Liying Wei

B.E. (Xidian University, China)
M.E. (Beijing University of Posts and Telecommunications, China)

September 2010

A THESIS SUBMITTED FOR THE DEGREE OF DOCTOR OF PHILOSOPHY
OF THE AUSTRALIAN NATIONAL UNIVERSITY

ANU

THE AUSTRALIAN NATIONAL UNIVERSITY

Applied Signal Processing Group
School of Engineering
College of Engineering and Computer Science
The Australian National University

Declaration

The contents of this thesis are the results of original research carried out by myself under the supervision of Prof. Rodney A. Kennedy. These have not been submitted for a higher degree to any other university or institution.

Much of the work in this thesis has been published or has been submitted for publication as journal papers or conference proceedings. These papers are:

Journal Publications

1. L. Wei, R. A. Kennedy and T. A. Lamahewa, "An Optimal Basis of Band-limited Functions for Signal Analysis and Design", IEEE Trans. Signal Processing, Vol.58, issue.11, pp.12, Nov. 2010.

2. R. A. Kennedy, T. A. Lamahewa and L. Wei, "On Azimuthally Symmetric 2-Sphere Convolution", submitted to Digital Signal Processing.

3. L. Wei and R. A. Kennedy, "A norvel spherical convolution on the 2-sphere", submitted to IEEE Signal Processing Letter.

4. L. Wei, R. A. Kennedy and T. A. Lamahewa, "Quadratic Variational Framework for Signal Design on the 2-Sphere", submitted to IEEE Transactions on Signal Processing.

5. L. Wei and R. A. Kennedy, "Statistical Reconstruction on the 2-Sphere", to be submitted to IEEE Transactions on Signal Processing.

6. L. Wei and R. A. Kennedy, "General Spatiospectral Signal Concentration on the 2-Sphere", to be submitted to IEEE Transactions on Signal Processing.

Conference Publications

1. L. Wei, R. A. Kennedy and T. A. Lamahewa, "Band-limited Signal Concentration in Time-frequency", Proc. 3rd International Conference on Signal

Processing and Communication System, ICSPCS'2009, Omaha, Nebraska, USA, 28 - 30 September 2009.

2. R. A. Kennedy, T. A. Lamahewa and L. Wei, "On Azimuthally Symmetric 2-Sphere Convolution", Proc. 6th U.S./Australia Joint Workshop on Defense Applications of Signal Processing, DASP'2009, Hilton Kauai Beach Resort Lihue, Hawaii, USA, 29 Sep. - 1 Oct. 2009.

3. L. Wei, R. A. Kennedy and T. A. Lamahewa, "Signal Concentration on Unit Sphere: A Local K-th Moment Zenithal Energy Concentration Measure", Proc. 11th Australian Communications Theory Workshop, AusCTW'2010, Canberra, Australia, Feb. 2010.

4. L. Wei, R. A. Kennedy and T. A. Lamahewa, "Further Results on Signal Concentration in Time-frequency", Proc. IEEE International Conference on Acoustics, Speech and Signal Processing, ICASSP'2010, Sheraton Dallas Hotel, Dallas, Texas, USA, Mar. 14 - 19, 2010.

5. L. Wei, R. A. Kennedy and T. A. Lamahewa, "Signal Concentration on Sphere: An Azimuthally Moment Weighting Approach", Proc. IEEE International Conference on Acoustics, Speech and Signal Processing, ICASSP'2010, Sheraton Dallas Hotel, Dallas, Texas, USA, Mar. 14 - 19, 2010.

6. L. Wei and R. A. Kennedy, "On Spectral Concentration of Signals on the 2-Sphere under a Generalized Moment Weighting Criterion", Proc. European Signal Processing Conference, EUSIPCO'2010, Aalborg, Demark, August 23 - 27, 2010.
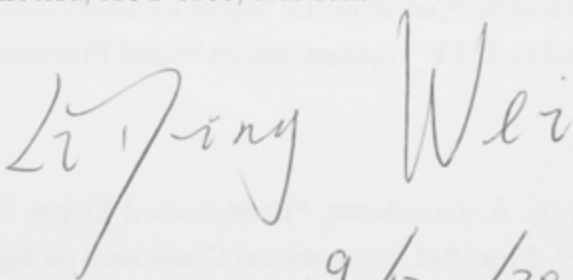
Liying Wei
School of Engineering
College of Engineering and Computer Science,
The Australian National University,
Canberra, ACT 0200, Australia.

Li Jing Wei

9/12/2010

Acknowledgements

I like to thank my supervisor Prof. Rodney A. Kennedy for his support and guidance over the years. I like to thank Rod for the brainstorming meetings, his deep insights into my research problems and his great freedom to allow me to do what I like to do.

I would like to thank Dr. Tharaka A. Lamhewa for his great help in my paper publish and paper revision, especially in English writing, speaking and material's organization. I would also like to thank Mr. Nick Boling (IT supporter) and Mr. Miles Hunty (summer scholar of ANU) who helped my paper and thesis revision.

I would like to thank Prof. Jonathan H. Manton in Melbourne University as my former supervisor when he was in Australian National University. His wonderful mathematical ideas gave me great help in my PhD study. I would also like to thank Dr. Ben Andrews, Prof. John Hutchinson and Dr. Paul Leopardi in Mathematic Sciences Institute, ANU, who discussed the partial differential equations, Hilbert space and spline functions with me.

I thank everyone in the school of engineering for providing a congenial working environment. In particular, Wen Zhang, Jennifer Wu, Thushara Abhayapala, Salman Durrani, Kim Blackmore, Jochen Trumpf and Yongxiang Xia. It is also my pleasure to acknowledge the help from Debbie Pioch, Lesley Goldburg, Elspeth Davies, James Ashton and Peter Shevchenko on various administrative and technical matters.

I would like to thank the Australian National University for provision of the PhD scholarship and National ICT Australia for the supplementary scholarship.

Finally, I thank my parents, my brother, my sister-in-law and their cute daughter, for their love and care without which I could not have completed my research work.

Abstract

Unit sphere signal processing is an increasingly active area of research with applications in computer vision, medical imaging, geophysics, cosmology and wireless communications. However, comparing with signal processing in time-frequency domain, characterization and processing of signals defined on the unit sphere is relatively unfamiliar for most of the engineering researchers. In order to better understand and analysis the current issues using the spherical model, such as analysis of brain neural electronic activities in medical imaging and neuroscience, target detection and tracking in radar systems, earthquake occurrence prediction and seismic origin detection in seismology, it is necessary to set up a systematic theory for unit sphere signal processing.

How to efficiently analyze and represent functions defined on the unit sphere are central for the unit sphere signal processing, such as filtering, smoothing, detection and estimation in the presence of noise and interference. Slepian-Landau-Pollak time-frequency energy concentration theory and the essential dimensionality of time-frequency signals by the Fourier transform are the fundamental tools for signal processing in the time-frequency domain. Therefore, our research work starts from the analogies of signals between time-frequency and spatial-spectral.

In this thesis, we first formulate the k-th moment time-duration weighting measure for a band-limited signal using a general constrained variational method, where a complete, orthonormal set of optimal band-limited functions with the minimum fourth moment time-duration measure is obtained and the prospective applications are discussed. Further, the formulation to an arbitrary signal with second and fourth moment weighting in both time and frequency domain is also developed and the corresponding optimal functions are obtained, which are helpful for practical waveform designs in communication systems.

Next, we develop a k-th spatially global moment azimuthal measure (GMZM) and a k-th spatially local moment zenithal measure (LMZM) for real-valued spectral-limited signals. The corresponding sets of optimal functions are solved and compared with the spherical Slepian functions.In addition, a harmonic multiplication

operation is developed on the unit sphere. Using this operation, a spectral moment weighting measure to a spatial-limited signal is formulated and the corresponding optimal functions are solved. However, the performance of these sets of functions and their perspective applications in real world, such as efficiently analysis and representation of spherical signals, is still in exploration.

Some spherical quadratic functionals by spherical harmonic multiplication operation are formulated in this thesis. Next, a general quadratic variational framework for signal design on the unit sphere is developed. Using this framework and the quadratic functionals, the general concentration problem to an arbitrary signal defined on the unit sphere to simultaneously achieve maximum energy in the finite spatial region and finite spherical spectrum is solved.

Finally, a novel spherical convolution by defining a linear operator is proposed, which not only specializes the isotropic convolution, but also has a well defined spherical harmonic characterization. Furthermore, using the harmonic multiplication operation on the unit sphere, a reconstruction strategy without consideration of noise using analysis-synthesis filters under three different sampling methods is discussed.

List of Acronyms

WMAP	Wilkinson microwave anisotropy probe
ISI	Inter-symbol interference
FOBE	Fraction out-of-band
PSWF	Prolate spheroidal wave function
RMS	Root-mean-square
DPSWF	Discrete prolate spheroidal wave function
DPSS	Discrete prolate spheroidal sequence
EEG	Electroencephalogram
FGCVM	Franks' general constrained variational method
CMB	Cosmic microwave background
GMAM	Global kth moment azimuthal measure
LMZM	Local kth moment zenithal measure
ECP	Equidistant Cylindrical Projection
GLEP	Gauss-Legendre pixelization

Notations and Symbols

$\mathcal{H}$	Complex Hilbert space
$L^2(\cdot, \cdot)$	Complex Hilbert space with an inner product
$T(\cdot, \cdot)$	Bilinear functional
i	$\sqrt{-1}$
$\mathbb{S}^2$	Unit sphere, also called the 2-sphere
$ds = \sin\theta\, d\theta\, d\phi$	measure on the unit sphere
$\boldsymbol{x} = (\theta, \phi)$	A point on the unit sphere
$\mathcal{F}^0(\mathbb{S}^2, ds)$	Linear subspace of $L^2(\mathbb{S}^2, ds)$ containing zonal functions
$SO(3)$	Special orthogonal group with determinant equal to 1
$g = (\alpha, \beta, \gamma)$	Rotation element on $SO(3)$
$ds = \sin\theta\, d\theta\, d\phi$	Lebesgue measure on the unit sphere
$\mathfrak{D}_\Gamma(\mathbb{S}^2, ds)$	subspace of spatial-limited signals in region $\Gamma \subset \mathbb{S}^2$
$\mathfrak{B}_N(\mathbb{S}^2, ds)$	subspace of spectral-limited signas with degree N
$*$	convolution in time-frequency domain
$\odot$	Harmonic multiplication
$\circledast$	isotropic convolution on the unit sphere
$\star$	left convolution on the unit sphere
$\otimes$	full convolution on the unit sphere
$\overline{[\cdot]}$	Complex Conjugate
$[\cdot]^T$	Hermitian Transpose
$Y_n^m(\cdot)$	Spherical harmonics of degree n and order m
$P_n(\cdot)$	Legendre polynomial of nth degree
$P_n^m(\cdot)$	Associated Legendre function of degree n and order m
$\delta_{(\cdot)}$	Kronecker delta function
$\delta(\cdot, \cdot)$	Spherical Dirac delta function
D	Differential operator
$\mathcal{B}$	Band-limited operator
$\mathcal{D}$	Time-limited operator
$\mathcal{B}_N$	Mode limiting operator

$\mathcal{D}_\Gamma$ — Spatial truncation operator

$\mathcal{R}$ — Rotation operator

$\mathcal{D}_a$ — Dilation operator with dilated factor a

$D_{mm'}^n(\alpha, \beta, \gamma)$ — Wigner-D function

$d_{mm'}^n(\beta)$ — Wigner-d function

$\chi_\Gamma(\cdot)$ — Characteristic function of region Γ

$\mathbf{B}_{nq}^{mp}$ — Infinite matrix representation of an operator

$A(\boldsymbol{x}, \boldsymbol{y})$ — Spatial kernel of an operator

$\Re\{\cdot\}$ — Real part of one complex number or complex function

$\begin{pmatrix} p & s & n \\ q & t & m \end{pmatrix}$ — Wigner 3j-symbol

Contents

List of Figures

List of Tables

Chapter 1

Introduction

1.1 Motivation and Background

Unit sphere signal processing is an increasingly active area of research with applications in computer vision, medical imaging, geophysics, cosmology and wireless communications, such as

- exact reconstruction of a signal from the scattered data in astrophysics, such as Wilkinson microwave anisotropy probe (WMAP) [2,3];

- highly concentrated spatial beam-forming in wireless communications systems [4–6];

- efficient function analysis and representation in geophysics [2,7–11];

- precise surface representation and smoothing in medical imaging [12,13];

- proper shape analysis in computer vision [14–16];

- correctly detecting objects in an embedded stochastic process and estimation of the power spectrum in cosmology [17–19].

However, comparing with signal processing in time-frequency domain, these research interests are more common in applied mathematics and physics than in engineering, especially ill-suited for practical engineering applications.

First, the concepts of signals defined on the unit sphere are different from those in time and frequency domains [20]:

- two variables (azimuthal and zenithal angles), rather than one single variable (time or frequency), arise;

1

- spherical harmonics transform replaces Fourier transform, where the Fourier coefficients on the unit sphere are discrete, not continuous any more;

- the region of interest is spatial area, not an interval (time or frequency), which requires more mathematical techniques to simple a problem and makes the optimization procedure complicated;

- translation in time-frequency domain changes into rotation on the unit sphere;

- dilation is not conformal any more on the unit sphere [21].

Accordingly, the processing techniques applied on the unit sphere, such as convolution, filtering and smoothing, are different from those in the time-frequency domain. Further, it is also improper to apply time-frequency techniques directly in practical applications using spherical models.

Therefore, in order to better understand the current issues using the spherical model for engineering researchers, it is necessary to develop a set of systematic theory and make it available to the engineering community. This thesis firstly explores the analogies of signals and processing techniques between time-frequency domain and spatial-spectral domain, then develops new spherical signal processing techniques and finally builds up a bridge for theoretical researches and practical researches.

1.1.1   Signal Concentration in the Time-frequency Domain and on the Unit Sphere

A central result in signal processing and information theory is the time-frequency concentration and the essential dimensionality of time-frequency signals [6]. Fourier theorem states that a signal cannot severely confine itself both in the time domain and the frequency domain. Slepian, Landau and Pollak provided an explicit theorem for such an uncertainty principal by introducing a fraction-out-band (FOBE) measure [22–26]: a bandlimited signal whose frequency vanishes outside $|\omega| > W$ achieves maximum energy in the time interval$[-T/2, T/2]$, or a time-limited signal which has finite support in the time interval $[-T/2, T/2]$, achieves maximum energy in the frequency interval $[-W, W]$. The optimal function is called prolate spheroidal wave function (PSWF) and this theorem plays a key role in waveform design [27], filter window design [28, 29] and signal representation [30].

Analogously, a signal defined on the unit sphere cannot be simultaneously concentrated in a spatial region and in the spherical harmonic spectrum. At present,

the spherical Slepian simultaneous concentration problems for both a spectral-limited signal which has finite spectral degree and a spatial-limited signal which vanishes outside a specified region on the unit sphere, have been solved in [31–33]. However, such an uncertainty principle for an arbitrary signal which is neither spatial-limited nor spectral-limited has not been solved yet on the unit sphere. Therefore, a general solution for an arbitrary signal which simultaneously achieves maximum energy both in the spatial region and in the spherical harmonic spectrum needs to be determined.

Recent research [34] also shows that a 4th moment bandwidth concentration gave a superior frequency roll-off than time-limited PSWFs, which is particularly important for an effective practical filter design to reduce the inter-band interference. However, a proper formulation for both time-duration and frequency bandwidth moment weighting and an investigation of such characteristics and perspective applications to corresponding set of functions are desirable. Further, for a more general case, whether such an analogy as a kth (k is not necessary equal to 4) moment weight measure exists on the unit sphere needs to be determined. In addition, the comparison should also be done with the spherical Slepian functions if such a set of optimal basis functions of this kth moment weighting on the unit sphere exists. Finally, the performance of the new set of basis functions to practical applications, such as analysis and representation of signals on the unit sphere, should also be verified.

Motivated by Franks' general framework which generalizes the uncertainty problem by measuring the energy concentrations relevant to duration and bandwidth in terms of arbitrarily weighted energy distributions in the time domain and frequency domain [1], it is natural to explore whether such generally variational framework exists on the unit sphere thereby could unify the existing scattered results which have been developed for concentration on the unit sphere.

1.1.2 Spherical Convolution and Reconstruction on the Unit Sphere

In mathematics and functional analysis, convolution is a mathematical operation on two functions, producing a third function that is typically viewed as a modified version of one of the original functions. The convolution theorem also conforms that the Fourier transform in the time domain corresponds to multiplication in the frequency domain, and vice versa. However, translation in the time-frequency domain changes into rotation on the unit sphere. Due to the invariant rotation on the unit sphere, some problems arise:

1. The left convolution developed by Driscoll and Healy [35] loses some Fourier coefficients of the spherical filter, where only the axisymmetric Fourier coefficients are captured.

2. The isotropic convolution [36–38] has a strict requirement to the spherical filter which must be axisymmetric. This gives a high requirement of telescopes and scanners.

3. Another spherical formulation (termed as spherical correlation), proposed by Wandelt and Gorski [39], renders the convolved function on $SO(3)$, not on the unit sphere $\mathbb{S}^2$ any more, therefore, a conformal projection from $SO(3)$ back to the unit sphere is required.

To overcome such difficulties, a noncircular beam strategy has been proposed [40, 41], where complicated calculation cost is involved. Therefore, to capture some anisotropic properties of the function of interest, such as the sky by cosmology microwave background (CMB) [18, 42–45], it is desirable to propose a new spherical convolution definition.

Reconstruction on the unit sphere from discretely sampled data is also an interest subject. At present, most of the reconstruction methods are based on the spherical wavelet transform [3, 46, 47], left convolution [15, 45] and isotropic convolution [39, 48, 49]. However, for the left convolution, only the zonal part of the spherical filter is used; the spherical filter has to be axisymmetric for the isotropic convolution; and higher calculation cost is expected for the spherical wavelet transform. Therefore, it is necessary to design a easier and simpler method to reconstruct the original signal.

In all, it is necessary to develop a new spherical convolution on the unit sphere with the following properties:

1. No requirements of the function of interest and the spherical filter, that is, both of the functions involved in the convolution are arbitrary;

2. The convolved function lies on the unit sphere, so there is no back-projection procedure;

3. No information is lost, that is, it can utilize all the Fourier coefficients of the function of interest and the spherical filter;

4. It could be equivalent to the isotropic convolution theorem;

5. The calculation, especially for the reconstruction based on the sample points, should be simple.

1.2   Aims of the Thesis

Relating to the problems proposed in the above section, the objective of this thesis is to develop a systematic theory for the characterization and processing of signals defined on the unit sphere, and use the developed theory in real world applications, including those in geodesy, human hearing modeling and wireless channel modeling.

The prospective work includes:

1. Further studies of the signal concentration in the time-frequency domain, in particular, the formulation of the moment weighting with duration and bandwidth;

2. A general solution to an arbitrary signal which simultaneously achieves the maximum energy both in the spatial domain and in the spherical harmonic spectrum;

3. A general variational framework for signal design to the unit sphere;

4. Development of a new spherical convolution on the unit sphere.

1.3   Outline of the Thesis

The present work is divided into seven chapters: Chapter 1 states the motivation and background of this thesis, then introduces the aims, structure and contributions of the thesis.

In the second chapter, we introduce the preliminary technical background of this thesis. Starting with the fundamentals of the signal space in Section 2.1, we review the Hilbert space, linear transforms, linear operations and linear functionals. Then in Section 2.3, we focus on spherical harmonics and their related concepts, the spherical harmonic transform and the inverse spherical harmonic transform. Motivated by the spherical convolution or the left convolution [35], Section 2.4 is devoted to the rotation operation, the relation of spherical harmonics and the Wigner-D functions. Finally, several useful operators and subspaces are introduced.

Chapter 3 is concerned with time-frequency signals' energy concentration with moment weighting both in the time domain and in the frequency domain. First, we review the Slepian-Landau-Pollak simultaneous concentration problem in the time-frequency domain; we also present Franks' general constrained variational method. Then, in Section 3.2, we focus on the formulation based on the Franks' method for the minimum 4th moment time-duration measure for a strictly band-limited signal, investigate the characteristics of this set of optimal basis functions, and

the potential applications of this set of functions. After that, we formulate an arbitrary time-limited signal concentration with 2nd and 4th bandwidth moment weighting for the practical waveform design in Section 3.3. Finally, we summarize all the optimal functions of the corresponding concentration problems in the time-frequency domain. The publication of our work involving this chapter includes:

- L. Wei, R. A. Kennedy and T. A. Lamahewa, "Band-limited Signal Concentration in Time-frequency", Proc. 3rd International Conference on Signal Processing and Communication System, ICSPCS'2009, Omaha, Nebraska, USA, 28 - 30 September 2009.

- L. Wei, R. A. Kennedy and T. A. Lamahewa, "Further Results on Signal Concentration in Time-frequency", Proc. IEEE International Conference on Acoustics, Speech and Signal Processing, ICASSP'2010, Sheraton Dallas Hotel, Dallas, Texas, USA, Mar. 14 - 19 2010.

- L. Wei, R. A. Kennedy and T. A. Lamahewa, "An Optimal Basis of Band-limited Functions for Signal Analysis and Design", IEEE Trans. Signal Processing, Vol.58, issue.11, pp.12, Nov. 2010.

The objective of the fourth chapter is to solve the general concentration problem on the unit sphere, that is, determine the signal that occupies the maximum spatial region subjected to fixed maximum spectral degree. In Section 4.2, we first introduce an infinite matrix represent to an operator and its corresponding spatial kernel. Section 4.3 defines a harmonic multiplication operation on the unit sphere. Then some useful quadratic functionals on the unit sphere are derived in Section 4.4. Further, Section 4.5 extends the Franks' general constrained variational method on the unit sphere. Section 4.6 addresses the full concentration problem on the unit sphere. Based on the spherical Slepian functions in Section 4.7 and the spherical Franks' framework, we solve the arbitrary signal's simultaneous concentration problem on the unit sphere in Section 4.8. The publication of our work involving this chapter includes:

- R. A. Kennedy, T. A. Lamahewa and L. Wei, "On Azimuthally Symmetric 2-Sphere Convolution", Proc. 6th U.S./Australia Joint Workshop on Defense Applications of Signal Processing, DASP'2009, Hilton Kauai Beach Resort Lihue, Hawaii, USA, 29 Sep. - 1 Oct. 2009.

- R. A. Kennedy, T. A. Lamahewa and L. Wei, "On Azimuthally Symmetric 2-Sphere Convolution", submitted to Elsevier Digital Signal Processing.

- L. Wei and R. A. Kennedy, "A Novel Spherical Convolution on the 2-Sphere", submitted to IEEE Signal Processing Letter.

- L. Wei and R. A. Kennedy, "Signal Concentration on The Unit Sphere", to be submitted to IEEE Transactions on Signal Processing.

Chapter 5 focuses on the formulation of the azimuthal and zenithal moment weighting of a spectral-limited signal and the harmonic multiplication operation of a spatial-limited signal on the unit sphere, which is an extension of the work introduced in Chapter 3 for time-frequency domain to the unit sphere. Section 5.2 not only formulates both global zenithal moment weighting and local zenithal moment weighting to a spectral-limited signal, but also makes the comparisons between these two sets of optimal functions and the spherical Slepian functions. Section 5.3 studies a spatial-limited signal concentration situation with harmonic multiplication weighting. The publication of our work involving this chapter includes:

- L. Wei, R. A. Kennedy and T. A. Lamahewa, "Signal Concentration on Unit Sphere: A Local K-th Moment Zenithal Energy Concentration Measure", Proc. 11th Australian Communications Theory Workshop, AusCTW'2010, Canberra, Australia, Feb. 2010.

- L. Wei, R. A. Kennedy and T. A. Lamahewa, "Signal Concentration on Sphere: An Azimuthally Moment Weighting Approach", Proc. IEEE International Conference on Acoustics, Speech and Signal Processing, ICASSP'2010, Sheraton Dallas Hotel, Dallas, Texas, USA, Mar. 14 - 19 2010.

- L. Wei and R. A. Kennedy, "On Spectral Concentration of Signals on the 2-Sphere under a Generalized Moment Weighting Criterion", Proc. European Signal Processing Conference, EUSIPCO'2010, Aalborg, Demark, August 23 - 27.

Chapter 6 deals with the spherical convolution development and the corresponding application on the unit sphere. Section 6.1 points out the shortcomings of the existing spherical convolutions. Then, we propose a spherical full convolution on the unit sphere in Section 6.4, which is equivalent to the spherical isotropic convolutions. However, some unexpected properties are also achieved comparing with the present spherical convolution definitions. Section 6.6 reconstructs an original signal defined on the unit sphere based on the harmonic multiplication operation. The publication of our work involving this chapter includes:

- L. Wei, R. A. Kennedy and T. A. Lamahewa, "A Novel Spherical Convolution on the 2-Sphere", submitted to IEEE Signal Processing Letter.

- L. Wei and R. A. Kennedy, "Reconstruction Base on Harmonic Multiplication Theorem on The Unit Sphere", to be submitted to IEEE Transactions on Signal Processing.

The last chapter provides conclusions and possible directions for future work.

1.4   Main Contributions

The main contributions of this thesis are as follows:

1. A kth moment time-duration measure of a band-limited signal with Franks' general constrained variational method in the time domain is formulated, where a complete, orthonormal set of band-limited functions with minimum fourth-moment time-duration measure is obtained and the applications of this set of functions are demonstrated by the radar waveform design and the representation of an arbitrary band-limited signal.

2. Using Franks' general constrained variational method, a kth moment time-duration weighting measure for an arbitrary signal with is proposed, and the corresponding optimal functions are solved. The bandwidth weighting to an arbitrary signal is also discussed.

3. A harmonic multiplication operation on the unit sphere is developed which can be be used for the frequency domain weighting. Then the equivalences between the harmonic multiplication operation and the existing convolution formulations are made. Further, some quadratic functionals using infinite matrix representation of an operator and the harmonic multiplication weighting are derived.

4. A kth global moment azimuthal measure (GMAM) for a real-valued spectral-limited signal on the whole unit sphere is developed; later, a kth local moment zenithal measure (LMZM) for a real-valued spectral-limited signal on one specified spatial region on the unit sphere is also proposed. The corresponding optimal functions for GMZM and LMZM are solved and compared with the spherical Slepian function, respectively.

5. The concentration problem of a spatial-limited signal with the harmonic multiplication weighting is studied and the corresponding optimal functions are obtained. Simulation results show that the decaying rate of the spectrum of this set of functions is slower than the spherical Slepian functions.

6. Franks general constrained variational framework is extended to the unit sphere, which generalizes the uncertainty problems by measuring the energy concentrations relevant to the spatial region and the spectral angular degree.

7. The general concentration problem for an arbitrary signal defined on the unit sphere is solved by the Franks framework and the quadratic functionals, where the arbitrary signal simultaneously achieves the maximum energy in the spatial region and in the finite spectral spectrum.

8. A novel spherical convolution definition is proposed based on a linear operator, which relaxes the requirement of the function of interest and the spherical filter and keeps all the information. It also specializes the spherical isotropic convolution.

9. A simple reconstruction method based on the harmonic multiplication operation on the unit sphere is proposed, which greatly reduces the calculation cost.

Chapter 2

Technical Background

This chapter provides mathematical preliminaries required for the thesis. Section 2.1 introduces some fundamentals about the signal space, including Hilbert space, linear transformations, linear operators and linear functionals. Then Section 2.2 describes the Fourier transform in the time-frequency domain. Section 2.3 deals with the spherical harmonics and the spherical transform on the unit sphere. Section 2.4 recalls some basic knowledge about the rotations on the unit sphere. Finally, several important operators which are often used in this thesis are introduced in Section 2.5.

2.1 Hilbert Space, Linear Transformations, Linear Operators and Linear Functionals

The development of this subsection follows closely to the book "Signal Theory" written by Lewis Franks [1].

Let $\mathcal{H}_1$ and $\mathcal{H}_2$ be two complex Hilbert spaces. A continuous linear transformation is a linear mapping $T : \mathcal{H}_1 \to \mathcal{H}_2$. That is, for $x \in \mathcal{H}_1$ and $y = \mathcal{H}_2$, we have a relation:

$$y = T(x).$$

The element y in $\mathcal{H}_2$ is called the image of x under the mapping T. The set $\mathcal{H}_1$ is the domain of the mapping, and the set of all images of elements of $\mathcal{H}_1$ (contained in $\mathcal{H}_2$) is the range of the mapping. When the input space $\mathcal{H}_1$ and the output space $\mathcal{H}_2$ are identical, denoted as $\mathcal{H}$, the linear transformation is called a *linear operator*.

Let L^2 denote a complex Hilbert space that contains all the square-integrable

11

functions defined in $(-\infty, \infty)$ with inner product

$$\langle x, y \rangle \triangleq \int_{-\infty}^{\infty} x(t)\overline{y(t)} \, dt, \quad \forall x, y \in L^2,$$

where $\overline{[\cdot]}$ denotes the complex conjugate. Note the inner product induces a norm, $\|x\| = \langle x, x \rangle^{1/2}$.

For any function $f \in L^2$, a linear operator $\mathcal{A}$ is defined as

$$(\mathcal{A}f)(t) \triangleq \int_{-\infty}^{\infty} A(t, \tau)f(\tau) \, d\tau, \tag{2.3}$$

where $A(t, \tau)$ is known as the kernel function.

Suppose $\mathcal{C}$ is a set containing all the complex numbers, then a linear functional is a linear mapping $T : \mathcal{H} \to \mathcal{C}$ having the property,

$$T(\alpha x + \beta y) = \alpha T(x) + \beta T(y)$$

for any $\alpha, \beta \in \mathcal{C}$ and any $x, y \in \mathcal{H}$.

A bilinear functional is a mapping of pairs of signals $x, y \in \mathcal{H}$ into numerical values: $\mathcal{H} \times \mathcal{H} \longrightarrow T(x, y)$. $T(x, y)$ has the following properties:

$$T(\alpha_1 x_1 + \alpha_2 x_2, y) = \alpha_1 T(x_1, y) + \alpha_2 T(x_2, y)$$
$$T(x, \beta_1 y_1 + \beta_2 y_2) = \overline{\beta_1} T(x, y_1) + \overline{\beta_2} T(x, y_2)$$

for any $\alpha_1, \alpha_2, \beta_1, \beta_2 \in \mathcal{C}$ and any $x_1, x_2, y_1, y_2 \in \mathcal{H}$. Note $T_\mathcal{A}(x, y) = \langle \mathcal{A}x, y \rangle$ also denotes a bilinear functional in x and y under the operation of an operator $\mathcal{A}$.

A quadratic functional is simply defined by replacing y by x in the bilinear functional $T_\mathcal{A}(x, y)$,

$$I_A(x) = \langle \mathcal{A}x, x \rangle = \int_T \int_T A(t, \tau)x(\tau)\overline{x(t)} \, d\tau \, dt. \tag{2.5}$$

2.2   Fourier Transform in Time-frequency Domain

Let t, ω and $f = \omega/2\pi$ denote time, angular frequency and frequency, respectively. A function $x \in L^2$ and its Fourier transform are related by

$$x(t) = \frac{1}{2\pi} \int_{-\infty}^{\infty} X(\omega)e^{i\omega t} \, d\omega = \int_{-\infty}^{\infty} X(f)e^{i2\pi ft} \, df,$$
$$X(f) = \int_{-\infty}^{\infty} x(t)e^{-i2\pi ft} \, dt,$$

where $i = \sqrt{-1}$. Then by Parseval's theorem, we have

$$\langle x, y \rangle = \langle X, Y \rangle,$$

where $\langle X, Y \rangle = \int_{-\infty}^{\infty} X(f)\overline{Y(f)}\, df$ for any $X, Y \in L^2$.

Since the Fourier transform is a unitary transform [1], the quadratical functional can be expressed by

$$I(x) = \langle \mathcal{A}x, x \rangle = \langle \mathcal{B}X, X \rangle, \tag{2.7}$$

where

$$A(t, \tau) = \int_{-\infty}^{\infty} \int_{-\infty}^{\infty} B(f, \nu) e^{i2\pi ft} e^{-i2\pi\nu\tau}\, df\, d\nu,$$

$$B(f, \nu) = \int_{-\infty}^{\infty} \int_{-\infty}^{\infty} A(t, \tau) e^{-i2\pi ft} e^{i2\pi\nu\tau}\, dt\, d\tau,$$

where $A(t, \tau)$ is the kernel function for the time domain operator $\mathcal{A}$ and $B(f, \nu)$ is the kernel function for the frequency domain operator $\mathcal{B}$.

2.2.1 Some Quadratic Functionals and Their Time-frequency Domain Operators

Assume $w(t)$ is an arbitrary real function and $w(t) > 0$ for all t; $V(f)$ is an arbitrary real function and $V(f) > 0$ for all frequency f. Table 2.1 shows some quadratical functionals and their corresponding operator kernels $A(t, \tau)$ in the time domain and $B(f, \nu)$ in the frequency domain [1].

2.3 Spherical Harmonics and Spherical Harmonic Transform

2.3.1 Notation

Let $\mathbb{S}^2 = \{x \in \mathbb{R}^3 : \|x\| = 1\}$ denote the unit sphere in $\mathbb{R}^3$. Let $x \equiv (\theta, \phi) \triangleq (\sin\theta\cos\phi, \sin\theta\sin\phi, \cos\theta) \in \mathbb{R}^3$ denotes a point on the sphere, where θ denotes the colatitude with $0 \le \theta \le \pi$ and ϕ denotes the longitude with $0 \le \phi < 2\pi$. The geodesic angular distance between two points $x_1 = (\theta_1, \phi_1)$ and $x_2 = (\theta_2, \phi_2)$ is given by $\cos\Delta$, where

$$\cos\Delta = x_1 \cdot y_2 = \cos\theta_1\cos\theta_2 + \sin\theta_1\sin\theta_2\cos(\phi_1 - \phi_2), \tag{2.8}$$

	Quadratic functionals	Time kernel	frequency kernel
I	$\langle \mathcal{A}x, x \rangle = \langle \mathcal{B}X, X \rangle$	$A(t, \tau)$	$B(f, \nu)$
I_1	$\langle x, x \rangle = \langle X, X \rangle$	$\delta(t - \tau)$	$\delta(f - \nu)$
I_2	$\langle wx, x \rangle$ $= \int_{-\infty}^{\infty} w(t)|x(t)|^2 dt$	$w(t)\delta(t - \tau)$	$W(f - \nu)$
I_3	$\langle VX, X \rangle$ $= \int_{-\infty}^{\infty} V(f)|X(f)|^2 df$	$v(t - \tau)$	$V(f)\delta(f - \nu)$
I_4	$\langle w[h \otimes x], [h \otimes x] \rangle$	$\int_{-\infty}^{\infty} w(\sigma)h(\sigma - \tau)\overline{h(\sigma - t)}\, d\sigma$	$\overline{H(f)}H(\nu)W(f - \nu)$
I_5	$\langle VHX, HX \rangle$	$\int_{-\infty}^{\infty} \int_{-\infty}^{\infty} v(\sigma)$ $\times h(\gamma - \sigma - \tau)\overline{h(\gamma - t)}\, d\gamma\, d\sigma$	$V(f)|H(f)|^2\delta(f - \nu)$
I_6	$\langle x, g \rangle \overline{\langle x, h \rangle}$ $= \langle X, G \rangle \overline{\langle X, H \rangle}$	$h(t)\overline{g(\tau)}$	$H(f)\overline{G(\nu)}$

Table 2.1: Some quadratic functionals and their time- and frequency-domain operators [1].

where $\boldsymbol{x}_1 \cdot \boldsymbol{y}_2$ is the dot/inner product between vector $\boldsymbol{x}_1$ and $\boldsymbol{y}_2$.

Let $L^2(\mathbb{S}^2, ds)$ be a complex Hilbert space containing all the square-integrable functions defined on the unit sphere $\mathbb{S}^2$. For $f, g \in L^2(\mathbb{S}^2, ds)$, the inner product is defined as

$$\langle f, g \rangle = \int_{\mathbb{S}^2} f(\boldsymbol{x})\overline{g(\boldsymbol{x})}\, ds(\boldsymbol{x}) = \int_0^{\pi} \int_0^{2\pi} f(\theta, \phi)\overline{g(\theta, \phi)} \sin\theta\, d\phi\, d\theta, \qquad (2.9)$$

where $ds(\boldsymbol{x}) = \sin\theta\, d\theta\, d\phi$. The induced norm is given by

$$\|f\|^2 = \int_{\mathbb{S}^2} |f(\boldsymbol{x})|^2\, ds(\boldsymbol{x}). \qquad (2.10)$$

2.3.2 Spherical Harmonics

There are two kinds of definitions for the spherical harmonics: real spherical harmonics and complex spherical harmonics. Both of them are used in this thesis, so both of the definitions are introduced.

The complex spherical harmonics are defined by [50]

$$Y_n^m(\boldsymbol{x}) = \sqrt{\frac{2n+1}{4\pi}\frac{(n-|m|)!}{(n+|m|)!}}\, P_n^{|m|}(\cos\theta)e^{im\phi},$$

$$n = 0, 1, \cdots, \quad m = -n, \cdots, n, \tag{2.11}$$

where $P_n^m(\cdot)$ are the associated Legendre functions, n is the angular (spectral) degree and m ($-n \le m \le n$) is the angular order.

The real spherical harmonics are defined by [33, 51]

$$Y_n^m(\theta, \phi) = \begin{cases} \sqrt{2}X_n^{|m|}(\theta)\sin|m|\phi, & -n \le m < 0; \\ X_n^0(\theta), & m = 0; \\ \sqrt{2}X_n^m(\theta)\cos m\phi, & 0 < m \le n, \end{cases} \tag{2.12}$$

where

$$X_n^m(\theta) = \left(\frac{2n+1}{4\pi}\right)^{1/2}\left[\frac{(n-|m|)!}{(n+|m|)!}\right]^{1/2}P_n^{|m|}(\cos\theta). \tag{2.13}$$

Important properties of the spherical harmonics:

1. $\{Y_n^m(\boldsymbol{x})\}$ forms a complete orthonormal sequence in $L^2(\mathbb{S}^2, ds)$,

$$\int_{\mathbb{S}^2} Y_n^m(\boldsymbol{x})\overline{Y_{n'}^{m'}(\boldsymbol{x})}\, ds(\boldsymbol{x}) = \delta_{nn'}\delta_{mm'}, \tag{2.14}$$

where $\delta_{nn'}$ is the Kronecker delta function with

$$\delta_{nn'} = \begin{cases} 1, & n = n'; \\ 0, & n \ne n'. \end{cases} \tag{2.15}$$

2. Addition theorem,

$$\sum_{m=-n}^{n} Y_n^m(\boldsymbol{x})\overline{Y_n^m(\boldsymbol{y})} = \frac{2n+1}{4\pi}P_n(\boldsymbol{x}\cdot\boldsymbol{y}), \quad \forall\boldsymbol{x}, \forall\boldsymbol{y} \in \mathbb{S}^2, \tag{2.16}$$

where $P_n(\cdot)$ are the Legendre polynomials of degree n.

3. The spherical Dirac delta function $\delta(\boldsymbol{x}, \boldsymbol{y})$ is defined by [33]

$$\delta(\boldsymbol{x}, \boldsymbol{y}) = \sum_{n=0}^{\infty} \sum_{m=-n}^{n} Y_n^m(\boldsymbol{x})\overline{Y_n^m(\boldsymbol{y})} = \sum_{n=0}^{\infty} \frac{2n+1}{4\pi} P_n(\boldsymbol{x} \cdot \boldsymbol{y}). \tag{2.17}$$

Note that $\delta(\boldsymbol{x}, \boldsymbol{y})$ has the sifting property

$$\int_{\mathbb{S}^2} \delta(\boldsymbol{x}, \boldsymbol{y})f(\boldsymbol{y}) \, ds(\boldsymbol{y}) = f(\boldsymbol{x}). \tag{2.18}$$

2.3.3 Spherical Harmonic Transform

The inverse spherical harmonic transform of $f \in L^2(\mathbb{S}^2, ds)$, can be represented, in the sense of convergence in the mean with the norm induced by (2.10),

$$f(\boldsymbol{x}) = \sum_{n=0}^{\infty} \sum_{m=-n}^{n} f_n^m Y_n^m(\boldsymbol{x}), \tag{2.19}$$

where the spherical harmonic coefficients f_n^m are given by the spherical harmonic transform,

$$f_n^m = \langle f, Y_n^m \rangle = \int_{\mathbb{S}^2} f(\boldsymbol{x})\overline{Y_n^m(\boldsymbol{x})} \, ds(\boldsymbol{x}). \tag{2.20}$$

Denote the ordered column vector of spherical harmonic coefficients as

$$\hat{\mathbf{f}} = (f_0^0, f_1^{-1}, f_1^0, f_1^1, ..., f_n^m, ...)^T, \tag{2.21}$$

where $[\cdot]^T$ denotes the complex transpose. Then the norm of a spatial-domain function $f(\boldsymbol{x})$ and its spectral-domain equivalent $\hat{\mathbf{f}}$ is [33]

$$\|f\|^2 = \int_{\mathbb{S}^2} |f(\boldsymbol{x})|^2 \, ds(\boldsymbol{x}), \quad \|\hat{\mathbf{f}}\|^2 = \sum_{n=0}^{\infty} \sum_{m=-n}^{n} |f_n^m|^2. \tag{2.22}$$

According to Parseval's theorem, we have

$$\|f\|^2 = \|\hat{\mathbf{f}}\|^2. \tag{2.23}$$

2.4 Rotations on the Sphere and Wigner-D Function

2.4.1 Basics of Rotations

In mathematics, a group is an algebraic structure consisting of a set G together with an operation " $\cdot$ " that combines any two of its elements a and b to form a third element $a \cdot b \in G$. The rotation group $SO(3)$ on $\mathbb{R}^3$ is the special orthogonal group. It consists of 3×3 matrices defined through

$$SO(3) = \{g \in \mathbb{R}^{3\times 3} : g^T g = 1, \quad \det g = 1\}, \tag{2.24}$$

where g is a rotation on the sphere.

The rotation g can be parameterized by three Euler anglers, i.e.,

$$g = (\alpha, \beta, \gamma) = R_z(\alpha) R_y(\beta) R_z(\gamma), \tag{2.25}$$

where $\alpha \in [0, 2\pi)$, $\beta \in [0, \pi]$, $\gamma \in [0, 2\pi)$, R_y and R_z denote the rotation about the y- and z-axis, respectively [14]. In matrix notation, R_y and R_z take the form

$$R_y(\beta) = \begin{bmatrix} \cos\beta & 0 & \sin\beta \\ 0 & 1 & 0 \\ -\sin\beta & 0 & \cos\beta \end{bmatrix}, \quad R_z(\alpha) = \begin{bmatrix} \cos\alpha & -\sin\alpha & 0 \\ \sin\alpha & \cos\alpha & 0 \\ 0 & 0 & 1 \end{bmatrix}. \tag{2.26}$$

2.4.2 Rotation Operators

Let $\mathcal{R}_g = \mathcal{R}(\alpha, \beta, \gamma)$ denote a rotation operator $\mathcal{R}$ under a rotation g. There are two different but equivalent viewpoints about the rotation computations. Driscoll and Healy, in their paper [35], showed that: under a rotation g, each spherical harmonic of degree n is transformed into a linear combination of only those Y_n^m, $-n \leq m \leq n$, with the same degree (n):

$$\mathcal{R}_g Y_n^m = \sum_{|m'| \leq n} D_{m'm}^n(g) Y_n^{m'}, \tag{2.27}$$

where $D_{m'm}^n(g)$ is the Wigner-D function (explored in more detail in section 2.4.3). Then the rotated function $f(\boldsymbol{x})$ expanded by the spherical harmonics (2.19) takes the form

$$(\mathcal{R}_g f)(\boldsymbol{x}) = \sum_{n=0}^{\infty} \sum_{m=-n}^{n} \sum_{m'=-n}^{n} f_n^m D_{m'm}^n(g) Y_n^{m'}(\boldsymbol{x}). \tag{2.28}$$

Another viewpoint says that the rotation operator should be implemented on the spherical coefficients [13], i.e.,

$$(\mathcal{R}_g)f_n^m = \sum_{|m'| \le n} D_{mm'}^n(g)f_n^{m'}. \tag{2.29}$$

Then the rotated function is

$$(\mathcal{R}_g f)(\boldsymbol{x}) = \sum_{n=0}^{\infty} \sum_{m=-n}^{n} \sum_{m'=-n}^{n} f_n^{m'} D_{mm'}^n(g) Y_n^m(\boldsymbol{x}). \tag{2.30}$$

Comparing (2.28) with (2.30), the results show that they are precisely identical. Therefore, in the rest of this thesis, the second definition, whereby the rotation operator acts on the spherical harmonic coefficients, is adopted.

2.4.3   Wigner-D Function

The Wigner-D function $D_{mm'}^n(g) = D_{mm'}^n(\alpha, \beta, \gamma)$ can be decomposed into [13]:

$$D_{mm'}^n(\alpha, \beta, \gamma) \triangleq e^{-im\alpha} d_{mm'}^n(\beta) e^{-im'\gamma}, \tag{2.31}$$

where $d_{mm'}^n(\beta)$ is the Wigner-d function,

$$d_{mm'}^n(\beta) \triangleq \sum_{j=\max(0,m-m')}^{\min(n+m,n-m')} (-1)^{j-m'+m} \frac{\sqrt{(n+m')!(n-m')!(n+m)!(n-m)!}}{(n+m'-j)!j!(n-j-m)!(j-m'+m)!}$$

$$\times (\cos\frac{\beta}{2})^{2n-2j+m'-m}(\sin\frac{\beta}{2})^{2j-m'+m}, \tag{2.32}$$

which is real. Recursion formula are available to compute rapidly the Wigner-d function in the basis of either complex [52, 53] or real [54, 55] spherical harmonics.

By Peter-Weyl theorem [56, 57], $D_{mm'}^n(g)$ forms an orthogonal basis in $L^2(SO(3))$, i.e.

$$\int_{SO(3)} D_{mm'}^n(g) \overline{D_{pp'}^q(g)} \, dg = \frac{8\pi^2}{2n+1} \delta_{nq} \delta_{mp} \delta_{m'p'}, \tag{2.33}$$

where $dg = \sin\beta d\alpha d\beta d\gamma$ [13]. The Wigner-d function also has a similar property

$$\int_{\beta} d_{mm'}^n(\beta) d_{mm'}^q(\beta) \sin\beta \, d\beta = \frac{2}{2l+1} \delta_{nq}. \tag{2.34}$$

Finally, the rotation can also be decomposed into two separate rotations for calcu-

lation convenience,

$$\mathcal{R}(\alpha, \beta, \gamma) = \mathcal{R}(\alpha + \frac{\pi}{2}, \frac{\pi}{2}, 0)\mathcal{R}(\beta + \pi, \frac{\pi}{2}, \frac{\pi}{2} + \gamma). \tag{2.35}$$

2.5 Some Useful Operators and Subspaces

In this subsection, several operators and subspaces which used in this thesis are introduced.

2.5.1 Operators in Time-frequency Domain

1. **Band-limited Operator** $\mathcal{B}_W$ is the operator which produces a function whose Fourier transform $F(f)$ vanishes on $|f| > W$,

$$(\mathcal{B}_W f)(t) \triangleq \int_{-W}^{W} F(f)e^{i2\pi ft} \, df. \tag{2.36}$$

2. **Time-limited Operator** $\mathcal{D}_T$ is the operator which produces a function with support $[-T/2, T/2]$, i.e.,

$$(\mathcal{D}_T f)(t) \triangleq \begin{cases} f(t), & |t| \leq T/2, \\ 0, & |t| > T/2. \end{cases} \tag{2.37}$$

2.5.2 Operators on Unit Sphere

1. **Mode Limiting Operator** $\mathcal{B}_N$ is defined by [20]:

$$\begin{aligned} (\mathcal{B}_N f)(\boldsymbol{x}) &\triangleq \sum_{n=0}^{N} \sum_{m=-n}^{n} f_n^m Y_n^m(\boldsymbol{x}) \\ &= \sum_{n=0}^{N} \sum_{m=-n}^{n} \left(\int_{\mathbb{S}^2} f(\boldsymbol{y})\overline{Y_n^m(\boldsymbol{y})} \, ds(\boldsymbol{y}) \right) Y_n^m(\boldsymbol{x}) \\ &= \int_{\mathbb{S}^2} \sum_{n=0}^{N} \sum_{m=-n}^{n} Y_n^m(\boldsymbol{x})\overline{Y_n^m(\boldsymbol{y})} f(\boldsymbol{y}) \, ds(\boldsymbol{y}) \\ &= \int_{\mathbb{S}^2} \sum_{n=0}^{N} \frac{2n+1}{4\pi} P_n(\boldsymbol{x} \cdot \boldsymbol{y}) f(\boldsymbol{y}) \, ds(\boldsymbol{y}, \end{aligned} \tag{2.38}$$

where we have used (2.20) in the second equality and (2.16) in the fourth equality.

In the above, the inverse spherical harmonics transform (2.20) and the additional theorem for spherical harmonics (2.16) have been used. Denote

$$B_N(\boldsymbol{x}, \boldsymbol{y}) \triangleq \sum_{n=0}^{N} \sum_{m=-n}^{n} Y_n^m(\boldsymbol{x})\overline{Y_n^m(\boldsymbol{y})} = \sum_{n=0}^{N} \frac{2n+1}{4\pi} P_n(\boldsymbol{x} \cdot \boldsymbol{y}). \qquad (2.39)$$

Then, $(\mathcal{B}_N f)$ can be simplified into

$$(\mathcal{B}_N f)(\boldsymbol{x}) = \int_{\mathbb{S}^2} B_N(\boldsymbol{x}, \boldsymbol{y}) f(\boldsymbol{y}) \, ds(\boldsymbol{y}). \qquad (2.40)$$

$B_N(\boldsymbol{x}, \boldsymbol{y})$ is the kernel of the mode limiting operator $\mathcal{B}_N$. $\mathcal{B}_N$ is proved to be a compact, projection, idempotent and self-adjoint operator [20].

2. **Spatial Truncation Operator** $\mathcal{D}_\Gamma$ is defined by [20]:

$$(\mathcal{D}_\Gamma f)(\boldsymbol{x}) \triangleq \int_{\mathbb{S}^2} \chi_\Gamma(\boldsymbol{y})\delta(\boldsymbol{x} - \boldsymbol{y}) f(\boldsymbol{y}) \, ds(\boldsymbol{y}) = \begin{cases} f(\boldsymbol{x}), & \boldsymbol{x} \in \Gamma; \\ 0, & \boldsymbol{x} \in \mathbb{S}^2 \backslash \Gamma, \end{cases} \qquad (2.41)$$

where

$$D_\Gamma(\boldsymbol{x}, \boldsymbol{y}) = \chi_\Gamma(\boldsymbol{y})\delta(\boldsymbol{x} - \boldsymbol{y}), \qquad (2.42)$$

is the kernel function and $\chi_\Gamma(\cdot)$ is the characteristic function of the region Γ. It is also proved in the paper [20] that $\mathcal{D}_\Gamma$ is a projection, idempotent and self-adjoint operator; but it is not compact.

It is easy to prove that

$$(\mathcal{B}_N \mathcal{D}_\Gamma f)(\boldsymbol{x}) = \int_\Gamma B_N(\boldsymbol{x}, \boldsymbol{y}) f(\boldsymbol{y}) \, ds(\boldsymbol{y}), \quad \boldsymbol{x} \in \mathbb{S}^2, \qquad (2.43)$$

$$(\mathcal{D}_\Gamma \mathcal{B}_N f)(\boldsymbol{x}) = \begin{cases} \int_{\mathbb{S}^2} B_N(\boldsymbol{x}, \boldsymbol{y}) f(\boldsymbol{y}) \, ds(\boldsymbol{y}), & \boldsymbol{x} \in \Gamma, \\ 0, & \boldsymbol{x} \in \mathbb{S}^2/\Gamma \end{cases} \qquad (2.44)$$

which shows $\mathcal{B}_N$ and $\mathcal{D}_\Gamma$ do not commute [20].

3. **Rotation Operator** $\mathcal{R}$ is defined by (see Section 2.4.2),

$$(\mathcal{R}(\alpha, \beta, \gamma) f)(\boldsymbol{x}) = \sum_{n=0}^{\infty} \sum_{m=-n}^{n} \sum_{m'=-n}^{n} f_n^{m'} D_{mm'}^n(\alpha, \beta, \gamma) Y_n^m(\boldsymbol{x}).$$

where $D_{mm'}^n(\alpha, \beta, \gamma)$ is the Wigner-D function.

4. **Dilation Operator** $\mathcal{D}_a$ for $a > 0$ is defined by [21]

$$(\mathcal{D}_a f)(\theta, \phi) = \frac{1 + \tan^2 \frac{\theta}{2}}{1 + (\frac{1}{a} \tan \frac{\theta}{2})^2} \times \frac{1}{a} f\left(2 \tan^{-1}(\frac{1}{a} \tan \frac{\theta}{2}), \phi\right) = \lambda_a f(\theta_a, \phi),$$

(2.46)

where

$$\lambda_a = \frac{1}{a} \frac{1 + \tan^2 \frac{\theta}{2}}{1 + (\frac{1}{a} \tan \frac{\theta}{2})^2}, \quad \theta_a = 2 \tan^{-1}(\frac{1}{a} \tan \frac{\theta}{2}).$$

(2.47)

When $a = 1$, $\lambda_a = 1$ and $\theta_a = \theta$. That is, $\mathcal{D}_{a=1} f = f$ is the un-dilated function.

2.5.3 Notations for Some Complete Subspaces

- $L^2([-W, W])$ denotes a complete subspace of L^2 which contains all the square-integrable functions whose Fourier transforms vanish outside $[-W, W]$.

- $L^2([-T, T])$ denotes a complete subspace of L^2 which contains all the square-integrable functions whose supports are in interval $[-T, T]$.

- $\mathfrak{D}_\Gamma(\mathbb{S}^2, ds)$ is a complete subspace of $L^2(\mathbb{S}^2, ds)$ which contains all spatial-limited functions with compact support in the region $\Gamma \in \mathbb{S}^2$.

- $\mathfrak{B}_N(\mathbb{S}^2, ds)$ is a complete subspace of $L^2(\mathbb{S}^2, ds)$ which contains all spectral-limited functions with the maximum spectral degree N.

Chapter 3

Results On Signal Concentration in the Time-frequency Domain

This chapter deals with the signal energy concentration problem in the time-frequency domain. More specifically, in Section 3.2, applying Franks' general constrained variational method, the minimum kth moment time-duration concentration measure for a strictly band-limited signal in the time-frequency domain is formulated. Then a complete, orthonormal set of optimal band-limited functions with minimum fourth-moment time-duration concentration measure, high energy in the main lobe and fast decaying side lobes is obtained. Further, the properties of this set of functions are studied and prospective applications of these functions are given. In Section 3.3, the minimum 2nd and 4th-moment weighting for arbitrary signals with γ ratio energy outside of specified interval $[-T/2, T/2]$ are solved, which completes Franks' framework in the arbitrary signal concentration problem. Finally, Section 3.4 summarizes all the optimal functions of the concentration problem in the time-frequency domain.

3.1 Introduction

It is well known that a signal with shorter pulse duration has better range resolution [30] and a signal with small bandwidth better utilizes scarce channel frequency resources. But according to the Fourier transform theory, a signal cannot be both time-limited and band-limited simultaneously. However, in tasks such as minimizing the error rate [22, 23, 27] or minimizing bias for high-resolution spectral estimation [28], researchers seek signal designs that have the greatest concentration simultaneously in both time and frequency domains [58].

Slepian and Pollak [22] developed a set of concentration results which are partic-

ularly relevant to practical application. For a band-limited signal which is confined
to the frequency range $[-W, W]$, the fraction out-of-band energy (FOBE) measure
was proposed to determine a signal that has the greatest portion of its energy in
the $[-T, T]$ time interval. These signals are the prolate spheroidal wave functions
(PSWF). There are similar results when we exchange the roles of the time and
frequency domains.

Further interest in concentration for time-limited signals saw the emergence of
other results, such as minimum bandwidth of M orthogonal signals [59] and mini-
mum root-mean-square (RMS) bandwidth of M time-limited signals [60]. Similarly,
band-limited signals with minimum time-duration also have wide applicability, such
as hearing sensation [61], extrapolation of band-limited signals [20, 62], optimal
waveform signal design [63] and resolution enhancement to the near-field acoustic
holography [64].

Slepian [26] also extended his results to the discrete case. The corresponding op-
timal functions are called the discrete prolate spheroidal wave functions (DPSWF).
Applications of this result include digital filter design [65], optimal windows design
in electroencephalogram (EEG) [66], reduction of the bias of multi-taper spectrum
estimation in geophysics [9], and local basis expansions for linear inverse prob-
lems [41]. Recently, the DPSWF functions have also been applied in constructing
wavelets for multi-resolution analysis [67–70], and shown potential in denoising for
image processing.

However, no explicit analytical formula for prolate spheroidal wave function
(PSWF) has been developed. In addition, the cost in calculating such a solution
to a second order differential operator which commutes with the PSWF integral
convolution operator [22] is expensive [71]. At present, only the discrete version of
PSWF is available [22, 72–74]. The PSWF decays slowly like $1/t$ for increasing time
t. In contrast, Gabor's optimal band-limited function, i.e., the half sinusoid signal,
which minimizes a second-moment concentration measure, decays more quickly as
$1/t^2$. In [34], an optimal time-limited function with the minimum fourth-moment
bandwidth was determined. This function has larger main lobe and decays as
$1/f^3$. However, a detailed formulation and analysis for band-limited signals and
their concentration properties with arbitrary moment weighting in the time-domain
is of interest here. Further, it is also desirable to investigate whether a new com-
plete, orthonormal set of band-limited functions, besides PSWFs, exists which have
better performances than PSWF in representing and approximating a band-limited
function. Furthermore, in reality, it is impossible to construct strictly band-limited
or strictly time-limited signals. There always is some energy leakage outside of the

desired interval in either domain. Therefore, it leads to practical optimal waveform (neither band-limited nor time-limited) design issues in communication systems.

3.1.1   Slepian's Concentration for Band-limited Signals

Slepian's formulation is addressed: suppose $\psi(t)$ is a band-limited signal in $[-\Omega, \Omega]$, to achieve the maximum energy in the time interval $[-T/2, T/2]$, i.e.,

$$\lambda = \frac{\int_{-T/2}^{T/2} |\psi(t)|^2 \, dt}{\int_{-\infty}^{\infty} |\psi(t)|^2 \, dt} = \textbf{Maximum}, \tag{3.1}$$

what is the optimal waveform of $\psi(t)$?

Denote $\Psi(f)$ is the Fourier transform of $\psi(t)$. According to inverse Fourier transform, we have

$$\psi(t) = \frac{1}{2\pi} \int_{-\Omega}^{\Omega} \Psi(\omega) e^{i\omega t} \, d\omega = \int_{-\Omega/(2\pi)}^{\Omega/(2\pi)} \Psi(f) e^{i2\pi f t} \, df. \tag{3.2}$$

Then this problem is equivalent to maximizing the energy ratio

$$\lambda = \frac{\int_{-\Omega/(2\pi)}^{\Omega/(2\pi)} \int_{-\Omega/(2\pi)}^{\Omega/(2\pi)} |\Psi(f)|^2 \frac{\sin \pi T(f-f')}{\pi (f-f')} \, df \, df'}{\int_{-\infty}^{\infty} |\Psi(f)|^2 \, df}, \quad |f| \le \frac{\Omega}{2\pi}. \tag{3.3}$$

under the bandwidth constraint. Slepian and Pollak, in their paper [22], showed that the optimal function is the eigenfunction of the following eigenvalue equation (3.4),

$$\int_{-\Omega/(2\pi)}^{\Omega/(2\pi)} \frac{\sin \pi T(f-f')}{\pi (f-f')} \Psi(f) \, df' = \lambda \Psi(f), \quad |f| \le \frac{\Omega}{2\pi}. \tag{3.4}$$

This set of optimal functions is called the prolate spheroidal wave functions (PSWFs).

Remark 3.1   *1. The eigenvalue equation in Slepian paper [22] is for the time-limited signal, not for the band-limited signal,*

$$\int_{-T/2}^{T/2} \frac{\sin \Omega(t-s)}{\pi (t-s)} \psi(s) \, ds = \lambda \psi(t), \quad |t| \le T/2. \tag{3.5}$$

That is, $\psi(t)$ is a time-limited signal in the time interval $[-T/2, T/2]$ which achieves maximal energy in the bandwidth $[-\Omega, \Omega]$.

2. *Equivalent eigenvalue equation to (3.5) (for a time-limited signal) is*

$$\int_{-1}^{1} \frac{\sin c(t-s)}{\pi(t-s)} \psi\left(\frac{T}{2}s\right) ds = \lambda\psi\left(\frac{T}{2}t\right), \quad |t| \le 1, \tag{3.6}$$

where $c = \Omega\frac{T}{2}$. This equation also shows that $\psi\left(\frac{T}{2}t\right)$ is a scaled version of $\psi(t)$.

3. *PSWFs $\psi(t)$ in Slepian's paper are normalized.*

4. *It also should be noted that the kernel $\frac{\sin c(t-s)}{\pi(t-s)}$ is finite, which means there are only a finite number of nonzero eigenvalues.*

PSWFs have the following properties [22]:

1. For any value of $c = 2\pi WT$, there is a countable set of real functions $\{\psi_i(c,t); i = 0,1,2,\cdots\}$ with corresponding real and positive distinct eigenvalues

$$1 > \lambda_0(c) > \lambda_1(c) > \lambda_2(c) > \cdots \tag{3.7}$$

where the ordering is maintained for all values of c.

2. The $\psi_i(t)$ are band-limited, orthonormal on the real line and complete in the $L^2(-\infty, \infty)$:

$$\int_{-\infty}^{\infty} \psi_i(t)\psi_j(t)\, dt = \delta_{ij}, \quad , i, j = 0, 1, 2, \cdots, \tag{3.8}$$

where $\delta_{(.)}$ is the Kronecker delta function defined in (2.15).

3. The $\psi_i(t)$ are orthogonal and complete in the interval $L^2([-T/2, T/2])$:

$$\int_{-T/2}^{T/2} \psi_i(t)\psi_j(t)\, dt = \lambda_i\delta_{ij}, \quad , i, j = 0, 1, 2, \cdots. \tag{3.9}$$

3.1.2 Landau's Concentration for Arbitrary Signals

This problem is stated thus: given the total energy constraint on an arbitrary signal $x(t) \in L^2(-\infty, \infty)$, its partial energy in the time interval $[-T/2, T/2]$ and its partial energy in the frequency band $[-W, W]$, to achieve the simultaneous time and frequency concentration, what is the optimal waveform of $x(t)$?

Landau and Pollak, in their paper [23], proved the uncertainty relations between α and β by Theorem 2, and the optimal signal that does the best job simultaneously in the time domain and frequency domain is provided.

Theorem 3.1.1 *(Uncertainty Principle [23]): given $\|x\| = 1$, $\|\mathcal{D}_T x\| = \alpha$ with $0 \le \alpha \le 1$ and $\|\mathcal{B}_W x\| = \beta$ with $0 \le \beta \le 1$, the uncertainty relation is:*

1. *If $\alpha = 0$, when $0 \le \beta < 1$;*

2. *If $0 < \alpha < \sqrt{\lambda_0}$, when $0 \le \beta \le 1$;*

3. *If $\sqrt{\lambda_0} \le \alpha < 1$, when $\cos^{-1}\alpha + \cos^{-1}\beta \ge \cos^{-1}\sqrt{\lambda_0}$;*

4. *If $\alpha = 1$, when $0 < \beta \le \sqrt{\lambda_0}$.*

where $\mathcal{D}_T$ is the time-limited operator and $\mathcal{B}_W$ is the band-limited operator defined in Subsection 2.5.1, λ_0 is the largest eigenvalue of the eigenvalue equation (3.4).

The optimal signal for the general concentration problem is

$$x(t) = p\psi_0(c, t) + qw(t)\psi_0(c, t) \tag{3.10}$$

where $\psi_0(c, t)$ is the first order PSWF, $w(t)$ is the window function

$$w(t) = \begin{cases} 1, & |t| \le T/2; \\ 0, & otherwise, \end{cases} \tag{3.11}$$

and

$$p = \sqrt{\frac{1 - \alpha^2}{1 - \lambda_0}}, \quad q = \frac{\alpha}{\sqrt{\lambda_0}} - \sqrt{\frac{1 - \alpha^2}{1 - \lambda_0}} \tag{3.12}$$

where α and β satisfy $\sqrt{\lambda_0} \le \alpha < 1$ and $\cos^{-1}\alpha + \cos^{-1}\beta \ge \cos^{-1}\sqrt{\lambda_0}$.

3.2 Band-limited Signal Concentration with kth Moment Weighting in the Time Domain

In this section, the general constrained variational method of Franks [1] is applied to formulate concentration with a kth time moment weighting for a band-limited signal [75–77]. The case $k = 4$ is taken as a central example. A complete, orthonormal set of optimal band-limited functions in $L^2([-W, W])$ with the minimum fourth-moment time-duration measure is obtained. The characteristics of the set of functions are discussed. Further, the minimum fourth-moment time-duration measure and the time-duration energy concentration measure are calculated. Furthermore, by comparing the PSWF and Gabor's functions, our optimal functions

can be a seen to be a good alternative in optimal waveform design for communication systems, and higher range resolution radar systems. Finally, this set of optimal functions can also be used for representation of any band-limited signal, extrapolation a band-limited function known only in the interval $[-T, T]$ or approximation a band-limited function in the interval $[-T, T]$.

3.2.1   Problem Statement

Let L^2 be the complex Hilbert space containing all square-integrable functions defined on the real line with inner product defined as

$$\langle x, y \rangle = \int_{-\infty}^{\infty} x(t)\overline{y(t)}\, dt.$$

for $x, y \in L^2$. This inner product induces the norm such that $\|x\| = \langle x, x \rangle^{1/2}$.

Find the optimal finite energy signal, $x(t) \in L^2$, band-limited to the frequency range $[-W, W]$ which minimizes the moment weighted energy $\int_{-\infty}^{\infty} t^k |x(t)|^2\, dt$. Here t^k, $k = 0, 2, 4, \cdots$, is the kth weighting function in the time-domain. Note that odd values of k and $k = 0$ are degenerate or trivial. For $k = 2$, this problem has been solved by Gabor [61]. In this paper, we concentrate on the $k = 4$, fourth moment time-domain weighting as an exemplar. For $k > 4$, the solution can be easily extended based on our methods. It is possible to treat the case of time-limited finite energy signals with frequency domain moment weighting, f^k, in an analogous way.

3.2.2   Franks' General Constrained Variational Method

In this section, Franks' general constrained variational method (FGCVM) [1, Chap. 6] is revisited. This method is applicable for any properly formulated extremization problem in the time and frequency domains, and is ideal for signal concentration problems.

The general constrained variational problem is stated: For a given signal with finite energy, extremize (minimize or maximize) the arbitrary weighted energy either in the time domain or in the frequency domain, to obtain the optimal waveform signal? Suppose $w(t) \geq 0$ is an arbitrary weighting function in the time-domain, $V(f) \geq 0$ is an arbitrary weighting function in the frequency domain. Following Franks [1], this general variational problem is equivalent to extremizing

$$G = \mu_1 I_1 + \mu_2 I_2 + I_3 \tag{3.14}$$

where μ_1 and μ_2 are two Lagrange multipliers and I_1–I_3 are three quadratic functionals defined as

$$I_1 \triangleq \langle wx, x \rangle = \int_{-\infty}^{\infty} w(t)|x(t)|^2 \, dt \tag{3.15a}$$

$$I_2 \triangleq \langle VX, X \rangle = \int_{-\infty}^{\infty} V(f)|X(f)|^2 \, df \tag{3.15b}$$

$$I_3 \triangleq \langle x, x \rangle = \langle X, X \rangle = 1. \tag{3.15c}$$

Here, I_1 represents a time weighted measure of energy in the time domain, I_2 represents a frequency weighted measure of energy in the frequency domain, and I_3 represents the total energy of a signal constrained to be unity (finite energy without loss of generality). The frequency domain inner product is defined in the obvious way.

By solving this optimization equation (3.14), the necessary conditions are obtained in both time domain and frequency domains [1]:

$$\mu_1 w(t)x(t) + \mu_2 \int_{-\infty}^{\infty} v(t - \tau)x(\tau) \, d\tau + x(t) = 0, \tag{3.16}$$

$$\mu_1 \int_{-\infty}^{\infty} W(f - \nu)X(\nu) \, d\nu + \mu_2 V(f)X(f) + X(f) = 0, \tag{3.17}$$

where $v(t)$ is the inverse Fourier transform of $V(f)$ and $W(f)$ is the Fourier transform of $w(t)$.

3.2.3 Optimization Formulation

Define frequency weighting, corresponding to band-limiting to frequencies $[-W, W]$,

$$V(f) = \begin{cases} 1, & |f| \leq W, \\ 0, & |f| > W \end{cases} \tag{3.18}$$

and time weighting $w(t) = t^4$, corresponding to fourth moment time-domain weighting. Then under the general constrained variational method of Franks, the optimization problem is to extremize

$$G(x) = \mu_1 I_1 + \mu_2 I_2 + I_3,$$

where

$$I_1 = \int_{-\infty}^{\infty} t^4 |x(t)|^2 \, dt$$

$$I_2 = \int_{-\infty}^{\infty} V(f) |X(f)|^2 \, df = \int_{-W}^{W} |X(f)|^2 \, df = 1$$

$$I_3 = \langle x, x \rangle = \langle X, X \rangle = 1.$$

Now to obtain the optimal function $X(f)$ that renders $G(x)$ or I_1 stationary, we only need to find the necessary condition in the frequency domain.

Using the Fourier transform of $t^n x(t)$

$$t^n x(t) \longleftrightarrow i^n \frac{d^n X(\omega)}{d\omega^n} = \frac{i^n}{(2\pi)^n} \frac{d^n X(f)}{df^n},$$

where $i = \sqrt{-1}$, the necessary condition equation (3.17) in the frequency domain is obtained

$$\mu_1 \frac{1}{(2\pi)^4} X^{(4)}(f) + \mu_2 V(f) X(f) + X(f) = 0, \quad |f| \leq W,$$

which further simplifies to the fourth order linear differential equation

$$X^{(4)}(f) = -\frac{1 + \mu_2}{\mu_1} (2\pi)^4 X(f), \quad |f| \leq W, \tag{3.23}$$

where the notation $X^{(4)}(f)$ represents the 4-th derivative of $X(f)$ with respect to frequency f. By defining $\lambda = -(1 + \mu_2)(2\pi)^4 / \mu_1 \in \mathbb{R}$ (real numbers), this equation can be written

$$\left(D^4 X \right)(f) = \lambda X(f), \quad |f| \leq W, \tag{3.24}$$

where D is the differential operator. Revealing this is an eigen-function equation with λ the eigenvalue.

3.2.4   Solutions

As shown in the Appendix A.1, a general solution to the fourth order linear differential equation (3.24) can be written as

$$X(f) = A \cos(mf) + B \sin(mf) + E \cosh(mf) + F \sinh(mf), \quad |f| \leq W \tag{3.25}$$

where A, B, E and F are arbitrary constants. Its first derivative is

$$X'(f) = m[-A\sin(mf) + B\cos(mf) + E\sinh(mf) + F\cosh(mf)], \quad |f| \leq W. \tag{3.26}$$

According to the characteristic of $X(f)$, the boundary conditions $X(-W) = X(W) = 0$ and $X'(-W) = X'(W) = 0$ and the total energy of $I_3 = \langle x, x \rangle = \langle X, X \rangle = 1$, there are three different solutions. Detailed deduction is provided in the Appendix A.2.

Case a) When $X(f)$ is an even function, i.e., $B = F = 0$, then

$$X_e(f) = A_e[\cos(mf) + \alpha\cosh(mf)], \quad |f| \leq W, \tag{3.27}$$

where $A_e = 1/\sqrt{(1 + \alpha^2)W}$, $\alpha = -\cos(mW)/\cosh(mW)$ and m is the positive solution of the following even condition equation

$$C_e(m) \triangleq \cos(mW)\sinh(mW) + \sin(mW)\cosh(mW) = 0. \tag{3.28}$$

Case b) When $X(f)$ is an odd function, i.e., $A = E = 0$, then

$$X_o(f) = B_o[\sin(mf) + \beta\sinh(mf)], \quad |f| \leq W, \tag{3.29}$$

where $B_o = 1/\sqrt{(1 - \beta^2)W}$, $\beta = -\sin(mW)/\sinh(mW)$ and m is the positive solution of the following odd condition equation:

$$C_o(m) \triangleq \cos(mW)\sinh(mW) - \sin(mW)\cosh(mW) = 0. \tag{3.30}$$

Case c) When $X(f)$ is neither an even nor an odd function, it can be expressed as a linear combination of (3.27) and (3.29). Note the values of m in equations (3.27) and (3.29) are not the same.

3.2.5 Inverse Fourier transform

Taking the inverse Fourier transform of $X(f)$, the optimal waveform of the signal $x(t)$ in the time domain is obtained.

For $|f| \leq W$, according to the Fourier transform pairs:

$$\frac{W}{2\pi}\left\{ \text{sinc}\left[W(t + \frac{m}{2\pi})\right] + \text{sinc}\left[W(t - \frac{m}{2\pi})\right] \right\} \longleftrightarrow \cos(mf)V(f)$$

and

$$\frac{-iW}{2\pi}\left\{\mathrm{sinc}\left[W(t+\frac{m}{2\pi})\right]-\mathrm{sinc}\left[W(t-\frac{m}{2\pi})\right]\right\}\longleftrightarrow\sin(mf)V(f),$$

where $\mathrm{sinc}(x)=\sin x/x$. Similarly,

$$\frac{W}{2\pi}\left\{\mathrm{sinc}\left[W(t+i\frac{m}{2\pi})\right]+\mathrm{sinc}\left[W(t-i\frac{m}{2\pi})\right]\right\}\longleftrightarrow\cosh(mf)V(f)$$

and

$$\frac{-iW}{2\pi}\left\{\mathrm{sinc}\left[W(t+i\frac{m}{2\pi})\right]-\mathrm{sinc}\left[W(t-i\frac{m}{2\pi})\right]\right\}\longleftrightarrow\sinh(mf)V(f).$$

Therefore,

$$\mathrm{sinc}\left[W(t+i\frac{m}{2\pi})\right]+\mathrm{sinc}\left[W(t-i\frac{m}{2\pi})\right]$$
$$=\frac{2Wt}{(Wt)^2+(\frac{Wm}{2\pi})^2}\sin(Wt)\cosh(\frac{Wm}{2\pi})+\frac{\frac{Wm}{\pi}}{(Wt)^2+(\frac{Wm}{2\pi})^2}\cos(Wt)\sinh(\frac{Wm}{2\pi}).$$

$$(3.31)$$

Similarly,

$$\mathrm{sinc}\left[W(t+i\frac{m}{2\pi})\right]-\mathrm{sinc}\left[W(t-i\frac{m}{2\pi})\right]$$
$$=i\left[\frac{\frac{-Wm}{\pi}}{(Wt)^2+(\frac{Wm}{2\pi})^2}\sin(Wt)\cosh(\frac{Wm}{2\pi})+\frac{2Wt}{(Wt)^2+(\frac{Wm}{2\pi})^2}\cos(Wt)\sinh(\frac{Wm}{2\pi})\right].$$

$$(3.32)$$

So the inverse Fourier transform of $X(f)$ leads to:

Case a) when $X(f)$ is even, then

$$x_e(t)=\frac{A_eW}{2\pi}\left\{\mathrm{sinc}\left[W(t+\frac{m}{2\pi})\right]+\mathrm{sinc}\left[W(t-\frac{m}{2\pi})\right]\right\}$$
$$+\alpha\frac{A_eW}{2\pi}\left\{\mathrm{sinc}\left[W(t+i\frac{m}{2\pi})\right]+\mathrm{sinc}\left[W(t-i\frac{m}{2\pi})\right]\right\},\qquad(3.33)$$

where A_e and α have the same definition as before, (3.29).

Substituting the equation (3.31), $x_e(t)$ equals to

$$x_e(t)=\frac{A_eW}{2\pi}\left\{\mathrm{sinc}\left[W(t+\frac{m}{2\pi})\right]+\mathrm{sinc}\left[W(t-\frac{m}{2\pi})\right]\right\}$$
$$+\alpha\frac{A_eW}{2\pi}\left\{\frac{2Wt}{(Wt)^2+(\frac{Wm}{2\pi})^2}\sin(Wt)\cosh(\frac{Wm}{2\pi})\right.$$

$$+ \frac{\frac{Wm}{\pi}}{(Wt)^2 + (\frac{Wm}{2\pi})^2} \cos(Wt) \sinh(\frac{Wm}{2\pi})\Big\}. \tag{3.34}$$

This shows that $x_e(t)$ is a real signal in the time domain.

Case b) when $X(f)$ is odd, then

$$x_o(t) = \frac{-iB_oW}{2\pi} \Big\{ \mathrm{sinc}\Big[W(t + \frac{m}{2\pi})\Big] - \mathrm{sinc}\Big[W(t - \frac{m}{2\pi})\Big]\Big\}$$
$$+ \beta\frac{-iB_oW}{2\pi} \Big\{ \mathrm{sinc}\Big[W(t + i\frac{m}{2\pi})\Big] - \mathrm{sinc}\Big[W(t - i\frac{m}{2\pi})\Big]\Big\}, \tag{3.35}$$

where B_o and β are the same as before, (3.29).

Substituting the equation (3.32), $x_o(t)$ equals to

$$x_o(t) = \frac{-iB_oW}{2\pi} \Big\{ \mathrm{sinc}\Big[W(t + \frac{m}{2\pi})\Big] - \mathrm{sinc}\Big[W(t - \frac{m}{2\pi})\Big]\Big\}$$
$$+ \beta\frac{B_oW}{2\pi} \Big\{ \frac{\frac{-Wm}{\pi}}{(Wt)^2 + (\frac{Wm}{2\pi})^2} \sin(Wt) \cosh(\frac{Wm}{2\pi})$$
$$+ \frac{2Wt}{(Wt)^2 + (\frac{Wm}{2\pi})^2} \cos(Wt) \sinh(\frac{Wm}{2\pi})\Big\}. \tag{3.36}$$

This shows that $x_o(t)$ is a complex signal in the time domain.

3.2.6 Properties of the solution functions

In this section, the properties of the solution functions are studied. The results are shown in the following theorems.

Theorem 3.2.1 *1. The sequence $\{m_j\}, j = 1, 2, 3, ...,$ consist of the values which satisfy the even condition function (3.28) and the even solution (3.27) function; and the sequence $\{m'_j\}, j = 1, 2, 3, ...,$ consist of the values which satisfy the odd condition function (3.30) and the odd solution function (3.29). Both of these two sets of sequences are monotonically increasing; m_j and m'_j are interleaved with each other.*

2. The union solution set $\{\psi_i(f)\} = \{X_{ej}(f) \cup X_{ok}(f)\}, i, j, k = 1, 2, 3, ..., |f| \le W$, which consists of the even optimal functions (3.27) and the odd optimal functions (3.29), can be ordered as

$$\sqrt{\frac{1}{(1 + \alpha_1^2)W}} \big(\cos(m_1 f) + \alpha_1 \cosh(m_1 f) \big),$$

$$\sqrt{\frac{1}{(1-\beta_1^2)W}}\big(\sin(m_1'f)+\beta_1\sinh(m_1'f)\big),$$

$$\sqrt{\frac{1}{(1+\alpha_2^2)W}}\big(\cos(m_2f)+\alpha_2\cosh(m_2f)\big),$$

$$\sqrt{\frac{1}{(1-\beta_2^2)W}}\big(\sin(m_2'f)+\beta_2\sinh(m_2'f)\big),$$

$$\vdots \tag{3.37}$$

Proof

See Appendix A.3.   □

Theorem 3.2.2 $\{\psi_i(f)\}$ *is a complete, orthonormal sequence in* $L^2([-W,W])$.

Proof

See Appendix A.4.   □

3.2.7   Time-duration Measure

In this chapter, two kinds of time-duration measures in the time-frequency domain are defined: the minimum fourth-moment time-duration measure on the whole real line and the time-duration energy concentration measure in the time interval $[-T,T]$.

The minimum fourth-moment time-duration measure is defined as

$$\eta \triangleq \frac{\int_{-\infty}^{\infty} t^4 |x(t)|^2 dt}{\int_{-\infty}^{\infty} |x(t)|^2 dt} = \frac{\lambda}{(2\pi)^4}, \tag{3.38}$$

where λ is defined by the fourth order differential equation (3.24). The latter equality is obtained using the Parseval's Theorem:

$$\int_{-\infty}^{\infty} t^4 |x(t)|^2 dt = \langle t^4 x, x \rangle = \langle \frac{1}{(2\pi)^4} X^{(4)}(f), X(f) \rangle = \frac{\lambda}{(2\pi)^4} \langle x(t), x(t) \rangle.$$

Here, the equation (3.23) has been used in the third equality "=".

The time-duration energy concentration measure in the time interval $[-T,T]$ is defined as

$$\gamma \triangleq \frac{\int_{-T}^{T} |x(t)|^2 dt}{\int_{-\infty}^{\infty} |x(t)|^2 dt}. \tag{3.39}$$

3.2.8   Distribution of m and m'

In Fig. 3.1, the x-axis denotes the values of mW and the y-axis denotes the condition function. We take the y-axis as $10 \log_{10} |C(m)|$. The label "even" means the even condition function, $C_e(m)$ in (3.28), and the label "odd" means the odd condition function, $C_o(m')$ in (3.30).
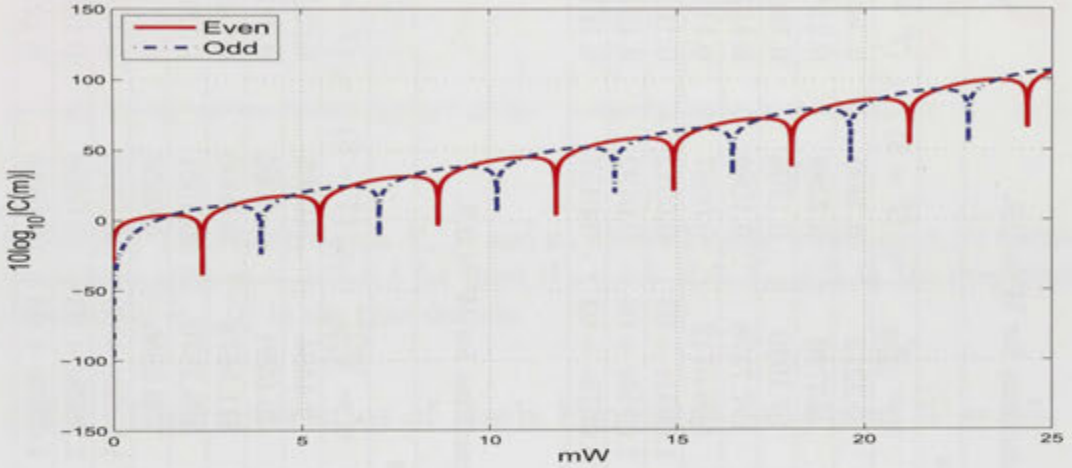
Figure 3.1: Trend of the even condition function (3.28) and odd condition function (3.30) versus mW.

The downward peak points in Fig. 3.1 show the zero points of the condition functions, respectively. This figure shows: 1) the condition functions present the periodicity of $\cos x$ and $\sin x$; 2) the zero points mW and $m'W$ for the functions are interleaved each other, asserted in Theorem 3.2.1; and 3) the trend of the condition functions are increasing by the hyperbolic functions $\cosh x$ and $\sinh x$.

Table. 3.1 and Table. 3.2 list the first 8 values of m and m' when $W = 0.5$ for the even and odd condition functions in (3.28) and (3.30), respectively. These two Tables also include the value of α, β, eigenvalues $\lambda = m^4$ and $\lambda' = (m')^4$, time-duration measure η, (3.38), and time-duration energy concentration measure γ_e, (3.39), corresponding to each m and m' values. From these tables, we can see that for fixed W, the values of α and β decrease very quickly. For index $j \geq 3$,

$$X_{ej}(f) \longrightarrow A_{ej} \cos(m_j f), \quad X_{oj}(f) \longrightarrow B_{oj} \sin(m_j')f. \qquad (3.40)$$

Table 3.1: Parameters for the even functions for $W = 0.5$.

			Even Functions				
Index	mW	m	$\lambda = m^4$	α	$\eta = \frac{m^4}{(2\pi)^4}$	$\gamma_e \ (T = 5)$	$\gamma_e \ (T = 13)$
1	2.365	4.7300	500.5467	0.1329	0.3212	0.3495	0.3693
2	5.4978	10.9956	$1.4618e+04$	-0.0058	9.3790	0.2288	0.2387
3	8.6394	17.2788	$8.9136e+04$	2.5031e-04	57.1919	0.1705	0.1806
4	11.781	23.5620	$3.0821e+05$	-1.0817e-05	197.7578	0.1080	0.1328
5	14.9226	29.8452	$7.9341e+05$	4.6744e-07	509.0712	0.0597	0.1157
6	18.0642	36.1284	$1.7037e+06$	-2.0200e-08	$1.0931e+03$	0.0312	0.1275
7	21.2057	42.4114	$3.2354e+06$	8.7292e-10	$2.0759e+03$	0.0192	0.1517
8	24.3473	48.6946	$5.6224e+06$	-3.7722e-11	$3.6075e+03$	0.0157	0.1679

Table 3.2: Parameters for the odd functions for $W = 0.5$.

			Odd Functions				
Index	$m'W$	m'	$\lambda' = (m')^4$	β	$\eta' = \frac{(m')^4}{(2\pi)^4}$	$\gamma_o \ (T = 5)$	$\gamma_o \ (T = 13)$
1	3.9266	7.8532	$3.8035e+03$	0.0279	2.4404	0.0205	0.0332
2	7.0686	14.1372	$3.9944e+04$	-0.0012	25.6291	0.0564	0.0917
3	10.2102	20.4204	$1.7388e+05$	5.2035e-05	111.5674	0.0900	0.1487
4	13.3518	26.7036	$5.0849e+05$	-2.2486e-06	326.2570	0.1051	0.1803
5	16.4934	32.9868	$1.1840e+06$	9.7172e-08	759.6985	0.0956	0.1797
6	19.635	39.2700	$2.3782e+06$	-4.1992e-09	$1.5259e+03$	0.0680	0.1583
7	22.7765	45.5530	$4.3059e+06$	1.8146e-10	$2.7628e+03$	0.0358	0.1359
8	25.9181	51.8362	$7.2199e+06$	-7.8417e-12	$4.6325e+03$	0.0118	0.1270
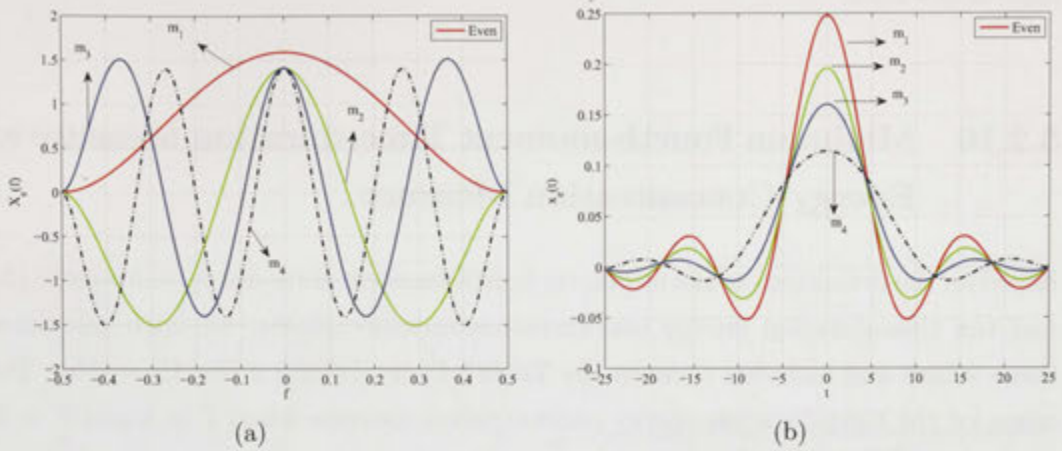
Figure 3.2: The even function $X_e(f)$ and its inverse Fourier transform $x_e(t)$ versus variable m with $m = 1, 2, 3, 4$ for fixed $W = 0.5$. (a) $X_{em_j}(f)$ in the frequency domain, (b) $x_{em_j}(t)$ in the time-domain.

3.2.9 Characteristics of Basis Functions for Fixed $W = 0.5$

The characteristics of the basis functions with different values of m_j for the even function and $m_{k'}$ for the odd function with fixed bandwidth $W = 0.5$ are shown in Fig. 3.2 and 3.3.

Fig. 3.2 shows the even functions $X_e(f)$ and their corresponding inverse Fourier transform $x_e(t)$ vary with different value m_j in the frequency domain. From Fig. 3.2(a), we know that for the even function $X_e(f)$, except the end points, there is no zero point when $m = m_1$, 2 zero points when $m = m_2$, 4 zero points when $m = m_3$, and 6 zero points when $m = m_4$, etc. So we can establish that there are $2j - 1$ zero points for the even function when $m = m_j$. The function $x_e(t)$ in Fig. 3.2(b) shows the waveform in the time-domain has sharper central portion, less main lobe and decays slowly when m_j decreases.

Fig. 3.3 depicts how the odd functions $X_o(f)$ and their inverse Fourier transforms $x_o(t)$ vary with different value m'_k in the frequency domain and in the time-domain. Fig. 3.3(a) indicates that for the odd function $X_{om'_k}(f)$, except the end points, there is 1 zero point when $m' = m'_1$, 3 zero points when $m' = m'_2$, 5 zero points when $m' = m'_3$ and 7 zero points when $m' = m'_4$. It is concluded that there are $2k - 1$ for the odd functions with $m' = m'_k$. Fig. 3.3(b) and Fig. 3.3(c) depict the real part and the imaginary part of the odd function $x_{om'_k}(t)$ versus the variable m' for fixed $W = 0.5$ in the time-domain. The magnitude of the real part is much smaller compared to the magnitude of the imaginary part. Therefore, as the value of m' increases, the odd signal approaches a pure complex signal as the real part

approaches zero.

3.2.10   Minimum Fourth-moment Time-duration Measure and Energy Concentration Measure

Based on the definitions of the minimum fourth-moment time-duration measure (3.38) and the time-duration energy concentration measure (3.39), we have calculated these values and included them in the Table 3.1 and Table 3.2 (for $W = 0.5$). Two cases for the time-duration energy concentration measure when $T = 5$ and $T = 13$ are considered. The tables indicate that: 1) the minimum fourth-moment time-duration measure η increases quickly; 2) the time-duration energy concentration measure γ_e decreases roughly as m increases; 3) γ_e increases as the measure interval T increases; and 4) $x_{e1}(t)$, the even function, has higher energy concentration measure than the other functions.

3.2.11   Comparison between PSWF, Gabor and our Basis Functions

Slepian's prolate spheroidal wave function (PSWF) is an optimal band-limited function bandwidth Ω which achieves the maximal energy in the time interval $[-T, T]$ [22]. PSWF satisfies the following eigenvalue equation,

$$\int_{-\Omega/(2\pi)}^{\Omega/(2\pi)} \frac{\sin 2\pi T(f - f')}{\pi(f - f')} \psi(f')\, df' = \lambda \psi(f), \quad |f| \le \frac{\Omega}{2\pi}.$$

It is well known that no explicitly analytical formula for the PSWF exists. And only the discrete approximation of the PSWF by numerical computation is available [22, 71, 73].

Gabor's function is defined by [61]

$$\phi(f) = \frac{1}{\sqrt{W}} \sin\left(\frac{k\pi}{2W} f + \frac{k\pi}{2}\right), \quad |f| \le W,$$

where $k \in \mathbf{Z} \backslash \{0\}$. The corresponding inverse Fourier transform is

$$\phi(t) = \frac{\sqrt{W}}{2\pi} \left\{ \operatorname{sinc}\left[W\left(t + \frac{k}{4W}\right)\right] + \operatorname{sinc}\left[W\left(t - \frac{k}{4W}\right)\right] \right\}.$$

(a)

(b)

(c)
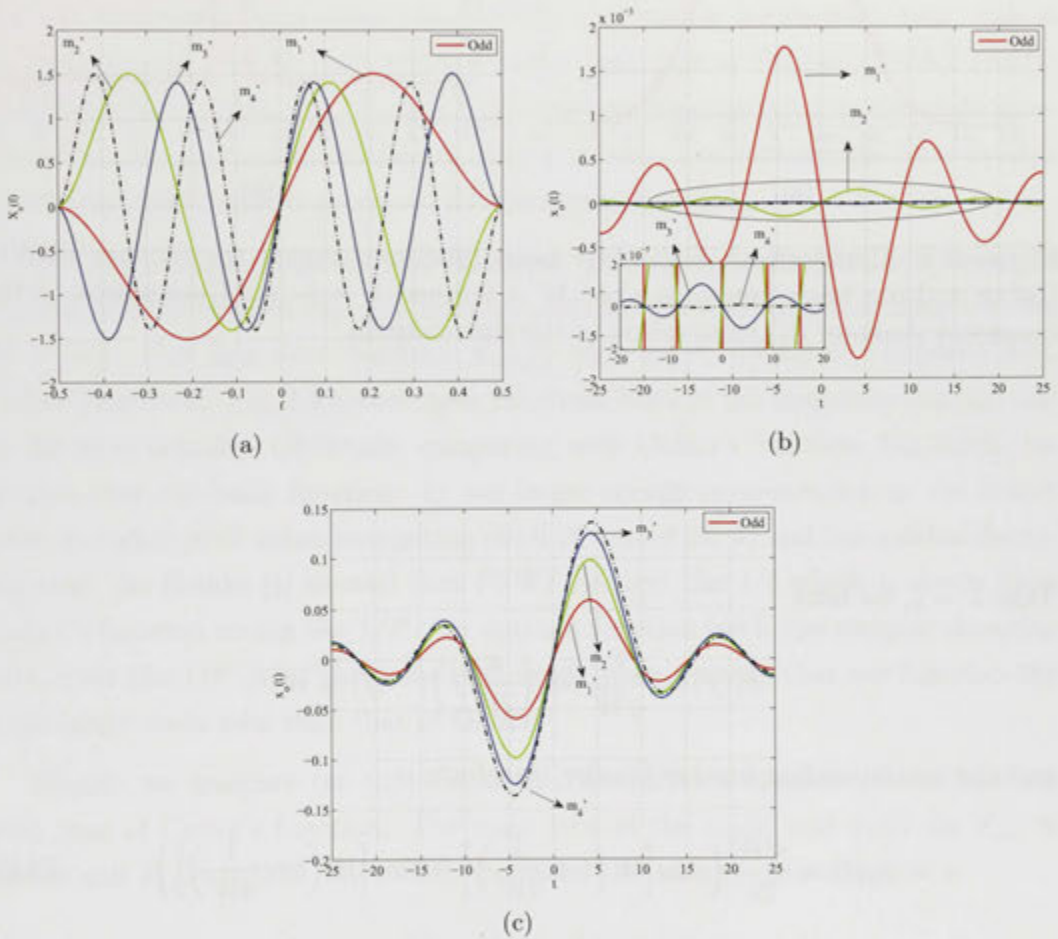
Figure 3.3: The odd function $X_o(f)$ and its inverse Fourier transform $x_o(t)$ versus
variable m' with $m' = 1, 2, 3, 4$ for fixed $W = 0.5$. (a) $X_{om'_k}(f)$ in the frequency
domain; (b) the real part of $x_{om'_k}(t)$ in the time-domain, where the amplitude of
Y-axis is 2×10^{-3}, the small panel is to show the real part of the waveform of
$x_{om'_3}(t)$ and $x_{om'_4}(t)$ whose amplitudes are only 2×10^{-5}; (c) the imaginary part of
$x_{om'_k}(t)$ in the time-domain, where the amplitude of Y-axis is 0.1. Comparing with
the real part in (b), the imaginary part in (c) dominates the whole waveform.
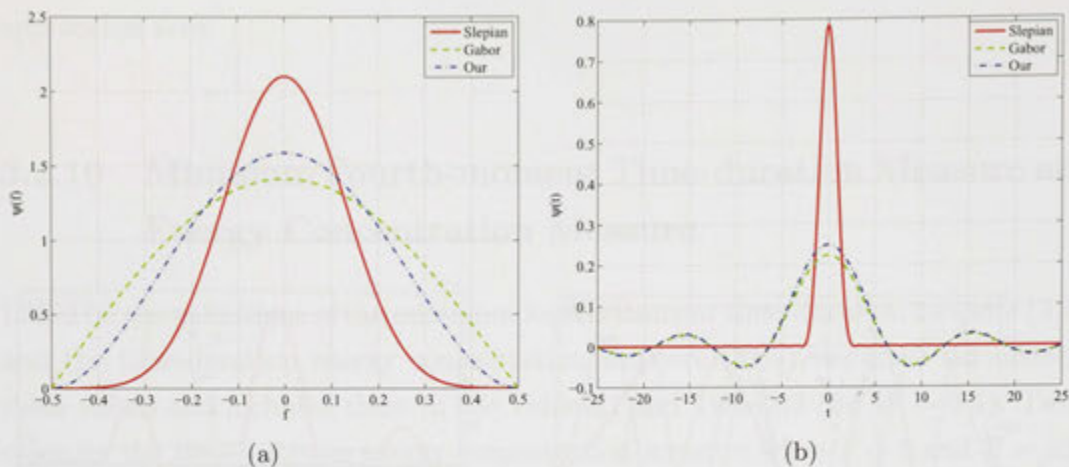
Figure 3.4: Comparison of the first basis functions among the Slepian PSWF, Gabor and our basis functions when $W = 0.5$ and $T = 5$. (a) Comparison in the frequency domain; (b) comparison in the time-domain.

Take $k = 1$, we have

$$\phi_1(f) = \frac{1}{\sqrt{W}} \cos\left(\frac{\pi}{2W} f\right), \quad |f| \leq W$$

and the corresponding inverse Fourier transform is

$$\phi_1(t) = \frac{\sqrt{W}}{2\pi}\left\{ \text{sinc}\left[W\left(t + \frac{1}{4W}\right)\right] + \text{sinc}\left[W\left(t - \frac{1}{4W}\right)\right]\right\}. \qquad (3.45)$$

Take the first basis functions of PSWF, Gabor and our basis functions as an example. Let the bandwidth $W = 0.5$ and the interested time-duration $T = 5$ for comparison. Then the time-bandwidth product for PSWF is $c = \Omega T = 2\pi W T = 15.7085$. Fig. 3.4 shows the first basis function of Slepian PSWF, Gabor and our basis functions both in the frequency domain and in the time-domain. The energy for these three functions in $[-T, T]$ is 0.9999, 0.2806 and 0.3495 for PSWF, Gabor and our basis function. From this figure, we can see that: 1) Slepian's PSWF absolutely holds the best performance both in the time-domain due to its maximum energy concentration in the center; 2) our basis functions are a bit better than Gabor's function; and 3) our basis functions have larger main lobes.

3.2.12   Application One – Optimal Waveforms for Communication Systems

The following study shows that the set of our optimal functions can be a better
choice of waveform for some systems, such as radar system with higher range resolution requirement and data transmission with higher information rate, due to
its fast decaying rate $O(1/t^3)$ which is faster than that of Slepian's PSWF $O(1/t)$
and Gabor's functions $O(1/t^2)$ and higher energy concentration in the main lobe.
Therefore, our optimal functions are more powerful to counteract the inter-symbol
interference (ISI) and more robust for the signal detection.

We now compare our optimal functions with Gabor's function [61] which is
optimal with respect to the minimum second-moment time-duration measure. Set
$W = 0.5$. Our first even function $X_{e1}(f)$ with $m_1 = 4.7300$ is compared with
Gabor's function. Fig. 3.5 shows these functions both in the frequency domain and
in the time domain. Obviously, comparing with Gabor's function, Fig. 3.5(b) indicates that our basis function: 1) has larger energy concentration in the center
lobe; 2) higher peak value, comparing the 0.25 with 0.22; 3) and has quicker decaying rate. As Franks [1] showed that PSWF decays[1] like $1/t$ which is slower than
Gabor's function acting like $1/t^2$, our optimal function holds the steepest decaying
rate, a bit like $1/t^3$ [34]. The embedded small figure denotes that our function has
a bit larger main lobe than that of Gabor.

Finally, we compare the time-duration concentration measure of our function
with that of Gabor's function. The main lobe of the $x_{e1}(t)$ and $\phi_1(t)$ are $T_{x_{e1}} \approx$
6.3536 and $T_{\phi_1} \approx 6.3236$. By (3.39), the main lobe energy concentration is

$$\gamma_{x_{e1}} = \frac{\int_{-T_{x_{e1}}}^{T_{x_{e1}}} \left|x_{e1}(t)\right|^2 dt}{\int_{-\infty}^{\infty} \left|x(t)\right|^2 dt} = 0.3524,$$

$$\gamma_{\phi_1(t)} = \frac{\int_{-T_{\phi_1}}^{T_{\phi_1}} \left|\phi_1(t)\right|^2 dt}{\int_{-\infty}^{\infty} \left|x(t)\right|^2 dt} = 0.2828.$$

It shows our function has much higher main lobe energy concentration than Gabor's
function's, though it has only a bit larger main lobe, which is a good alternative
for radar system with higher resolution requirement.

---

[1]We noted that although PSWFs decays like $1/t$, they are also uniformly small outside the
interval of concentration and as a result the decay rate is irrelevant. The results obtained from
the example in Fig. 3.4 confirms this observation.
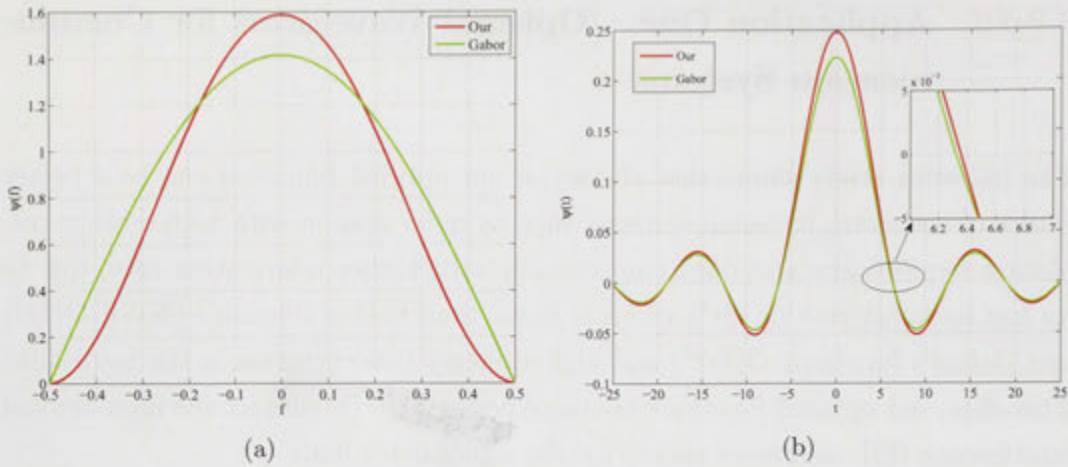
Figure 3.5: Comparison of our optimal function $X_{e1}(f)$ with Gabor's function $\Phi_1(f)$ with $W = 0.5$. (a) Our optimal function $X_{e1}(f)$ and Gabor's function $\Phi_1(f)$ in the frequency domain; (b) Our optimal function $x_{e1}(t)$ and Gabor's function $\phi_1(t)$ in the time-domain. The small panel in (c) shows the main lobes of both functions, where the red (our optimal function) is a bit larger than the green one (Gabor's function).

3.2.13   Application Two – Representation and Finite Dimensional Approximations

The eigenfunctions $\{\psi_i(f)\}$ form a complete, orthonormal basis in $L^2(-W, W)$, so we can use them to represent any band-limited function with maximal bandwidth W, extrapolate a band-limited function known only on the interval $(-T, T)$ and make an approximation in an interval to a band-limited function [22].

Suppose $S(f) \in L^2([-W, W])$ is a band-limited signal. Since $\{\psi_i(f)\}$ is an orthonormal basis in $L^2([-W, W])$, then we can represent

$$S(f) = \sum_{i=1}^{\infty} s_i \psi_i(f), \tag{3.46}$$

where $s_i = \int_{-W}^{W} S(f)\psi_i(f)df$. Based on the above Theorem 3.2.2 and the orthonormality of the basis functions, we can make a further detailed representation

$$S(f) = \sum_{j=1}^{\infty} a_j X_{ej}(f) + \sum_{k=1}^{\infty} b_k X_{ok}(f) \tag{3.47}$$

with

$$a_j = \int_{-W}^{W} S(f)X_{ej}(f)df, \quad b_k = \int_{-W}^{W} S(f)X_{ok}(f)df.$$

Now we consider the dimensionality of the generic expansion (3.46) or (3.47) by a finite number of terms [6, 24],

$$S_N(f) = \sum_{i=1}^{N} s_i \psi_i(f)$$

with squared error

$$\delta_N = \left\| S(f) - S_N(f) \right\|^2 = \sum_{i=N+1}^{\infty} |s_i|^2.$$

where N is the degree of freedom. Here, we take the square norm in $L^2([-W, W])$. It is well known that the dimensionality mainly depends on the basis functions $\{\psi_i(f)\}$, the explicit function $S(f)$ and the truncated error δ_N. As $\{\psi_i(f)\}$ is the optimum basis, it will achieve the best performance comparing with other basis functions. As our basis functions are complete, according to Fourier transform, we can also represent a signal in the time-domain,

$$s_N(t) = \sum_{j=1}^{N} a_j x_{ej}(t) + \sum_{k=1}^{N} b_k x_{ok}(t).$$

Take the rectangle function (also called box function) as an example,

$$G(f) = \begin{cases} 1, & |f| < W; \\ 0, & |f| \geq W. \end{cases}, \quad g(t) = \frac{W}{\pi} \text{sinc}(Wt).$$

Since $G(f)$ is an even function in the frequency interval $[-W, W]$, according to the representation (3.47), we get

$$\begin{aligned} a_j &= \int_{-W}^{W} G(f) A_{ej} \big(\cos(m_j f) + \alpha_j \cosh(m_j f) \big) \, df \\ &= 2 \int_{0}^{W} A_{ej} \big(\cos(m_j f) + \alpha_j \cosh(m_j f) \big) \, df \\ &= 2 A_{ej} \left[\frac{\sin(m_j W)}{m_j} + \alpha_j \frac{\sinh(m_j W)}{m_j} \right] \\ &= \frac{4 A_{ej} \sin(m_j W)}{m_j}. \end{aligned}$$

The last equality is obtained by substituting $\alpha_j = -\cos(m_j W)/\cosh(m_j W)$. We

also have $b_k = 0$ for all k. Therefore,

$$G(f) = \sum_{j=1}^{\infty} a_j X_{ej}(f), \quad G_N(f) = \sum_{j=1}^{N} a_j X_{ej}(f),$$

and the truncated squared error δ_N is

$$\delta_N = \left\| G(f) - G_N(f) \right\|^2 = \sum_{j=N+1}^{\infty} |a_j|^2.$$

Since $A_{ej} = 1/\sqrt{(1 + \alpha_j^2)W}$ and $\alpha_j \longrightarrow 0$ as $j > 4$, we get

$$A_{ej} = 1/\sqrt{(1 + \alpha_j^2)W} < 1/\sqrt{W}$$

and

$$|a_j| = \left| \frac{4A_{ej} \sin(m_j W)}{m_j} \right| \leq \left| \frac{4A_{ej}}{m_j} \right| < \frac{4}{\sqrt{W} m_j},$$

therefore, the truncated squared error is

$$\delta_N = \frac{16}{W} \sum_{j=N+1}^{\infty} \frac{\sin^2(m_j W)}{(1 + \alpha_j^2)m_j^2} < \frac{16}{W} \sum_{j=N+1}^{\infty} \frac{1}{m_j^2}.$$

As we have shown in the above Theorem 3.2.2 and subsection 3.2.6 that the values of $m_j \longrightarrow \infty$ as $j \longrightarrow \infty$. So δ_N can be made as small as desired by making N sufficiently large. Similarly, we have

$$g_N(t) = \sum_{j=1}^{N} a_j x_{ej}(t).$$

Set $W = 0.5$. We depict the function $G_N(f)$ and $g_N(t)$ when $N = 8, 16, 50$ in Fig. 3.6. Obviously, when the number of items N increases, the approximation is better.

3.3   Arbitrary Signal's Concentration with Second and Fourth Moment Weighting in the Frequency Domain

In this section, an arbitrary signal's concentration with moment weighting in the frequency domain is studied [78]. This is motivated by the practical waveform
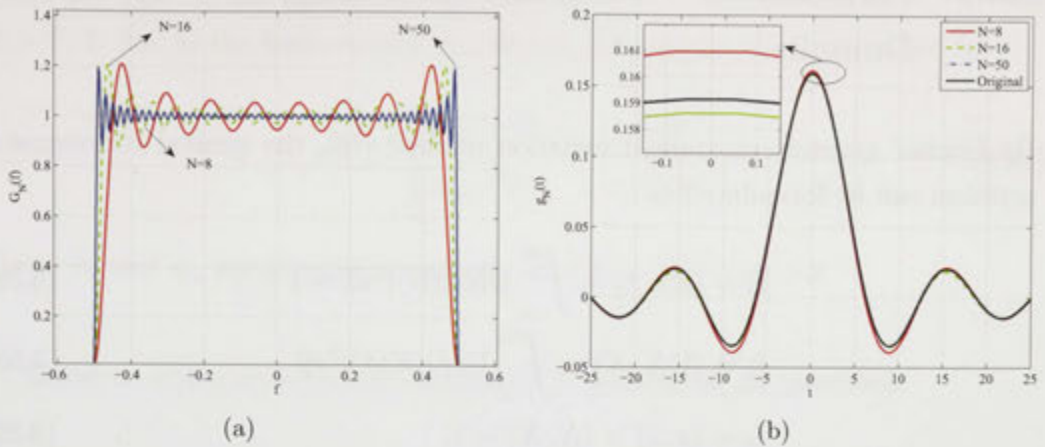
Figure 3.6: Representation of a rectangle function with our optimal basis functions. N is the number of basis functions used, here $N = 8, 16, 50$. (a) Approximated function $G_N(f)$ in the frequency domain, (b) approximated function $g_N(t)$ in the time-domain, the small panel in (b) is to show the difference around the peak value. When $N = 50$, $g_N(t)$ is approaching the original function.

design due to the energy leakage outside of the specified interval. In reality, it is impossible to construct strictly band-limited or strictly time-limited signals.

3.3.1 Problem Statement

Suppose $x(t)$ is a complex-valued, absolutely square-integrable signal on the Hilbert space $L^2(-\infty, \infty)$ and $X(f)$ is its Fourier transformation. The problem being addressed is: given the total energy constraint on $x(t)$ and its partial energy in the time interval $[-T/2, T/2]$ (or in the frequency interval $[-W, W]$), what is the signal waveform that achieves the minimum frequency moment weighting (or the minimum time moment weighting)?

The problem can be divided into two parts: i) time moment weighting; ii) frequency moment weighting. In this section, we mainly discuss the second part and derive the optimal waveforms for second and fourth moment weighting in the frequency domain. For the time moment weighting, results are briefly given.

3.3.2   Formulation – Moment Weighting in the Frequency Domain

By Franks' general constrained variation method [76], the general concentration problem can be formulated as

$$I_1 = \langle wx, x \rangle = \int_{-\infty}^{\infty} w(t)|x(t)|^2 \, dt = 1 - \gamma \tag{3.59a}$$

$$I_2 = \langle VX, X \rangle = \int_{-\infty}^{\infty} V(f)|X(f)|^2 \, df \tag{3.59b}$$

$$I_3 = \langle x, x \rangle = \langle X, X \rangle = 1. \tag{3.59c}$$

Here, $w(t) = 1$ for $|t| \leq T/2$, 0 otherwise; $0 < \gamma < 1$ is the energy outside the interval $[-T/2, T/2]$; $V(f) = f^n$, $n = 0, 2, 4, \cdots$. According to FGCVM [1], it is equivalent to minimizing

$$\mu_1 I_1 + \mu_2 I_2 + I_3, \tag{3.60}$$

where μ_1 and μ_2 are the two Lagrange multipliers. The necessary condition of a stationary solution of (3.59) is [1, (6.95)]

$$\mu_1 w(t)x(t) + \mu_2 \int_{-\infty}^{\infty} v(t - \tau)x(\tau) \, d\tau + x(t) = 0. \tag{3.61}$$

Let $x^{(n)}(t)$ represent the nth derivative of $x(t)$. Substituting the inverse Fourier transform of $f^n X(f)$

$$x^{(n)}(t) \longleftrightarrow (j2\pi)^n f^n X(f), \tag{3.62}$$

and $w(t)$ into (3.61), the final necessary conditions are

$$x^{(n)}(t) = -(j2\pi)^n \frac{\mu_1 + 1}{\mu_2} x(t), \qquad |t| \leq T/2, \tag{3.63a}$$

$$x^{(n)}(t) = -(j2\pi)^n \frac{1}{\mu_2} x(t), \qquad |t| > T/2. \tag{3.63b}$$

3.3.3   Second-moment Weighting for $n = 2$

In this case, substituting $n = 2$ into (3.63), for $|t| \leq T/2$, the general solution is given by

$$x(t) = A_1 \cos \sqrt{(-\lambda_1)}t + A_2 \sin \sqrt{(-\lambda_1)}t, \tag{3.64}$$

where A_1 and A_2 are arbitrary constants, and $\lambda_1 = 4\pi^2(1 + \mu_1)/\mu_2 < 0$. For
$|t| > T/2$, due to the finite energy constraint, the general solution is given by

$$x(t) = \begin{cases} A_3 e^{-\sqrt{\lambda_2}t}, & t > T/2 \\ A_4 e^{\sqrt{\lambda_2}t}, & t < -T/2, \end{cases} \tag{3.65}$$

where A_3 and A_4 are arbitrary constants, and $\lambda_2 = 4(\pi)^2/\mu_2 > 0$.

Based on different boundary conditions, two solutions are provided:

Case a) If $x(t)$ is an even function with boundary conditions: $x(-T/2) = x(T/2) = x_0$,

$$x(t) = \begin{cases} A\cos\sqrt{(-\lambda_1)}t, & |t| \leq T/2 \\ A(\cos\sqrt{(-\lambda_1)}T/2)e^{\sqrt{\lambda_2}(\frac{T}{2}-|t|)}, & |t| > T/2, \end{cases} \tag{3.66}$$

where A, λ_1 and λ_2 satisfy

$$A\cos\left(\sqrt{-\lambda_1}\frac{T}{2}\right) = x_0, \quad \sqrt{\lambda_2} = \frac{x_0^2}{\gamma}, \quad \frac{2(1-\gamma)}{A^2} = T\left[1 + \frac{\sin(\sqrt{-\lambda_1}T)}{\sqrt{-\lambda_1}T}\right].$$

Case b) If $x(t)$ is an odd function with boundary conditions: $x(-T/2) = -x(T/2) = x_0$,

$$x(t) = \begin{cases} A\sin\sqrt{(-\lambda_1)}t, & |t| \leq T/2 \\ A(\sin\sqrt{(-\lambda_1)}T/2)e^{\sqrt{\lambda_2}(\frac{T}{2}-t)}, & t > T/2 \\ -A(\sin\sqrt{(-\lambda_1)}T/2)e^{\sqrt{\lambda_2}(\frac{T}{2}+t)}, & t < -T/2, \end{cases} \tag{3.68}$$

where A, λ_1 and λ_2 satisfy

$$A\sin\left(\sqrt{-\lambda_1}\frac{T}{2}\right) = x_0, \quad \sqrt{\lambda_2} = x_0^2/\gamma, \quad \frac{2(1-\gamma)}{A^2} = T\left[1 - \frac{\sin(\sqrt{-\lambda_1}T)}{\sqrt{-\lambda_1}T}\right].$$

Fig. 3.7 shows the variation of the optimal even function with time for $\gamma = 0, 0.05, 0.15$ and 0.35. In the figure, $T = 3$ and $x_0 = A/2$. Note that $\gamma = 0$ corresponds to the time-limited signal, which is the work of Nuttall [59]. This figure shows that as γ increases, i.e., the energy in the main lobe decreases, the decaying rate of the function $x(t)$ becomes slow and flat.
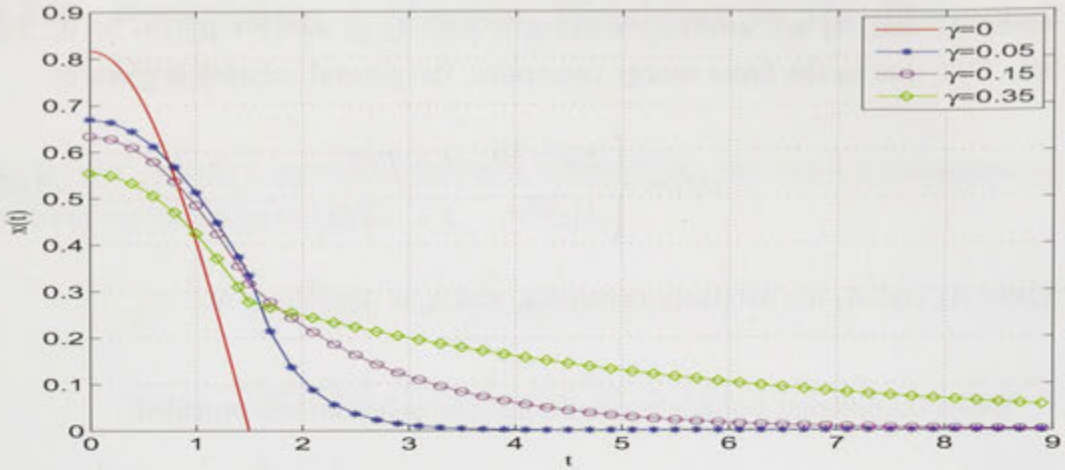
Figure 3.7: The optimal even functions with the second moment weighting vs time for different γ

3.3.4   Fourth-moment Weighting for $n = 4$

In this case, substituting $n = 4$ into (3.63), for $|t| < T/2$, the general solution is given by [76]

$$x(t) = A\cos(mt) + B\sin(mt) + C\cosh(mt) + D\sinh(mt). \qquad (3.70)$$

where A, B, C and D are arbitrary constants, and $m^4 = -(1 + \mu_2)/\mu_1(2\pi)^4 > 0$ with $m > 0$. For $|t| > T/2$, using the stability requirement of the solution, i.e., $x(\pm\infty) = 0$, the general solution can be written by

$$x(t) = \begin{cases} Ee^{-\tau t}, & t > T/2 \\ Fe^{\tau t}, & t < -T/2, \end{cases} \qquad (3.71)$$

where E and F are arbitrary constants, and $\tau^4 = -(2\pi)^4/\mu_2 > 0$ with $\tau > 0$. Similar to the $n = 2$ case considered above, two cases are considered and solutions are provided:

Case a) If $x(t)$ is an even function with boundary conditions: $x(-T/2) = x(T/2) = x_0$ and $x^{(1)}(-T/2) = x^{(1)}(T/2) = 0$, then for $|t| \leq T/2$

$$x(t) = A\big(\cos(mt) + \alpha\cosh(mt)\big), \quad |t| \leq T/2 \qquad (3.72)$$

where A, α and m satisfy

$$\alpha = \sin(mT/2)/\sinh(mT/2)$$

$$A = \frac{x_0}{\cos(mT/2) + \alpha \cosh(mT/2)}$$

$$\frac{1-\gamma}{A^2} = (1+\alpha^2)T/2 + \frac{3\sin(mT)}{2m} + \frac{3\alpha^2 \sinh(mT)}{2m},$$

and for $|t| > T/2$,

$$x(t) = x_0 e^{\frac{x_0^2}{\gamma}(\frac{T}{2}-|t|)}, \quad |t| > T/2. \tag{3.73}$$

Case b) If $x(t)$ is an odd function with boundary conditions: $x(-T/2) = -x(T/2) = x_0$ and $x^{(1)}(-T/2) = x^{(1)}(T/2) = 0$, then for $|t| \leq T/2$

$$x(t) = B\big(\sin(mt) + \beta \sinh(mt)\big), \quad |t| \leq T/2 \tag{3.74}$$

where B, β and m satisfy

$$\beta = -\cos(mT/2)/\cosh(mT/2)$$

$$B = \frac{x_0}{\sin(mT/2) + \beta \sinh(mT/2)}$$

$$\frac{1-\gamma}{B^2} = (1+\beta^2)T/2 - \frac{3\sin(mT)}{2m} + \frac{3\beta^2 \sinh(mT)}{2m},$$

and for $|t| > T/2$,

$$x(t) = \begin{cases} x_0 e^{\frac{x_0^2}{\gamma}(T/2-t)}, & t > T/2; \\ -x_0 e^{\frac{x_0^2}{\gamma}(T/2+t)}, & t < -T/2. \end{cases} \tag{3.75}$$

Fig. 3.8 depicts the the optimal even functions vs time for $\gamma = 0, 0.05, 0.15$ and 0.35. $T = 3$, $x_0 = \frac{A}{2}$. Note that $\gamma = 0$ corresponds to the time-limited signal which is the work of Fain [34]. As γ increases, the energy in the main lobe decreases and the tail decays slowly. It is shown in [34] that for $\gamma = 0$, the optimal function with minimum fourth-moment weighting has larger main lobe than the half sinusoid and the truncated PSWF [22] and a quicker decaying rate of side-lobe than the others. As shown in Fig. 3.9, this situation is similar for $\gamma > 0$. Also according to the inverse Fourier transform, it shows that: 1) the optimal function with the minimum fourth-moment weighting has more energy in the main lobe in comparison with that of the minimum second-moment weighting; 2) it has larger amplitude in the tail and quicker decaying rate due to the same out-of-bandwidth energy.
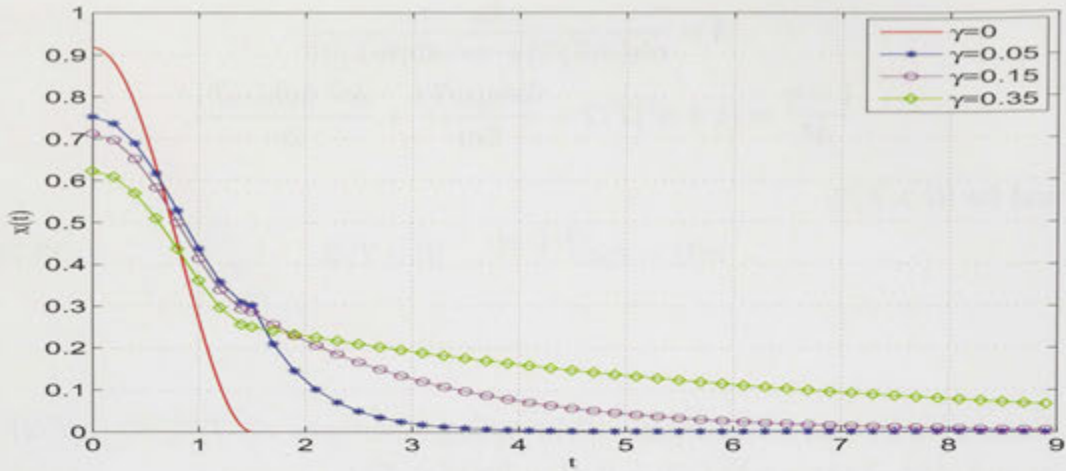
Figure 3.8: The optimal even functions with the fourth moment vs time for different γ
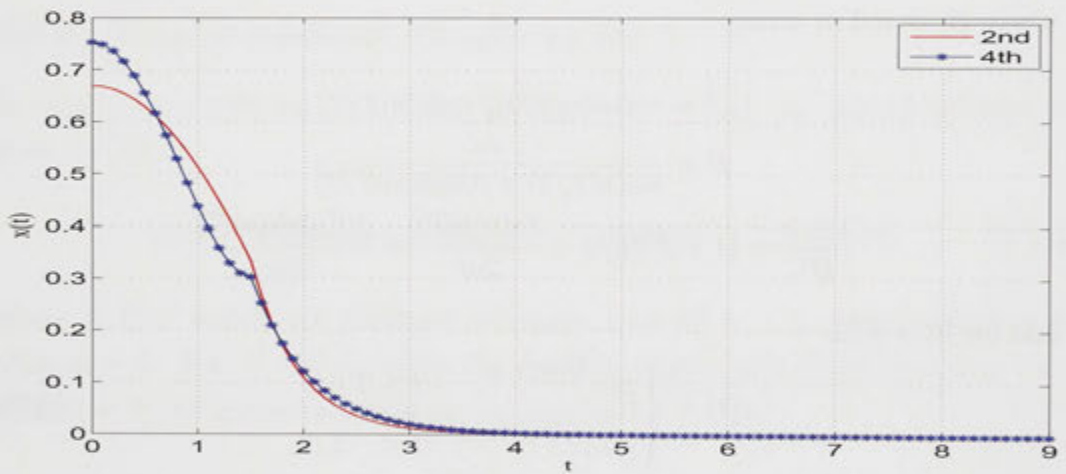
Figure 3.9: The comparison of the 2-nd function and 4-th function when $\gamma = 0.05$

3.3.5 Moment Weighting in the Time Domain

For this case, the problem is to minimize I_1 subject to $I_2 = 1 - \delta$ and $I_3 = 1$ where $V(f) = 1$ if $|f| \leq W$, 0 otherwise; $w(t) = t^n$ and $0 \leq \delta < 1$ is the energy outside of the bandwidth $[-W, W]$. The necessary condition of a stationary solution is now given by [1, (6.96)]

$$\mu_1 \int_{-\infty}^{\infty} W(f - \nu)X(\nu) \, d\nu + \mu_2 V(f)X(f) + X(f) = 0. \tag{3.76}$$

Substituting the Fourier transform of $t^n x(t) \longleftrightarrow \frac{i^n}{(2\pi)^n} \frac{d^n X(f)}{df^n}$ in (3.76) and by similar procedure, this problem can be easily solved.

3.3.6   Summary of Results of Signal Concentration in Time-frequency Domain

Table 3.3 summaries the known and our contributions on the signal concentration in the time-frequency domain. In the table,

$$\chi_{[-T/2,T/2]} = \begin{cases} 1, & |t| \le T/2; \\ 0, & |t| > T/2. \end{cases} \qquad \chi_{[-W,W]} = \begin{cases} 1, & |f| \le W; \\ 0, & |f| > W. \end{cases}$$

3.4   Summary of all the optimal functions for the concentration problem

In this section, all the optimal functions to the different cases of the concentration in the time-frequency domain are summarized in Table 3.4. Here, for convenience, $x(t)$ is a unit energy signal for all the optimal functions. $X(f)$ is the Fourier transform of $x(t)$. Also due to the huge work required to unify all the parameters for the different cases, the original forms are kept. But our work does provide the reader a rough understanding of the optimal functions. So for interested readers, please refer to the original papers or books referred in Table 3.3.

Table 3.4: A summary of optimal functions for signal concentration work in the time-frequency domain.

Problem	Optimal functions
SLEPIAN PROBLEM	
Strictly bandlimited signal for time concentration	Prolate spheroidal Wave functions $\psi_i(t)$
Strictly time-limited signal for frequency concentration	Special solution: $\chi_{[-T/2,T/2]}\psi_i(t)$
General concentration	$p\psi_i(t) + q\chi_{[-T/2,T/2]}\psi_i(t)$
SECOND MOMENT WEIGHTING PROBLEM	
Strictly bandlimited signal for time concentration	$A\cos(\frac{\pi f}{2W}), |f| \le W$
Arbitrary signal with γ ratio	

Table 3.4: *continuoued*

Problem	Optimal functions
energy for time concentration	$x(t) = \begin{cases} A \cos 2\pi \frac{\alpha f}{W}, & \|f\| \le W \\ A e^{2\pi\beta}(\cos 2\pi\alpha)e^{-2\pi\beta\frac{\|f\|}{W}}, & \|f\| > W \end{cases}$
Strictly time-limited signal for bandwidth concentration	Two cases: 1). Even function: $x(t) = A \cos \sqrt{(-\lambda)}t, \quad \|t\| \le T/2,$ 2). Odd function: $x(t) = A \sin \sqrt{(-\lambda)}t, \|t\| \le T/2,$
Arbitrary signal with γ ratio energy for bandwidth concentration	Three cases: 1). Even function: $x(t) = \begin{cases} A \cos \sqrt{(-\lambda)}t, & \|t\| \le T/2 \\ A e^{2\pi\beta}(\cos \sqrt{(-\lambda)}T/2)e^{-4\pi\beta\frac{\|t\|}{T}}, & \|t\| > T/2 \end{cases}$ 2). Odd function: $x(t) = \begin{cases} A \sin \sqrt{(-\lambda)}t, & \|t\| \le T/2 \\ A e^{2\pi\beta}(\sin \sqrt{(-\lambda)}T/2)e^{-4\pi\beta\frac{t}{T}}, & t > T/2 \\ -A e^{2\pi\beta}(\sin \sqrt{(-\lambda)}T/2)e^{4\pi\beta\frac{t}{T}}, & t < -T/2 \end{cases}$
Arbitrary signal (Heisenberg concentration problem)	Gaussian function
FOURTH MOMENT WEIGHTING PROBLEM	
Strictly time-limited signal for bandwidth concentration	$\psi_k(t) = \begin{cases} \sqrt{\frac{2}{T(1+\alpha_k^2)}}(\cos(\phi_k t) + \alpha_k \cosh(\phi_k t)), \\ \sqrt{\frac{2}{T(1+\alpha_k^2)}}(\sin(\phi_k t) + \alpha_k \sinh(\phi_k t)), \end{cases}$
Arbitrary signal with γ ratio ratio energy for bandwidth concentration	Two cases: 1). Even function: $x(t) = \begin{cases} A\big(\cos(mt) + \alpha \cosh(mt)\big), \|t\| \le T/2 \\ x_0 e^{\frac{x_0^2}{\gamma}(T/2-\|t\|)}, & \|t\| > T/2 \end{cases}$ 2). Odd function:

Table 3.4: *continuoued*

Problem	Optimal functions
	$x(t) = \begin{cases} B\big(\sin(mt) + \beta \sinh(mt)\big), |t| \leq T/2 \\ x_0\, e^{\frac{x_0^2}{\gamma}(T/2-f)}, \quad t > T/2 \\ -x_0\, e^{\frac{x_0^2}{\gamma}(T/2+f)}, \quad t < -T/2 \end{cases}$
Strictly bandlimited signal for time concentration	Two cases: 1). Even function: $X(f) = \sqrt{\frac{1}{(1+\alpha^2)W}}\big(\cos(mf) + \alpha \cosh(mf)\big)$ 2). Odd function: $X(f) = \sqrt{\frac{1}{(1-\beta^2)W}}\big(\sin(mf) + \beta \sinh(mf)\big)$
Arbitrary signal with γ ratio energy for time concentration	Two cases: 1). Even function: $X(f) = \begin{cases} A\big(\cos(mf) + \alpha \cosh(mf)\big), |f| \leq W \\ X_0 e^{\frac{X_0^2}{\gamma}(W-|f|)}, \quad |f| > W \end{cases}$ 2). Odd function: $X(f) = \begin{cases} B\big(\sin(mf) + \beta \sinh(mf)\big), |f| \leq W \\ X_0\, e^{\frac{X_0^2}{\gamma}(W-f)}, \quad f > W \\ -X_0\, e^{\frac{X_0^2}{\gamma}(W+f)}, \quad f < -W \end{cases}$

3.5   Summary and Contributions

In this chapter, we reviewed Slepian-Pollak-Landau's signal concentration problem in the time-frequency; then Frank's general constrained variational method (FGCVM) was revisited. Based on FGCVM, some specific contributions are made:

1. Detailed formulation framework to a band-limited signal's energy concentration with minimum kth moment time-duration measure is set up [77].

2. A complete, orthonormal set of optimal band-limited functions with minimum 4th moment time-duration concentration measure, high energy in the main lobe and fast decaying tails are obtained; the prospective applications in radar system and representation of any band-limited signal are provided [76, 77].

3. Detailed formulation framework to an arbitrary signal has γ energy ratio outside of the bandwidth interval $[-W, W]$ and has 2nd and 4th moment

Table 3.3: A summary of signal concentration work in the time-frequency domain.

Problem	Time domain weighting function $w(t)$	Freq. domain weighting function $V(f)$	Ref.
SLEPIAN PROBLEM			
Strictly bandlimited for time concentration	$\chi_{[-T/2,T/2]}(t)$	1	Slepian [22]
Strictly time-limited for frequency concentration	1	$\chi_{[-W,W]}(f)$	Slepian [22]
General concentration	$\chi_{[-T/2,T/2]}(t)$	$\chi_{[-W,W]}(f)$	Landau [23]
SECOND MOMENT WEIGHTING PROBLEM			
Strictly bandlimited for time concentration	t^2	$\chi_{[-W,W]}(f)$	Gabor [61]
Arbitrary signal with γ ratio energy for time concentration	t^2	$\chi_{[-W,W]}(f)$	Franks [1]
Strictly time-limited for bandwidth concentration	$\chi_{[-T/2,T/2]}(t)$	f^2	Nuttall [59]
Arbitrary signal with γ ratio energy for bandwidth concentration	$\chi_{[-T/2,T/2]}(t)$	f^2	**this thesis**
Heisenberg concentration Arbitrary signal	t^2	f^2	Well known
FOURTH MOMENT WEIGHTING PROBLEM			
Strictly bandlimited for time concentration	t^4	$\chi_{[-W,W]}(f)$	**Wei [76]**
Arbitrary signal with γ ratio energy for time concentration	t^4	$\chi_{[-W,W]}(f)$	**this thesis**
Strictly time-limited for bandwidth concentration	$\chi_{[-T/2,T/2]}(t)$	f^4	Fain [34]
Arbitrary signal with γ ratio energy for bandwidth concentration	$\chi_{[-T/2,T/2]}(t)$	f^4	**this thesis**

weighting in the frequency domain are given; the optimal function with 2nd and 4th moment weighting are solved, which can be applied to practical waveform design [78].

Chapter 4

General Concentration Problem On $\mathbb{S}^2$

The objective of this chapter is to solve the general concentration problem for an arbitrary signal on the unit sphere. To solve this problem, we need to develop a class of operators which have an appropriate frequency domain interpretation, while could also play an analogous role how convolution enters in defining quadratic functionals of interest in the time frequency case. It is convenient to introduce the harmonic multiplication in the spectral weighting for this purpose by defining quadratic functions of interest on the unit sphere.

Section 4.2 introduces a matrix representation of a bounded operator on the unit sphere. Section 4.3 defines a harmonic multiplication operation on the unit sphere, where the equivalence of the harmonic multiplication to the isotropic convolution is given. Section 4.4 also derives some useful spherical quadratic functionals. Further, motivated by Franks general constrained variational method (FGCVM) and Landau-Pollak's uncertainty principle in the time-frequency domain, FGCVM is extended on the unit sphere in Section 4.5. Section 4.6 proposes the full concentration problem relating to an arbitrary signal on the unit sphere. Finally, based on the spherical Slepian functions given in Section 4.7 and the spherical Franks framework (FGCVM) in Section 4.5, Section 4.8 solves the spherical general concentration problem.

4.1 Introduction

According to the Fourier transform, a signal cannot have finite support in the time domain and in the frequency domain simultaneously. Similarly, the spherical harmonic transform tells us that a signal cannot strictly confine itself in a region on

the unit sphere, $\mathbb{S}^2$, and in its spherical harmonic coefficients. As a central result in information theory, the simultaneous time-frequency concentration theory and the essential dimensionality of time-frequency signals provide a good criterion in filter window design, such as the Kaiser window [29], and in signal analysis and representation [79]. Whether an analogous simultaneous concentration theorem exists on the unit sphere and how it could be applied in analyzing and representing signals defined on the unit sphere is central in geophysics, cosmology and medical image processing.

Franks general constrained variational method (FGCVM) in Chapter 3 generalizes all properly formulated uncertainty problems by measuring the concentrations related to duration and bandwidth in terms of arbitrarily weighted energy distributions in the time domain and the frequency domain [1]. Analogously, the general constrained variational concentration problems to functions defined on the unit sphere relating to the arbitrary weighting is desirable. In this chapter, we extend FGCVM on the unit sphere, which unifies all possibly previous work on the energy concentration including not only the spatial region, but also the spherical harmonic coefficients, such as Slepian-style simultaneous concentration theorem.

In the past, little study has been made on the Slepian-style simultaneous concentration theorem for signals defined on the unit sphere, except Gillbert and Slepian's work on concentrated Legendre polynomials [80] and Grunbaum et al. on the commutativity of an differential operator with a finite convolution integral operator [81]. Recently, due to its relevance to engineering applications, such as beam-forming and channel modeling in wireless communications [6,79,82], analysis and representation of signals in geodesy [8,33] and cosmic microwave background (CMB) estimation in astrophysics [49], it has received much attention. Albertella et al. extended the Slepian concentration problem on the unit sphere and solved this problem for a spectral-limited signal on the belt and the cap [31]. Miranian solved this problem based on a second-order differential operator found by Grunbaum and his colleagues [81] on the polar cap [32]. And Simons etc. solved this problem for both spectral-limited signal concentration on an arbitrary region on the sphere and spatial-limited signal concentration in a finite spectral interval [33].

It is well known that the uncertainty principle for an arbitrary signal which is neither band-limited nor time-limited that "does the best job of simultaneous time and frequency concentration" has been proved by Landau and Pollak [23]. But whether this relation applies for an arbitrary signal which is neither spatial-limited nor spectral-limited on the unit sphere has not been determined. In this thesis, it is proved that there does exist such a signal and this relation does exist on the

unit sphere. This is the full concentration problem for a general signal on the unit sphere which is solved in this thesis.

4.2   Matrix Representation of Bounded Operators

4.2.1   Infinite Matrix Representation of Operator $\mathcal{A}$

A linear operator $\mathcal{A}$ defined in (2.3) is bounded if there exists a constant M, such that

$$\|\mathcal{A}f\| \leq M\|f\|, \quad \forall f \in L^2(\mathbb{S}^2, ds).$$

Theorem 4.2.2 in [83] claims: A bounded operator on a separable infinite dimensional Hilbert space can be represented by an infinite matrix. It has been pointed out in Chapter 2 that the spherical harmonics $Y_n^m(\boldsymbol{x})$ form a complete orthonormal sequence in $L^2(\mathbb{S}^2, ds)$. Therefore, any bounded linear operator $\mathcal{A}$ defined on $L^2(\mathbb{S}^2, ds)$ admits an infinite matrix representation with respect to $Y_n^m(\boldsymbol{x})$ [38],

$$\mathbf{B}_{nq}^{mp} \triangleq \langle \mathcal{A}Y_q^p, Y_n^m \rangle \tag{4.2}$$

for all $n = 0, 1, 2, \cdots$, $m = -n, \cdots, n$ and $q = 0, 1, 2, \cdots$, $p = -q, \cdots, q$. $\mathbf{B}_{nq}^{mp}$ represents how much of Y_q^p as an input gets projected along the Y_n^m direction of the output under $\mathcal{A}$.

4.2.2   Spatial Kernel $A(\boldsymbol{x}, \boldsymbol{y})$ of Operator $\mathcal{A}$

It is useful to find the kernel of operator $\mathcal{A}$. Since

$$
\begin{aligned}
\mathbf{B}_{nq}^{mp} &= \langle \mathcal{A}Y_q^p, Y_n^m \rangle \\
&= \int_{\mathbb{S}^2} \left(\mathcal{A}Y_q^p \right)(\boldsymbol{x}) \overline{Y_n^m(\boldsymbol{x})} \, ds(\boldsymbol{x}) \\
&= \int_{\mathbb{S}^2} \left(\int_{\mathbb{S}^2} A(\boldsymbol{x}, \boldsymbol{y}) Y_q^p(\boldsymbol{y}) \, ds(\boldsymbol{y}) \right) \overline{Y_n^m(\boldsymbol{x})} \, ds(\boldsymbol{x}),
\end{aligned}
$$

according to the spherical harmonics transform (2.19) and the inverse spherical harmonics transform (2.20), we have

$$\int_{\mathbb{S}^2} A(\boldsymbol{x}, \boldsymbol{y}) Y_q^p(\boldsymbol{y}) \, ds(\boldsymbol{y}) = \sum_{n=0}^{\infty} \sum_{m=-n}^{n} \mathbf{B}_{nq}^{mp} Y_n^m(\boldsymbol{x}). \tag{4.3}$$

So taking the conjugate on both sides, it is easy to obtain

$$\int_{\mathbb{S}^2} \overline{A(\boldsymbol{x}, \boldsymbol{y})}\, \overline{Y_q^p(\boldsymbol{y})}\, ds(\boldsymbol{y}) = \sum_{n=0}^{\infty} \sum_{m=-n}^{n} \overline{\mathbf{B}_{nq}^{mp}}\, \overline{Y_n^m(\boldsymbol{x})}.$$

That is,

$$\overline{A(\boldsymbol{x}, \boldsymbol{y})} = \sum_{q=0}^{\infty} \sum_{p=-q}^{q} \left(\sum_{n=0}^{\infty} \sum_{m=-n}^{n} \overline{\mathbf{B}_{nq}^{mp}}\, \overline{Y_n^m(\boldsymbol{x})} \right) Y_q^p(\boldsymbol{y}).$$

Therefore,

$$A(\boldsymbol{x}, \boldsymbol{y}) = \sum_{q=0}^{\infty} \sum_{p=-q}^{q} \sum_{n=0}^{\infty} \sum_{m=-n}^{n} \mathbf{B}_{nq}^{mp} Y_n^m(\boldsymbol{x}) \overline{Y_q^p(\boldsymbol{y})}. \tag{4.6}$$

This is the kernel of operator $\mathcal{A}$.

4.3   Harmonic Multiplication on $\mathbb{S}^2$

For any $f, h \in L^2(\mathbb{S}^2, ds)$, the harmonic multiplication on $\mathbb{S}^2$ is defined by [38],

$$(h \odot f)(\boldsymbol{x}) \triangleq \sum_{n=0}^{\infty} \sum_{m=-n}^{n} h_n^m f_n^m Y_n^m(\boldsymbol{x}), \tag{4.7}$$

where $h_n^m = \langle h, Y_n^m \rangle$ and $f_n^m = \langle f, Y_n^m \rangle$. $\odot$ is commutative, that is, $h \odot f = f \odot h$. If $h\odot$ is regarded as a bounded linear operator, then according to the matrix representation (4.2), the elements $\mathbf{H}_{nq}^{mp}$ of the infinite matrix are given by

$$\mathbf{H}_{nq}^{mp} = \langle h \odot Y_q^p, Y_n^m \rangle = h_q^p \delta_{nq} \delta_{mp}. \tag{4.8}$$

Introducing a linear operator $\mathcal{K}_h$, we have

$$(\mathcal{K}_h f)(\boldsymbol{x}) = (h \odot f)(\boldsymbol{x}) = \int_{S^2} K_h(\boldsymbol{x}, \boldsymbol{y}) f(\boldsymbol{y})\, ds(\boldsymbol{y}), \tag{4.9}$$

where the kernel function

$$K_h(\boldsymbol{x}, \boldsymbol{y}) = \sum_{n=0}^{\infty} \sum_{m=-n}^{n} h_n^m Y_n^m(\boldsymbol{x}) \overline{Y_n^m(\boldsymbol{y})} \tag{4.10}$$

is a compact, Hilbert-Schmidt kernel.

4.3.1 Isotropic Convolution on $\mathbb{S}^2$

Define $\mathcal{F}^0(\mathbb{S}^2, ds)$, a linear subspace of $L^2(\mathbb{S}^2, ds)$ [38],

$$\mathcal{F}^0(\mathbb{S}^2, ds) = \{z \in L^2(\mathbb{S}^2, ds) : z(\theta, \phi) = z(\theta)\}.$$

Therefore, for any axisymmetric function $z(\theta, \phi) = z(\theta)$ defined on the unit sphere, it can be expressed as

$$z(\theta) = \sum_{n=0}^{\infty} \sum_{m=-n}^{n} z_n^m \delta_{m0} Y_n^m(\theta, \phi)$$

$$= \sum_{n=0}^{\infty} z_n^0 Y_n^0(\theta, \phi) = \sum_{n=0}^{\infty} \sqrt{\frac{2n+1}{4\pi}} z_n^0 P_n(\cos\theta),$$

where $z_n^0 = \langle z, Y_n^0 \rangle$. For any two points $\boldsymbol{x}$ and $\boldsymbol{y}$ on the unit sphere, according to (2.8), we have $\boldsymbol{x} \cdot \boldsymbol{y} = \cos\gamma$. Further, we have

$$z(\gamma) = \sum_{n=0}^{\infty} \sqrt{\frac{2n+1}{4\pi}} z_n^0 P_n(\cos\gamma)$$

$$= \sum_{n=0}^{\infty} \sqrt{\frac{2n+1}{4\pi}} z_n^0 P_n(\boldsymbol{x} \cdot \boldsymbol{y})$$

$$= \sum_{n=0}^{\infty} z_n^0 \sqrt{\frac{4\pi}{2n+1}} \sum_{m=-n}^{n} Y_n^m(\boldsymbol{x}) \overline{Y_n^m(\boldsymbol{y})},$$

where the addition theorem for the spherical harmonics Y_n^m (2.16) in the last equality has been used.

The isotropic convolution for $f \in L^2(\mathbb{S}^2, ds)$ and an axisymmetric filter $z(\theta) \in \mathcal{F}^0(\mathbb{S}^2, ds)$ is defined by [37]

$$(\mathcal{I}_z f)(\boldsymbol{x}) = (z \circledast f)(\boldsymbol{x}) = \int_{\mathbb{S}^2} I_z(\boldsymbol{x} \cdot \boldsymbol{y}) f(\boldsymbol{y}) \, ds(\boldsymbol{y}), \tag{4.12}$$

where the kernel function $I_z(\boldsymbol{x} \cdot \boldsymbol{y})$ is given by

$$I_z(\boldsymbol{x} \cdot \boldsymbol{y}) = z(\gamma) = \sum_{n=0}^{\infty} z_n^0 \sqrt{\frac{4\pi}{2n+1}} \sum_{m=-n}^{n} Y_n^m(\boldsymbol{x}) \overline{Y_n^m(\boldsymbol{y})}. \tag{4.13}$$

Theorem 4.3.1 *Isotropic Convolution Theorem on $\mathbb{S}^2$: The Fourier transform of the isotropic convolution between $f \in L^2(\mathbb{S}^2, ds)$ and $z(\theta) \in \mathcal{F}^0(\mathbb{S}^2, ds)$ is*

given by:

$$(\widehat{z \circledast f})_n^m = \sqrt{\frac{4\pi}{2n+1}} z_n^0 f_n^m, \tag{4.14}$$

where $z_n^0 = \langle z, Y_n^0 \rangle$ and $f_n^m = \langle f, Y_n^m \rangle$.

4.3.2   Equivalence between Harmonic Multiplication and Isotropic Convolution

If the harmonic multiplication operation (4.9) is equivalent to the isotropic convolution (4.12), we must have $K_h(\boldsymbol{x}, \boldsymbol{y}) = I_z(\boldsymbol{x} \cdot \boldsymbol{y})$ [38],

$$
\begin{aligned}
K_h(\boldsymbol{x}, \boldsymbol{y}) &= \sum_{n=0}^{\infty} \sum_{m=-n}^{n} z_n^0 \sqrt{\frac{4\pi}{2n+1}} Y_n^m(\boldsymbol{x}) \overline{Y_n^m(\boldsymbol{y})} \\
&= \sum_{n=0}^{\infty} z_n^0 \sqrt{\frac{4\pi}{2n+1}} \frac{2n+1}{4\pi} P_n(\boldsymbol{x} \cdot \boldsymbol{y}) \\
&= \sum_{n=0}^{\infty} z_n^0 \sqrt{\frac{2n+1}{4\pi}} P_n(\boldsymbol{x} \cdot \boldsymbol{y}),
\end{aligned} \tag{4.15}
$$

or equivalent, $h_n^m = z_n^0 \sqrt{\frac{4\pi}{2n+1}}$ for all m and n. Let $h_n^0 = z_n^0 \sqrt{\frac{4\pi}{2n+1}}$, then we have

$$h(\boldsymbol{x}) = \sum_{n=0}^{\infty} h_n^0 \sum_{m=-n}^{n} Y_n^m(\boldsymbol{x}). \tag{4.16}$$

We denote this relation as $\widetilde{\odot}$,

$$(h \widetilde{\odot} f)(\boldsymbol{x}) = \int_{S^2} K_h(\boldsymbol{x} \cdot \boldsymbol{y}) f(\boldsymbol{y}) \, ds(\boldsymbol{y}) \tag{4.17}$$

with kernel

$$K_h(\boldsymbol{x} \cdot \boldsymbol{y}) = \sum_{n=0}^{\infty} h_n^0 \frac{2n+1}{4\pi} P_n(\boldsymbol{x} \cdot \boldsymbol{y}). \tag{4.18}$$

And the infinite matrix representation (4.8) becomes

$$\mathbf{H}_{nq}^{mp} = h_n^0 \delta_{nq}^{mp}. \tag{4.19}$$

That is, if the convolution is isotropic, then the infinite matrix is a diagonal matrix with elements h_n^0.

4.4   Some Quadratic Functionals On the Spatial-spectral Domain

A function d which is obtained by a bounded linear operator $\mathcal{A}$ mapping to $f \in L^2(\mathbb{S}^2, ds)$ can be expressed by

$$d = \mathcal{A}f = \sum_{n=0}^{\infty} \sum_{m=-n}^{n} d_n^m Y_n^m(\boldsymbol{x}),$$

where $d_n^m = \langle d, Y_n^m \rangle = \langle \mathcal{A}f, Y_n^m \rangle = \sum_{q=0}^{\infty} \sum_{p=-q}^{q} \mathbf{B}_{nq}^{mp} f_q^p$. That is,

$$d = \mathcal{A}f = \sum_{n=0}^{\infty} \sum_{m=-n}^{n} \sum_{q=0}^{\infty} \sum_{p=-q}^{q} \mathbf{B}_{nq}^{mp} f_q^p Y_n^m(\boldsymbol{x}). \tag{4.21}$$

Therefore, analogous to (2.7) in the time-frequency domain, a quadratic functional $I(f)$ under the operator $\mathcal{A}$ can be defined as [84]

$$I(f) = \langle \mathcal{A}f, f \rangle = \left\langle \sum_{n=0}^{\infty} \sum_{m=-n}^{n} \sum_{q=0}^{\infty} \sum_{p=-q}^{q} \mathbf{B}_{nq}^{mp} f_q^p Y_n^m(\boldsymbol{x}), \sum_{n=0}^{\infty} \sum_{m=-n}^{n} f_n^m Y_n^m(\boldsymbol{x}) \right\rangle$$

$$= \sum_{n=0}^{\infty} \sum_{m=-n}^{n} \overline{f_n^m} \sum_{q=0}^{\infty} \sum_{p=-q}^{q} \mathbf{B}_{nq}^{mp} f_q^p. \tag{4.22}$$

According to Parseval theorem, we have

$$I(f) = \langle \mathcal{A}f, f \rangle = \langle \mathbf{B}\hat{\mathbf{f}}, \hat{\mathbf{f}} \rangle, \tag{4.23}$$

where $\mathbf{B}$ is an infinite matrix containing elements $\mathbf{B}_{nq}^{mp}$ and $\hat{\mathbf{f}}$ is the ordered column vector containing all the spherical harmonic coefficients of f.

Analogous to Table 2.1 that shows the quadratic functionals in the time-frequency domain and their corresponding time- and frequency-domain operators, Table 4.1 shows the quadratic functionals and the corresponding operators' kernel $A(\boldsymbol{x}, \boldsymbol{y})$ and the infinite matrix representation $\mathbf{B}_{nq}^{mp}$ on the unit sphere. In this table,

$$\mathbf{B}_{nq}^{mp} = \langle \mathcal{A}Y_q^p, Y_n^m \rangle,$$

$$A(\boldsymbol{x}, \boldsymbol{y}) = \sum_{q=0}^{\infty} \sum_{p=-q}^{q} \sum_{n=0}^{\infty} \sum_{m=-n}^{n} \mathbf{B}_{nq}^{mp} Y_n^m(\boldsymbol{x}) \overline{Y_q^p(\boldsymbol{y})},$$

$\odot$ denotes the general harmonic multiplication and $\widetilde{\odot}$ denotes the special harmonic multiplication which is equivalent to the isotropic convolution.

Table 4.1: Some quadratic functionals and their spatial- and spectral-domain operators' kernels. $\odot$ denotes the harmonic multiplication, $\widetilde{\odot}$ denotes the harmonic multiplication equivalent to the isotropic convolution.

Index	Quadratic Functionals	Kernel $A(\boldsymbol{x}, \boldsymbol{y})$	Infinite matrix representation $\mathbf{B}_{nq}^{mp}$
I	$\langle \mathcal{A}f, f \rangle$	$A(\boldsymbol{x}, \boldsymbol{y})$	$\mathbf{B}_{nq}^{mp}$
I_1	$\langle f, f \rangle$ $= \int_{S^2} \|f(\boldsymbol{x})\|^2 \, ds(\boldsymbol{x})$ $= \sum_{n=0}^{\infty} \sum_{m=-n}^{n} \|f_n^m\|^2$	$\delta(\boldsymbol{x}, \boldsymbol{y})$	δ_{nq}^{mp}
I_2	$\langle wf, f \rangle$ $= \int_{S^2} w(\boldsymbol{x}) \|f(\boldsymbol{x})\|^2 \, ds(\boldsymbol{x})$	$w(\boldsymbol{x}) \delta(\boldsymbol{x}, \boldsymbol{y})$	$\int_{S^2} w(\boldsymbol{x}) Y_q^p(\boldsymbol{x}) \overline{Y_n^m(\boldsymbol{x})} \, ds(\boldsymbol{x})$
I_3	$\langle z \widetilde{\odot} f, f \rangle$ $= \sum_{n=0}^{\infty} \sum_{m=-n}^{n} z_n^0 \|f_n^m\|^2$	$z(\boldsymbol{x} \cdot \boldsymbol{y})$ $= \sum_{n=0}^{\infty} z_n^0 \frac{2n+1}{4\pi} P_n(\boldsymbol{x} \cdot \boldsymbol{y})$	$z_n^0 \delta_{nq}^{mp}$
I_4	$\langle z \odot f, f \rangle$ $= \sum_{n=0}^{\infty} \sum_{m=-n}^{n} z_n^m \|f_n^m\|^2$	$\sum_{n=0}^{\infty} \sum_{m=-n}^{n} z_n^m Y_n^m(\boldsymbol{x}) \overline{Y_n^m(\boldsymbol{y})}$	$z_q^p \delta_{nq}^{mp}$
I_5	$\langle w(z \widetilde{\odot} f), z \widetilde{\odot} f \rangle$	$\sum_{q=0}^{\infty} z_q^0 \frac{2q+1}{4\pi}$ $\times \sum_{n=0}^{\infty} \frac{2n+1}{4\pi} \overline{z_n^0}$ $\times \int_{S^2} w(\boldsymbol{t}) P_q(\boldsymbol{t} \cdot \boldsymbol{y})$ $\times P_n(\boldsymbol{x} \cdot \boldsymbol{t}) \, ds(\boldsymbol{t})$	$\overline{z_n^0} z_q^0 \quad \times$ $\int_{S^2} w(\boldsymbol{x}) Y_q^p(\boldsymbol{x}) \overline{Y_n^m(\boldsymbol{x})} \, ds(\boldsymbol{x})$
I_6	$\langle w(z \odot f), z \odot f \rangle$	$\sum_{q=0}^{\infty} \sum_{p=-q}^{q} z_q^p$ $\times \sum_{n=0}^{\infty} \sum_{m=-n}^{n} \overline{z_n^m}$	$\overline{z_n^m} z_q^p \quad \times$

Table 4.1: *continuoued*

Index	Quadratic Functionals	Kernel $A(\boldsymbol{x}, \boldsymbol{y})$	Infinite matrix representation B_{nq}^{mp}
		$\times \int_{S^2} w(\boldsymbol{t}) Y_q^p(\boldsymbol{t}) \overline{Y_n^m(\boldsymbol{t})}\, ds(\boldsymbol{t})$ $\times Y_n^m(\boldsymbol{x}) \overline{Y_q^p(\boldsymbol{y})}$	$\int_{S^2} w(\boldsymbol{x}) Y_q^p(\boldsymbol{x}) \overline{Y_n^m(\boldsymbol{x})}\, ds(\boldsymbol{x})$
I_7	$\langle v \widetilde{\odot}(z \widetilde{\odot} f), z \widetilde{\odot} f \rangle$ $= \sum_{n=0}^{\infty} \sum_{m=-n}^{n}$ $v_n^0 |z_n^0|^2 |f_n^m|^2$	$\sum_{n=0}^{\infty} \sum_{m=-n}^{n} v_n^0 |z_n^0|^2$ $\times Y_n^m(\boldsymbol{x}) \overline{Y_n^m(\boldsymbol{y})}$	$v_n^0 |z_n^0|^2 \delta_{nq}^{mp}$
I_8	$\langle v \odot (z \odot f), z \odot f \rangle$ $= \sum_{n=0}^{\infty} \sum_{m=-n}^{n} v_n^m |z_n^m|^2 |f_n^m|^2$	$\sum_{n=0}^{\infty} \sum_{m=-n}^{n} v_n^m |z_n^m|^2$ $\times Y_n^m(\boldsymbol{x}) \overline{Y_n^m(\boldsymbol{y})}$	$v_q^p \overline{z_n^m} z_q^p \delta_{nq}^{mp}$
I_9	$\langle v \widetilde{\odot}(z \odot f), z \odot f \rangle$ $= \sum_{n=0}^{\infty} \sum_{m=-n}^{n} v_n^0 |z_n^m|^2 |f_n^m|^2$	$\sum_{n=0}^{\infty} \sum_{m=-n}^{n} v_n^0 |z_n^m|^2$ $\times Y_n^m(\boldsymbol{x}) \overline{Y_n^m(\boldsymbol{y})}$	$v_q^0 \overline{z_n^m} z_q^p \delta_{nq}^{mp}$
I_{10}	$\langle v \odot (z \widetilde{\odot} f), z \widetilde{\odot} f \rangle$ $= \sum_{n=0}^{\infty} \sum_{m=-n}^{n} v_n^m |z_n^0|^2 |f_n^m|^2$	$\sum_{n=0}^{\infty} \sum_{m=-n}^{n} v_n^m |z_n^0|^2$ $\times Y_n^m(\boldsymbol{x}) \overline{Y_n^m(\boldsymbol{y})}$	$v_q^p \overline{z_n^0} z_q^0 \delta_{nq}^{mp}$
I_{11}	$\langle f, z \rangle \overline{\langle f, h \rangle}$ $= \langle \hat{\mathbf{f}}, \hat{\mathbf{z}} \rangle \overline{\langle \hat{\mathbf{f}}, \hat{\mathbf{h}} \rangle}$	$\sum_{n=0}^{\infty} \sum_{m=-n}^{n} z_n^m \overline{h_n^m}$ $\times Y_n^m(\boldsymbol{x}) \overline{Y_n^m(\boldsymbol{y})}$	$\sum_{n=0}^{\infty} \sum_{m=-n}^{n} z_n^m \overline{h_n^m} \delta_{nq}^{mp}$

4.5 Franks' General Variational Framework on $\mathbb{S}^2$

In this section, a generalization of the uncertainty problem is formulated by measuring the energy concentrations relevant to the spatial region and the spectral angular degree in terms of arbitrarily weighted energy distributions in the spatial and the spectral domains on the sphere. Then Franks' general variational framework [1] in the time-frequency domain is extended to the unit sphere. Two necessary conditions for the general variational problem are obtained both in the spatial domain and in the spectral domain.

4.5.1 The General Variational Problem On $\mathbb{S}^2$

The general variational problem on the sphere is stated: suppose $w(\boldsymbol{x})$ is an arbitrary real square-integrable function on the unit sphere and $w(\boldsymbol{x}) \geq 0$, $v(\boldsymbol{x})$ is an arbitrary square-integrable function on the unit sphere with all the spherical harmonic coefficients v_n^m real and $v_n^m \geq 0$ where $v_n^m = \int_{\mathbb{S}^2} v(\boldsymbol{x}) \overline{Y_n^m(\boldsymbol{x})} \, ds(\boldsymbol{x})$. For any $f \in L^2(\mathbb{S}^2, ds)$, if its spatially weighted energy by $w(\boldsymbol{x})$ is fixed, to maximize (minimize) the spectrally weighted energy by v_n^m, what is the optimal function of $f(\boldsymbol{x})$? Or if the spectrally weighted energy by v_n^m is fixed, to maximize (minimize) the spectrally weighted energy by $w(\boldsymbol{x})$, what is the optimal function of $f(\boldsymbol{x})$? In this section, we solve this problem by Franks' spherical framework [1] which is extended from the time-frequency domain to the spatial-spectral domain on the unit sphere.

4.5.2 Formulation

For the purpose of normalization, the function $f(\boldsymbol{x})$ is constrained to be unit energy. Three quadratic functionals on the unit sphere are defined,

$$I_1 \triangleq \langle \mathcal{A}_1 f, f \rangle = \langle wf, f \rangle = \int_{\mathbb{S}^2} w(\boldsymbol{x}) |f(\boldsymbol{x})|^2 \, ds(\boldsymbol{x}) \tag{4.24a}$$

$$I_2 \triangleq \langle \mathcal{A}_2 f, f \rangle = \langle v \odot f, f \rangle$$

$$= \left\langle \sum_{n=0}^{\infty} \sum_{m=-n}^{n} v_n^m f_n^m Y_n^m(\boldsymbol{x}), \sum_{n=0}^{\infty} \sum_{m=-n}^{n} f_n^m Y_n^m(\boldsymbol{x}) \right\rangle = \sum_{n=0}^{\infty} \sum_{m=-n}^{n} v_n^m |f_n^m|^2 \tag{4.24b}$$

$$I_3 \triangleq \langle f, f \rangle = \left\langle \hat{\mathbf{f}}, \hat{\mathbf{f}} \right\rangle = \int_{\mathbb{S}^2} |f(\boldsymbol{x})|^2 \, ds(\boldsymbol{x}) = \sum_{n=0}^{\infty} \sum_{m=-n}^{n} |f_n^m|^2 = 1. \tag{4.24c}$$

In the above equations (4.24a) – (4.24c), I_1 represents an arbitrary weighted measure of energy in the spatial domain; I_2 represents an arbitrary weighted measure

of energy in the spectral domain; I_3 represents the total energy of $f(\boldsymbol{x})$. $\mathcal{A}_1$ is the spatial multiplication operator which is defined as

$$\mathcal{A}_1 f \triangleq w(\boldsymbol{x}) f(\boldsymbol{x}). \tag{4.25}$$

and $\mathcal{A}_2$ is the harmonic multiplication operator which is defined as [38]

$$\mathcal{A}_2 f \triangleq (v \odot f)(\boldsymbol{x}) \triangleq \sum_{n=0}^{\infty} \sum_{m=-n}^{n} v_n^m f_n^m Y_n^m(\boldsymbol{x}). \tag{4.26}$$

The general variational problem on the sphere being addressed is to find a function which maximizes I_1 (I_2) under the constraints I_2 (I_1) and I_3. According to the analogous property in the time-frequency domain [1], on the unit sphere, extremizing I_1 (I_2) subject to I_2 (I_1) and I_3 is also equivalent to extremizing

$$G \triangleq \mu_1 I_1 + \mu_2 I_2 + I_3, \tag{4.27}$$

where μ_1 and μ_2 are two Lagrange multipliers. This is the objective function. We attempt to find the necessary condition for a stationary solution to (4.27) both in the spatial domain and in the spectral domain on the sphere.

4.5.3 Necessary Conditions

Generally, finding a stationary function f that extremizes a quadratic functional $I(f)$, is usually done in two steps: 1) Obtain the directional derivative $D_u I(f)$ at a point f along any arbitrary function u; 2). Solve the equation $D_u I(f) = 0$ to get the necessary condition. In relation to our problem, it is necessary to find the directional derivative $D_u G(f)$ and then solve $D_u G(f) = 0$.

Directional Derivative of a Quadratic Functional

For a quadratic functional $I(f) = \langle \mathcal{A}f, f \rangle$ where $\mathcal{A}$ is a linear operator, the directional derivative of at a point f along u, where $u(\boldsymbol{x}) \in L^2(\mathbb{S}^2, ds)$ is an arbitrary unit vector (function) on the sphere, is defined as

$$D_u I(f) \triangleq \langle \mathcal{A}u, f \rangle + \langle \mathcal{A}f, u \rangle = \langle \mathcal{A}f, u \rangle + \langle u, \mathcal{A}'f \rangle, \tag{4.28}$$

where $\mathcal{A}'$ is the adjoint operator of $\mathcal{A}$. If $\mathcal{A}$ is also a self-adjoint operator, i.e., $\mathcal{A} = \mathcal{A}'$, then

$$D_u I(f) = \langle \mathcal{A}f, u \rangle + \langle u, \mathcal{A}f \rangle = 2\Re\{\langle \mathcal{A}f, u \rangle\}, \tag{4.29}$$

where $\Re\{\cdot\}$ denotes the real part of $\langle \mathcal{A}f, u \rangle$.

Two Self-adjoint Operators

It is necessary to prove that both $\mathcal{A}_1$ and $\mathcal{A}_2$ are self-adjoint operators. For any $f, g \in L^2(\mathbb{S}^2, ds)$, according to the definition (4.25) and the adjoint operator property, we have

$$\langle \mathcal{A}_1 f, g \rangle = \langle wf, g \rangle = \int_{\mathbb{S}^2} w(\boldsymbol{x}) f(\boldsymbol{x}) \overline{g(\boldsymbol{x})} \, ds(\boldsymbol{x}),$$

and

$$\langle f, \mathcal{A}_1 g \rangle = \langle f, wg \rangle = \int_{\mathbb{S}^2} f(\boldsymbol{x}) \overline{w(\boldsymbol{x}) g(\boldsymbol{x})} \, ds(\boldsymbol{x}) = \int_{\mathbb{S}^2} f(\boldsymbol{x}) w(\boldsymbol{x}) \overline{g(\boldsymbol{x})} \, ds(\boldsymbol{x}).$$

In the above, $w(\boldsymbol{x})$ is used as a real-valued function. Therefore,

$$\langle \mathcal{A}_1 f, g \rangle = \langle f, \mathcal{A}_1' g \rangle = \langle f, \mathcal{A}_1 g \rangle. \tag{4.30}$$

So $\mathcal{A}_1$ is a self-adjoint operator.

Similarly, using the definition (4.26), the orthonormality (2.14) of the spherical harmonics $Y_n^m(\boldsymbol{x})$ and real value of v_n^m, we have

$$\langle \mathcal{A}_2 f, g \rangle = \langle v \odot f, g \rangle$$
$$= \left\langle \sum_{n=0}^{\infty} \sum_{m=-n}^{n} v_n^m f_n^m Y_n^m(\boldsymbol{x}), \sum_{n=0}^{\infty} \sum_{m=-n}^{n} \overline{g_n^m} Y_n^m(\boldsymbol{x}) \right\rangle = \sum_{n=0}^{\infty} \sum_{m=-n}^{n} v_n^m f_n^m \overline{g_n^m},$$

and

$$\langle f, \mathcal{A}_2 g \rangle = \langle f, v \odot g \rangle = \left\langle \sum_{n=0}^{\infty} \sum_{m=-n}^{n} f_n^m Y_n^m(\boldsymbol{x}), \sum_{n=0}^{\infty} \sum_{m=-n}^{n} v_n^m g_n^m Y_n^m(\boldsymbol{x}) \right\rangle$$
$$= \sum_{n=0}^{\infty} \sum_{m=-n}^{n} f_n^m \overline{v_n^m g_n^m} = \sum_{n=0}^{\infty} \sum_{m=-n}^{n} v_n^m f_n^m \overline{g_n^m}$$

therefore,

$$\langle \mathcal{A}_2 f, g \rangle = \langle f, \mathcal{A}_2' g \rangle = \langle f, \mathcal{A}_2 g \rangle. \tag{4.31}$$

So $\mathcal{A}_2$ is also a self-adjoint operator.

Directional directive of an Objective Function

The directional derivative of the objective function G at point f along u is

$$D_u G(f) = D_u \left[\mu_1 I_1 + \mu_2 I_2 + I_3 \right] = \mu_1 D_u I_1 + \mu_2 D_u I_2 + D_u I_3.$$

We must now solve

$$D_u G(f) = 0. \tag{4.32}$$

Since both $\mathcal{A}_1$ and $\mathcal{A}_2$ are self-adjoint, according to (4.29), we have

$$D_u I_1(f) = 2\Re\{\langle wf, u \rangle\}, \tag{4.33}$$

$$D_u I_2(f) = 2\Re\{\langle v \odot f, u \rangle\}. \tag{4.34}$$

For the third quadratic functional I_3, it is easy to obtain

$$D_u I_3(f) = \langle u, f \rangle + \langle f, u \rangle = 2\Re\{\langle f, u \rangle\}. \tag{4.35}$$

Substituting (4.33), (4.34) and (4.35) in (4.32), we obtain

$$D_u G(f) = 2\Re\{\mu_1 \langle wf, u \rangle\} + 2\Re\{\mu_2 \langle v \odot f, u \rangle\} + 2\Re\{\langle f, u \rangle\} = 0,$$

i.e.,

$$\Re\{\langle \mu_1 wf + \mu_2 v \odot f + f, u \rangle\} = 0. \tag{4.36}$$

An angle $\theta(f_1, f_2)$ between functions $f_1, f_2 \in L^2(\mathbb{S}^2, ds)$ is defined by [23]

$$\theta(f_1, f_2) = \cos^{-1} \frac{\Re\{\langle f_1, f_2 \rangle\}}{\|f_1\| \cdot \|f_2\|}. \tag{4.37}$$

Then, $\Re\{\langle f_1, f_2 \rangle\} = \|f_1\| \cdot \|f_2\| \cdot \cos \theta(f_1, f_2) = 0$ is obtained under $\|f_2\| = 1$ if and only if $\|f_1\| = 0$ (i.e., $f_1 = 0$, according to the norm definition) or f_1 is orthogonal to f_2.

Therefore, to ensure (4.36), since u is an arbitrary function with $\|u\| = 1$ on the unit sphere, the only posibility is that

$$\mu_1 wf + \mu_2 v \odot f + f = 0. \tag{4.38}$$

Therefore, (4.38) is the general necessary condition for the stationary solution of (4.32) in the spatial domain.

Note that

$$
\begin{aligned}
v \odot f &= \sum_{n=0}^{\infty} \sum_{m=-n}^{n} v_n^m f_n^m Y_n^m(\boldsymbol{x}) \\
&= \sum_{n=0}^{\infty} \sum_{m=-n}^{n} v_n^m \left(\int_{\mathbb{S}^2} f(\boldsymbol{y}) \overline{Y_n^m(\boldsymbol{y})} \, ds(\boldsymbol{y}) \right) Y_n^m(\boldsymbol{x}) \\
&= \int_{\mathbb{S}^2} \left(\sum_{n=0}^{\infty} \sum_{m=-n}^{n} v_n^m Y_n^m(\boldsymbol{x}) \overline{Y_n^m(\boldsymbol{y})} \right) f(\boldsymbol{y}) \, ds(\boldsymbol{y}). \tag{4.39}
\end{aligned}
$$

In the above, (2.19) and the interchangeability of integration and summation are used. Therefore, substituting (4.39) in (4.38), the general spatial necessary condition for the stationary solution of (4.32) in the spatial domain can also be expressed in the form of an eigenvalue equation as,

$$
(-\mu_2) \int_{\mathbb{S}^2} \left(\sum_{n=0}^{\infty} \sum_{m=-n}^{n} v_n^m Y_n^m(\boldsymbol{x}) \overline{Y_n^m(\boldsymbol{y})} \right) f(\boldsymbol{y}) \, ds(\boldsymbol{y}) + (-\mu_1) w(\boldsymbol{x}) f(\boldsymbol{x}) = f(\boldsymbol{x}). \tag{4.40}
$$

This is a Fredholm integral equation of the second kind.

Now taking the inverse spherical harmonic transform of (4.38), the general necessary condition for the stationary solution of (4.32) in the spectrum domain can be written as

$$
\mu_1 \left(w(\boldsymbol{x}) f(\boldsymbol{x}) \right)_n^m + \mu_2 v_n^m f_n^m + f_n^m = 0. \tag{4.41}
$$

Using the spherical harmonic transform (2.20), we can write

$$
\begin{aligned}
\left(w(\boldsymbol{x}) f(\boldsymbol{x}) \right)_n^m &= \int_{\mathbb{S}^2} w(\boldsymbol{x}) f(\boldsymbol{x}) \overline{Y_n^m(\boldsymbol{x})} \, ds(\boldsymbol{x}) \\
&= \sum_{s=0}^{\infty} \sum_{t=-s}^{s} f_s^t \int_{\mathbb{S}^2} w(\boldsymbol{x}) Y_s^t(\boldsymbol{x}) \overline{Y_n^m(\boldsymbol{x})} \, ds(\boldsymbol{x}) \\
&= \sum_{s=0}^{\infty} \sum_{t=-s}^{s} f_s^t \sum_{q=0}^{\infty} \sum_{p=-q}^{q} w_q^p \int_{\mathbb{S}^2} Y_q^p(\boldsymbol{x}) Y_s^t(\boldsymbol{x}) \overline{Y_n^m(\boldsymbol{x})} \, ds(\boldsymbol{x}) \\
&= \sum_{s=0}^{\infty} \sum_{t=-s}^{s} f_s^t \sum_{q=0}^{\infty} \sum_{p=-q}^{q} w_q^p D_{qsn}^{ptm}, \tag{4.42}
\end{aligned}
$$

where D_{qsn}^{ptm} are given by

$$
D_{qsn}^{ptm} \triangleq \int_{\mathbb{S}^2} Y_q^p(\boldsymbol{x}) Y_s^t(\boldsymbol{x}) \overline{Y_n^m(\boldsymbol{x})} \, ds(\boldsymbol{x}). \tag{4.43}
$$

The general necessary condition for the stationary solution of equation (4.27)

in the spectrum domain is given by

$$\mu_1 \sum_{s=0}^{\infty} \sum_{t=-s}^{s} f_s^t \sum_{q=0}^{\infty} \sum_{p=-q}^{q} w_q^p \overline{D_{qsn}^{ptm}} + \mu_2 v_n^m f_n^m + f_n^m = 0, \tag{4.44}$$

or for a given weighting function $w(\boldsymbol{x})$,

$$\mu_1 \sum_{s=0}^{\infty} \sum_{t=-s}^{s} f_s^t \int_{\mathbb{S}^2} w(\boldsymbol{x}) \overline{Y_s^t(\boldsymbol{x}) Y_n^m(\boldsymbol{x})} \, ds(\boldsymbol{x}) + \mu_2 v_n^m f_n^m + f_n^m = 0. \tag{4.45}$$

Finally, summing over all n from 0 to ∞ and $-n \le m \le n$ for the equation (4.45), we have

$$\mu_1 \sum_{n=0}^{\infty} \sum_{m=-n}^{n} \sum_{s=0}^{\infty} \sum_{t=-s}^{s} f_s^t \int_{\mathbb{S}^2} w(\boldsymbol{x}) \overline{Y_s^t(\boldsymbol{x}) Y_n^m(\boldsymbol{x})} \, ds(\boldsymbol{x})$$

$$+ \mu_2 \sum_{n=0}^{\infty} \sum_{m=-n}^{n} v_n^m f_n^m + \sum_{n=0}^{\infty} \sum_{m=-n}^{n} f_n^m = 0. \tag{4.46}$$

Taking $\mathbf{K}$ as a matrix containing all the elements $\int_{\mathbb{S}^2} w(\boldsymbol{x}) \overline{Y_s^t(\boldsymbol{x}) Y_n^m(\boldsymbol{x})} \, ds(\boldsymbol{x})$ and also introducing two column vectors $\hat{\mathbf{h}}$ whose individual elements are defined as

$$h_n^m \triangleq v_n^m f_n^m$$

and $\hat{\mathbf{f}}$ defined in (2.21), the spectral necessary condition for (4.32) can be expressed in the matrix form

$$\mu_1 \mathbf{K} \hat{\mathbf{f}} + \mu_2 \hat{\mathbf{h}} + \hat{\mathbf{f}} = 0. \tag{4.47}$$

4.6 General Concentration Problem on $\mathbb{S}^2$

In the spatial-spectral domain, the issue of signal concentration for signals defined on the unit sphere has not been thoroughly studied. At present, only the special cases, i.e., the spectral concentration problem for a spatial-limited signal and the spatial concentration problem for a spectral-limited signal, have been solved [31–33, 85]. But for an arbitrary signal which is neither spatial-limited nor spectral-limited on the unit sphere, the concentration problem is still open. In this chapter, this problem is solved which fills the gap based on the spherical Franks' framework [84].

For the purpose of normalization, the function $f(\boldsymbol{x})$ is constrained to be of unit energy. The general concentration problem under consideration can be stated as follows: Suppose f is any square-integrable function defined on the unit sphere

with its total energy $\|f\| = 1$. Suppose $\alpha^2 = \|\mathcal{D}_\Gamma f\|^2$ is the energy of f in the spatial region $\Gamma \subset \mathbb{S}^2$, $\beta^2 = \|\mathcal{B}_N f\|^2$ is the energy of f in the spectral interval $[0, N]$ where N is a positive integer, and $0 \le \alpha, \beta \le 1$. What is the optimal signal waveform of $f(\boldsymbol{x})$ that simultaneously achieves maximum energy α^2 concentrated both in the spatial domain and maximum energy β^2 concentrated in the spectral domain? (The definitions of $\mathcal{D}_\Gamma f$ and $\mathcal{B}_N f$ are given below.)

Here, due to the topologically compact property for a sphere $\mathbb{S}^2$, we do not consider the situation: $\alpha = \beta = 0$. Cases $\alpha = 1$ and $\beta = 1$ have been widely studied [31–33], so they are briefly reviewed and some important results are summarized, such as the relation of the eigenfunctions and eigenvalues and some geometrical properties of the eigenfunctions for the $\alpha = 1$ and $\beta = 1$ cases are deduced. More focus of the study is on the $0 < \alpha, \beta < 1$ case.

4.7 Special Signals Concentration on $\mathbb{S}^2$

The special concentration problem on the unit sphere has been solved by [31–33]. In this section, we review them and summarize some results.

4.7.1 Spatial Concentration of a Spectral-limited Signal ($\beta = 1$, $0 < \alpha \le \lambda_0^{(N)}$)

$f(\boldsymbol{x}) \in L^2(\mathbb{S}^2, ds)$ is assumed to be a spectral-limited signal with maximum spectral degree N, i.e.,

$$f(\boldsymbol{x}) \triangleq \sum_{n=0}^{N} \sum_{m=-n}^{n} f_n^m Y_n^m(\boldsymbol{x}). \tag{4.48}$$

So $\mathcal{B}_N f = f$, where $\mathcal{B}_N$ is the mode limiting operator defined in (2.38), and $f \in \mathfrak{B}_N(\mathbb{S}^2, ds)$ where $\mathfrak{B}_N(\mathbb{S}^2, ds)$ is the complete subspace containing all spatial-limited functions on the region $\Gamma \subset \mathbb{S}^2$. To achieve the maximum energy concentration in the spatial region $\Gamma \in \mathbb{S}^2$, we may equivalently maximize

$$\lambda^{(N)} \triangleq \frac{\langle \mathcal{D}_\Gamma f, f \rangle}{\langle f, f \rangle} = \frac{\int_\Gamma |f(\boldsymbol{x})|^2 \, ds(\boldsymbol{x})}{\int_{\mathbb{S}^2} |f(\boldsymbol{x})|^2 \, ds(\boldsymbol{x})}. \tag{4.49}$$

Substituting (4.48) into (4.49) and interchanging the summation and integration, we get

$$\lambda^{(N)} = \frac{\sum_{n=0}^{N} \sum_{m=-n}^{n} \overline{f_n^m} \sum_{n'=0}^{N} \sum_{m'=-n'}^{n'} D_{nn'}^{mm'} f_{n'}^{m'}}{\sum_{n=0}^{N} \sum_{m=-n}^{n} |f_n^m|^2}, \tag{4.50}$$

where f_n^m are the spherical harmonic coefficients and

$$D_{nn'}^{mm'} = \int_\Gamma \overline{Y_n^m(\boldsymbol{x})} Y_{n'}^{m'}(\boldsymbol{x})\, ds(\boldsymbol{x}).$$

It has been showed that solving (4.49) or (4.50), is equivalent to solving an algebraic eigenvalue equation [33]

$$\mathbf{D}_N \hat{\mathbf{f}} = \lambda^{(N)} \hat{\mathbf{f}}, \tag{4.52}$$

where $\mathbf{D}_N$ is a $(N+1)^2 \times (N+1)^2$ matrix

$$\mathbf{D}_N = \begin{pmatrix} D_{00}^{00} & \cdots & D_{0N}^{0N} \\ \vdots & & \vdots \\ D_{N0}^{N0} & \cdots & D_{NN}^{NN} \end{pmatrix} \tag{4.53}$$

with elements $D_{nn'}^{mm'}$, and $\hat{\mathbf{f}}$ is the column vector with the elements f_n^m. Solving (4.52), the eigenvalues $\{\lambda_i^{(N)}\}$ and the corresponding eigenvectors $\{\hat{\mathbf{f}}_i^{(N)}\}$, $i = 0, 1, \cdots, (N+1)^2 - 1$, are obtained. Using the spherical harmonics transform (2.19),

$$f_i^{(N)}(\boldsymbol{x}) = \sum_{n=0}^{N} \sum_{m=-n}^{n} (f_n^m)_i^{(N)} Y_n^m(\boldsymbol{x}), \tag{4.54}$$

the associated eigenfunctions $\{f_i^{(N)}(\boldsymbol{x})\}$ are achieved. We have also applied a normalization to the eigenvectors and eigenfunctions. The following theorem summarises some properties to the eigenvalues and eigenfunctions. Though the detailed proof is not provided, a key reference to understand the theorem based on functional analysis is given.

Theorem 4.7.1 *For a spectral-limited signal $f(\boldsymbol{x})$ with maximum spectral degree N, the optimal normalized vector $\hat{\boldsymbol{f}}$ composed of the spherical harmonic coefficients of the signal having the maximum energy in a spatial region $\Gamma \subset \mathbb{S}^2$ satisfies (4.52) and has the following properties:*

1. *The eigenvalues $\{\lambda_i^{(N)}\}$, $i = 0, 1, \cdots, (N+1)^2 - 1$, are the maximum energy concentration in the region Γ; $\{\lambda_i^{(N)}\}$ are real and can be ordered: $1 > \lambda_0^{(N)} \geq \lambda_1^{(N)} \geq \lambda_2^{(N)} \ldots \geq \lambda_{(N+1)^2-1}^{(N)} > 0$;*

2. *The ordered associated eigenfunctions $\{f_i^{(N)}(\boldsymbol{x})\}$ obtained by (4.54) have the double orthogonal property:*

$$\int_{\mathbb{S}^2} f_i^{(N)}(\boldsymbol{x}) f_j^{(N)}(\boldsymbol{x})\, ds(\boldsymbol{y}) = \delta_{ij}, \quad \int_\Gamma f_i^{(N)}(\boldsymbol{x}) f_j^{(N)}(\boldsymbol{x})\, ds(\boldsymbol{y}) = \lambda_i^{(N)} \delta_{ij}$$

for any $i, j = 0, 1, \cdots, (N+1)^2 - 1$.

3. *The ordered associated eigenfunctions $\{f_i^{(N)}(\boldsymbol{x})\}$ consist of a complete, orthonormal basis for the subspace $\mathfrak{B}_N(\mathbb{S}^2, ds)$;*

4. *The ordered eigenvalues $\{\lambda_i^{(N)}\}$ are the maximum energy concentration ratio in the spatial region Γ; in particular, $\lambda_0^{(N)}$ is the largest eigenvalue, which is also the largest concentration ratio for (4.49); and the corresponding spectral-limited $f_0^{(N)}(\boldsymbol{x})$ is the largest energy concentrated function in the region Γ.*

Proof

Please note that we only provide the key points to the proof. Detailed information refers to [33]. The matrix $\mathbf{D}_N$ (4.53) is a compact and Hermitian (self-adjoint) matrix. According to the finite-dimensional Spectral Theorem [83], $\mathfrak{B}_N(\mathbb{S}^2, ds)$ has an orthonormal basis consisting of the eigenvectors of $\mathbf{D}_N$; each eigenvalue is real.

The self-adjoint property of $\mathbf{D}_N$ guarantees the eigenvectors $\{\hat{\mathbf{f}}_i^{(N)}\}$ and the associated eigenfunctions $\{f_i^{(N)}(\boldsymbol{x})\}$ are orthogonal.

From definition (4.49), $0 < \lambda_i^{(N)} < 1$. We order the eigenvalues into

$$1 > \lambda_0^{(N)} \geq \lambda_1^{(N)} \geq \lambda_2^{(N)} \ldots \geq \lambda_{(N+1)^2-1}^{(N)} > 0$$

and also order the corresponding eigenvectors $\{\hat{\mathbf{f}}_i^{(N)}\}$ and the associated eigenfunctions $\{f_i^{(N)}(\boldsymbol{x})\}$. □

Therefore, according to Theorem 4.7.1, for any spectral-limited function $f^{(N)} \in \mathfrak{B}_N(\mathbb{S}^2, ds)$, it can be also represented by the new basis functions $\{f_i^{(N)}(\boldsymbol{x})\}$,

$$f^{(N)} = \sum_{i=0}^{(N+1)^2-1} a_i^{(N)} f_i^{(N)}(\boldsymbol{x}) \tag{4.57}$$

with $a_i^{(N)} = \left\langle f^{(N)}, f_i^{(N)}(\boldsymbol{x}) \right\rangle$ for $i = 0, 1 \cdots, (N+1)^2 - 1$.

4.7.2 Spectral Concentration of a Spatial-limited Signal ($\alpha = 1, 0 < \beta \leq \mu_0^{(\Gamma)}$)

$g(\boldsymbol{x}) \in L^2(\mathbb{S}^2, ds)$ is assumed to be a spatial-limited signal in the region Γ, i.e.,

$$g(\boldsymbol{x}) \triangleq \begin{cases} g(\boldsymbol{x}), & \boldsymbol{x} \in \Gamma; \\ 0, & \boldsymbol{x} \notin \Gamma. \end{cases} \tag{4.58}$$

According to the spatial truncation operator (2.41), we have $\mathcal{D}_\Gamma g = g$. Further, $g \in \mathfrak{D}_\Gamma(\mathbb{S}^2, ds)$ which is a complete subspace of $L^2(\mathbb{S}^2, ds)$ containing all spatial-limited functions with compact support in the region $\Gamma \in \mathbb{S}^2$.

Achieving the maximum energy concentration in the spectral interval $0 \leq n \leq N$ is equivalent to maximizing

$$\mu^{(\Gamma)} \triangleq \frac{\langle \mathcal{B}_N g, g \rangle}{\langle g, g \rangle} = \frac{\sum_{n=0}^{N} \sum_{m=-n}^{n} |g_n^m|^2}{\sum_{n=0}^{\infty} \sum_{m=-n}^{n} |g_n^m|^2}, \tag{4.59}$$

where g_n^m are the spherical harmonic coefficients of $g(\boldsymbol{x})$. Substituting (4.58) into (4.59) and interchanging the order of summation and integration, we obtain

$$\mu^{(\Gamma)} = \frac{\int_\Gamma \int_\Gamma \overline{g(\boldsymbol{x})} B_N(\boldsymbol{x}, \boldsymbol{y}) g(\boldsymbol{y}) \, ds(\boldsymbol{x}) \, ds(\boldsymbol{y})}{\int_\Gamma |g(\boldsymbol{x})|^2 \, ds(\boldsymbol{x})}, \tag{4.60}$$

where $B_N(\boldsymbol{x}, \boldsymbol{y})$ is given by (2.39).

It has been showed that solving (4.59) or (4.60) is equivalent to solving the Fredholm integral equation of the second kind [33]

$$\int_\Gamma B_N(\boldsymbol{x}, \boldsymbol{y}) g(\boldsymbol{y}) \, ds(\boldsymbol{y}) = \mu^{(\Gamma)} g(\boldsymbol{x}), \quad \boldsymbol{x} \in \Gamma. \tag{4.61}$$

Comparing (4.61) with (2.44), if $f(\boldsymbol{x}) = \mathcal{D}_\Gamma f(\boldsymbol{x}) = g(\boldsymbol{x})$, i.e., spatial-limited signal in the region Γ, then (2.44) and (4.61) are the same.

Solving (4.61), the eigenfunctions (optimal spatial-limited functions) are achieved. The following theorem summarises some key properties of the eigenfunctions and eigenvalues. We have also applied a normalization to the eigenfunctions. For the proof, only basic functional analysis is provided.

Theorem 4.7.2 *For a spatial-limited signal $g(\boldsymbol{x})$ within a spatial region Γ, the optimal normalized function having the maximum energy in the spectral interval $[0, N]$ satisfies (4.61) and have the following properties:*

1. *There are $(N+1)^2$ ordered orthonormal eigenfunctions $\{g_i^{(\Gamma)}(\boldsymbol{x})\}$ with ordered non-zero corresponding eigenvalues $1 > \mu_0^{(\Gamma)} \geq \mu_1^{(\Gamma)} \geq \ldots \geq \mu_{(N+1)^2-1}^{(\Gamma)} > 0$; there is also an infinite-dimensional null space of eigenfunctions $\{g_i^{(\Gamma)}(\boldsymbol{x})\}$ with associated eigenvalue $\mu_i^{(\Gamma)} = 0$ when $i \geq (N+1)^2$;*

2. *The eigenfunctions $g_i^{(\Gamma)}(\boldsymbol{x})$ are orthonormal on the whole sphere and orthog-*

onal on the region Γ:

$$\int_{\mathbb{S}^2} g_i^{(\Gamma)}(\boldsymbol{x})\overline{g_j^{(\Gamma)}(\boldsymbol{x})}\, ds(\boldsymbol{x}) = \delta_{ij}, \quad \int_{\Gamma} g_i^{(\Gamma)}(\boldsymbol{x})\overline{g_j^{(\Gamma)}(\boldsymbol{x})}\, ds(\boldsymbol{x}) = \mu_i^{(\Gamma)}\delta_{ij}$$

for any $i, j = 0, 1, \cdots$.

3. *The eigenfunctions* $\{g_i^{(\Gamma)}(\boldsymbol{x})\}$, $i = 0, 1, \cdots$, *consist of a complete, orthonormal basis for the subspace* $\mathfrak{D}_\Gamma(\mathbb{S}^2, ds)$;

4. *In particular,* $\mu_0^{(\Gamma)}$ *is the largest eigenvalue which is also the largest concentration ratio for* (4.59) *and* $g_0^{(\Gamma)}(\boldsymbol{x})$ *is the corresponding spatial-limited function having maximum energy in the spectral interval* $[0, N]$.

Proof

As Theorem 4.7.1, only the key points are provided. $B_N(\boldsymbol{x}, \boldsymbol{y})$ is a finite-rank (compact) and Hermitian symmetric kernel of the Mode Limiting Operator $\mathcal{B}_N$. According to the Spectral Theorem for a compact and self-adjoint operator on a Hilbert space [83], $\mathfrak{D}_\Gamma(\mathbb{S}^2, ds)$ has an orthonormal basis consisting of eigenfunctions of $\mathcal{B}_N$ and each eigenvalue is real. Since $B_N(\boldsymbol{x}, \boldsymbol{y})$ is a matrix with rank $(N+1)^2$, there are only $(N+1)^2$ non-zero eigenvalues. However, there are an infinite number of eigenfunctions corresponding to the eigenvalues equal to 0 in the null space. $\square$

Similarly, any spatial-limited function $g^{(\Gamma)} \in \mathfrak{D}_\Gamma(\mathbb{S}^2, ds)$, according to Theorem 4.7.2 can also be represented by

$$g^{(\Gamma)}(\boldsymbol{x}) = \sum_{j=0}^{\infty} b_j^{(\Gamma)} g_j^{(\Gamma)}(\boldsymbol{x}) \tag{4.63}$$

with $b_j^{(\Gamma)} = \left\langle g^{(\Gamma)}(\boldsymbol{x}), g_j^{(\Gamma)}(\boldsymbol{x}) \right\rangle$ and $j = 0, 1, \cdots$.

4.7.3   Duality of Basis Functions between Two Operators

Paper [33] showed that the truncated spectral-limited function in the region Γ is the optimal spatial-limited function. However, as it has been showed in Theorem 4.7.1 and Theorem 4.7.2, for the matrix operator $\mathbf{D}_N$, there are only $(N+1)^2$ eigenfunctions that are spectral-limited signals with maximum spectral degree N; while for the integral operator $\mathcal{B}_N$ with kernel $B_N(\boldsymbol{x}, \boldsymbol{y})$, there are infinite eigenfunctions which are spatial-limited signal in the region Γ. So it is impossible to determine all the eigenfunctions of $\mathcal{B}_N$ from the eigenfunctions of $\mathbf{D}_N$. Grunbaum etc., in

their paper [81], showed the duality between "finite Fourier operators" and "convolution integral operator" on a topological group G and its so-called dual group $\hat{G}$ by **Lemma 1**.

In this section, one theorem is given to show the duality of basis functions between the matrix $\mathbf{D}_N$ and the operator $\mathcal{B}_N$ with the kernel $B_N(\boldsymbol{x}, \boldsymbol{y})$ for the arbitrary region on the unit sphere.

Theorem 4.7.3 *Given any positive integer $N > 0$ and any spatial region $\Gamma \subset \mathbb{S}^2$.*
$\{f_i^{(N)}(\boldsymbol{x})\}$ *and* $\{\lambda_i^{(N)}\}$, $i = 0, 1, \cdots, (N+1)^2 - 1$, *are the associated eigenfunctions and corresponding eigenvalues to*

$$D_N \hat{f} = \lambda^{(N)} \hat{f},$$

where $f_i^{(N)}(\boldsymbol{x}) = \sum_{n=0}^{N} \sum_{m=-n}^{n} (f_n^m)_i^{(N)} Y_n^m(\boldsymbol{x})$ and $\hat{f}$ is the column vector containing the spherical harmonics coefficients f_n^m.

$\{g_i^{(\Gamma)}(\boldsymbol{x})\}$ *and* $\mu_i^{(\Gamma)}$, $i = 0, 1, \cdots$, *are the eigenfunctions and corresponding eigenvalues to*

$$\int_\Gamma B_N(\boldsymbol{x}, \boldsymbol{y}) g(\boldsymbol{y}) \, ds(\boldsymbol{y}) = \mu^{(\Gamma)} g(\boldsymbol{x}), \quad \boldsymbol{x} \in \Gamma.$$

For $0 \le i \le (N+1)^2 - 1$, there exist relations:

$$\lambda_i^{(N)} = \mu_i^{(\Gamma)} \tag{4.65}$$

$$\left(\mathcal{B}_N g_i^{(\Gamma)}\right)(\boldsymbol{x}) = \sqrt{\lambda_i^{(N)}} f_i^{(N)}(\boldsymbol{x}) \tag{4.66}$$

$$\left(\mathcal{D}_\Gamma f_i^{(N)}\right)(\boldsymbol{x}) = \sqrt{\mu_i^{(\Gamma)}} g_i^{(\Gamma)}. \tag{4.67}$$

Proof

The proof is provided in Appendix A.5.

Remark 4.1 *It should be noted that $\{f_i^{(N)}(\boldsymbol{x})\}$ can be determined from the algebraic eigenvalue equation (4.52); while $\{g_j^{(\Gamma)}(\boldsymbol{x})\}$ are the optimal functions of the Fredholm integral equation of the second kind (4.61) and they are not determined.*

4.7.4 Least Angle between Two Subspaces

In this section, one angle between $\mathfrak{D}_\Gamma(\mathbb{S}^2, ds)$ and $\mathfrak{B}_N(\mathbb{S}^2, ds)$ is introduced, and a least angle is also derived.

The angle $\theta(f_1, f_2)$ between functions $f_1 \in L^2(\mathbb{S}^2, ds)$ and $f_2 \in L^2(\mathbb{S}^2, ds)$ is defined as [23]

$$\theta(f_1, f_2) = \cos^{-1} \frac{\Re\{\langle f_1, f_2 \rangle\}}{\|f_1\| \cdot \|f_2\|}. \tag{4.68}$$

The extreme values 0 and π for $\theta(f_1, f_2)$ are obtained if and only if f_1 and f_2 are proportional and $\langle f_1, f_2 \rangle$ is real. According to $\Re\{\langle f_1, f_2 \rangle\} = \|f_1\| \cdot \|f_2\| \cdot \cos \theta(f_1, f_2)$, when both f_1 and f_2 are non-zero, $\Re\{\langle f_1, f_2 \rangle\} = 0$ (i.e., $\cos \theta(f_1, f_2) = 0$) is obtained if and only if f_1 and f_2 are orthogonal.

Theorem 4.7.4 *There exists an least angle θ_0 between the subspaces $\mathfrak{B}_N(\mathbb{S}^2, ds)$ and $\mathfrak{D}_\Gamma(\mathbb{S}^2, ds)$ and it is equal to $\sqrt{\lambda_0^{(N)}}$ (or $\sqrt{\mu_0^{(\Gamma)}}$). I.e., suppose $f^{(N)} \in \mathfrak{B}_N(\mathbb{S}^2, ds)$, $g^{(\Gamma)} \in \mathfrak{D}_\Gamma(\mathbb{S}^2, ds)$,*

$$\begin{aligned}
\theta_0 &= \min_{f^{(N)} \in \mathfrak{B}_N} \inf_{g^{(\Gamma)} \in \mathfrak{D}_\Gamma} \theta(f^{(N)}, g^{(\Gamma)}) \\
&= \cos^{-1} \sqrt{\lambda_0^{(N)}} \\
&= \cos^{-1} \sqrt{\mu_0^{(\Gamma)}},
\end{aligned} \tag{4.69}$$

the equality is obtained when $f^{(N)} = f_0^{(N)}(\boldsymbol{x})$ and $g^{(\Gamma)} = k\mathcal{D}_\Gamma f^{(N)} = k\mathcal{D}_\Gamma f_0^{(N)}(\boldsymbol{x}) = k\sqrt{\mu_0^{(\Gamma)}} g_0^{(\Gamma)}$ where k is an arbitrary positive constant.

Proof

The proof is provided in Appendix A.6. $\square$

4.8   Arbitrary Signal Concentration on $\mathbb{S}^2$ ($0 < \alpha, \beta < 1$)

In this section, we turn our attention to the general concentration problem on the unit sphere: for an arbitrary signal $f(\boldsymbol{x}) \in L^2(\mathbb{S}^2, ds)$ which is neither strictly spatial-limited nor spectral-limited, we aim to find an optimal function $f(\boldsymbol{x})$ that achieves the most concentrated energy both in the spatial domain and in the spectral domain, i.e., where $\|f\| = 1$, $0 < \|\mathcal{D}_\Gamma f\| = \alpha < 1$ and $0 < \|\mathcal{B}_N f\| = \beta < 1$, we seek $f(\boldsymbol{x})$ such that α and β are simultaneously maximized.

For simplicity, we divide this problem into two steps: 1) for fixed α, based on our spherical Franks' framework [84], obtain the first optimal function which has the maximum weighted spectral energy $\|\beta\|^2$; 2) maximize α to achieve the final optimal solution. Here, without loss of generality, α and β can be interchanged.

4.8.1 Spherical Franks' framework

In this section, the spherical Franks' framework derived in section 4.5 is used. The first objective is to maximize $I_2 = \|\mathcal{B}_N f\|^2 = \beta^2$ under the constraints $I_1 = \|\mathcal{D}_\Gamma f\|^2 = \alpha^2$ and $I_3 = \|f\|^2 = 1$. According to the spherical Franks' framework, it is equivalent to maximize

$$G = \mu_1 I_1 + \mu_2 I_2 + I_3, \tag{4.70}$$

where μ_1 and μ_2 are two Lagrange multipliers and

$$I_1 = \langle \mathcal{D}_\Gamma f, f \rangle = \int_\Gamma |f(\boldsymbol{x})|^2 \, ds(\boldsymbol{x}) \tag{4.71a}$$

$$I_2 = \langle \mathcal{B}_N f, f \rangle = \sum_{n=0}^{N} \sum_{m=-n}^{n} |f_n^m|^2 \tag{4.71b}$$

$$I_3 = \langle f, f \rangle = \left\langle \hat{\mathbf{f}}, \hat{\mathbf{f}} \right\rangle = \int_{\mathbb{S}^2} |f(\boldsymbol{x})|^2 \, ds(\boldsymbol{x}) = \sum_{n=0}^{\infty} \sum_{m=-n}^{n} |f_n^m|^2 = 1. \tag{4.71c}$$

It is well known that finding a stationary function f that extremizes a quadratic functional $I(f)$ is usually achieved in two steps: 1) obtain the directional derivative $D_u I(f)$ at a point f along any arbitrary function u; 2). solve the equation $D_u I(f) = 0$ to get the necessary condition. In our case, since G is a linear combination of three quadratic functionals, we can find the directional derivative $D_u G(f)$ and then solve $D_u G(f) = 0$.

For a quadratic function $I(f) = \langle \mathcal{A}f, f \rangle$ where $\mathcal{A}$ is a linear operator, its directional derivative at a point f along u, where u is an arbitrary unit vector in $L^2(\mathbb{S}^2, ds)$, is defined as [1]

$$D_u I(f) = \langle \mathcal{A}f, u \rangle + \langle \mathcal{A}u, f \rangle = \langle \mathcal{A}f, u \rangle + \langle u, \mathcal{A}'f \rangle.$$

And if $\mathcal{A}$ is a self-adjoint operator, i.e., $\mathcal{A} = \mathcal{A}'$, then

$$D_u I(f) = \langle \mathcal{A}f, u \rangle + \langle u, \mathcal{A}f \rangle = 2\Re\{\langle \mathcal{A}f, u \rangle\}, \tag{4.72}$$

where $\Re\{\cdot\}$ denotes the real part of $\langle \mathcal{A}f, u \rangle$.

Because both $\mathcal{D}_\Gamma$ and $\mathcal{B}_N$ are self-adjoint, we have

$$D_u I_1(f) = 2\Re\{\langle \mathcal{D}_\Gamma f, u \rangle\} \tag{4.73a}$$

$$D_u I_2(f) = 2\Re\{\langle \mathcal{B}_N f, u \rangle\} \tag{4.73b}$$

$$D_u I_3(f) = 2\Re\{\langle f, u \rangle\}. \tag{4.73c}$$

Therefore, the directional derivative of G at a point f along u is given by

$$
\begin{aligned}
D_u G(f) &= D_u \left[\mu_1 I_1 + \mu_2 I_2 + I_3 \right] \\
&= \mu_1 D_u I_1 + \mu_2 D_u I_2 + D_u I_3 \\
&= 2\Re\{\langle \mu_1 \mathcal{D}_\Gamma f + \mu_2 \mathcal{B}_N f + f, u \rangle\} \\
&= 2\|\mu_1 \mathcal{D}_\Gamma f + \mu_2 \mathcal{B}_N f + f\| \cdot \|u\| \cdot \cos\theta(\mu_1 \mathcal{D}_\Gamma f + \mu_2 \mathcal{B}_N f + f, u) \\
&= 0,
\end{aligned}
\tag{4.74}
$$

where we have used (4.73a) – (4.73c) and the angle definition between two functions (4.68).

Since $\|u\| = 1$, the necessary condition of (4.74) for a stationary point f which makes $D_u G(f) = 0$ is

$$
\|\mu_1 \mathcal{D}_\Gamma f + \mu_2 \mathcal{B}_N f + f\| = 0,
\tag{4.75}
$$

or

$$
\cos\theta(\mu_1 \mathcal{D}_\Gamma f + \mu_2 \mathcal{B}_N f + f, u) = 0.
\tag{4.76}
$$

According to norm property: $\|f\| = 0$ is satisfied if and only if $f = 0$, (4.75) is changed into

$$
\mu_1 \mathcal{D}_\Gamma f + \mu_2 \mathcal{B}_N f + f = 0.
\tag{4.77}
$$

Eqn (4.76) implies $\mu_1 \mathcal{D}_\Gamma f + \mu_2 \mathcal{B}_N f + f$ is orthogonal to u. As u is an arbitrary function on the unit sphere, this condition is hard to satisfy. Therefore, only (4.75) is possible. Therefore, after adjusting (4.75) and making variable substitutions, we get

$$
f = \lambda \mathcal{D}_\Gamma f + \mu \mathcal{B}_N f,
\tag{4.78}
$$

where $\lambda = -\mu_1$ and $\mu = -\mu_2$. Eq. (4.78) is the first optimal function with maximum β for fixed α and $\|f\| = 1$. Subsequently, we solve the final optimal function to obtain the maximum α based on the suboptimal function (4.78).

4.8.2   General Solution to the General Concentration Problem on $\mathbb{S}^2$

In this section, we focus on finding a function which maximizes α under the constraints $f = \lambda \mathcal{D}_\Gamma f + \mu \mathcal{B}_N f$, $\|f\| = 1$, $\|\mathcal{D}_\Gamma f\| = \alpha$ and $\|\mathcal{B}_N f\| = \beta$. Following a similar procedure as in [23] and taking the inner product of (4.78) with f, $\mathcal{D}_\Gamma f$ and $\mathcal{B}_N f$, we have

$$
1 = \langle f, f \rangle = \langle \lambda \mathcal{D}_\Gamma f + \mu \mathcal{B}_N f, f \rangle = \lambda \alpha^2 + \mu \beta^2
\tag{4.79a}
$$

$$\alpha^2 = \langle f, \mathcal{D}_\Gamma f \rangle = \langle \lambda \mathcal{D}_\Gamma f + \mu \mathcal{B}_N f, \mathcal{D}_\Gamma f \rangle = \lambda \alpha^2 + \mu \langle \mathcal{B}_N f, \mathcal{D}_\Gamma f \rangle \tag{4.79b}$$

$$\beta^2 = \langle f, \mathcal{B}_N f \rangle = \langle \lambda \mathcal{D}_\Gamma f + \mu \mathcal{B}_N f, \mathcal{B}_N f \rangle = \lambda \langle \mathcal{D}_\Gamma f, \mathcal{B}_N f \rangle + \mu \beta^2. \tag{4.79c}$$

By eliminating λ and μ from (4.79a) – (4.79c), we have

$$\alpha^2 - 2\Re\{\langle \mathcal{D}_\Gamma f, \mathcal{B}_N f \rangle\} + \beta^2 = 1 - \frac{|\langle \mathcal{D}_\Gamma f, \mathcal{B}_N f \rangle|^2}{\alpha^2 \beta^2}. \tag{4.80}$$

By definition (4.68), we have

$$\Re\{\langle \mathcal{D}_\Gamma f, \mathcal{B}_N f \rangle\} = \|\mathcal{D}_\Gamma f\| \cdot \|\mathcal{B}_N f\| \cdot \cos\theta(\mathcal{D}_\Gamma f, \mathcal{B}_N f) = \alpha\beta \cos\theta(\mathcal{D}_\Gamma f, \mathcal{B}_N f). \tag{4.81}$$

As $\Re\{\langle \mathcal{D}_\Gamma f, \mathcal{B}_N f \rangle\}$ is only the real part of $\langle \mathcal{D}_\Gamma f, \mathcal{B}_N f \rangle$, we then have

$$|\Re\{\langle \mathcal{D}_\Gamma f, \mathcal{B}_N f \rangle\}| \le |\langle \mathcal{D}_\Gamma f, \mathcal{B}_N f \rangle|. \tag{4.82}$$

This equality is obtained when $\langle \mathcal{D}_\Gamma f, \mathcal{B}_N f \rangle$ is real.

By the Cauchy-Schwarz inequality,

$$|\langle \mathcal{D}_\Gamma f, \mathcal{B}_N f \rangle|^2 \le |\langle \mathcal{D}_\Gamma f, \mathcal{D}_\Gamma f \rangle| \cdot |\langle \mathcal{B}_N f, \mathcal{B}_N f \rangle| = \alpha^2 \beta^2.$$

The equality is obtained when $\mathcal{D}_\Gamma f$ is proportional to $\mathcal{B}_N f$, which is impossible due to the least angle between two subspaces $\mathfrak{D}_\Gamma(\mathbb{S}^2, ds)$ and $\mathfrak{B}_N(\mathbb{S}^2, ds)$.

Therefore,

$$0 < 1 - \frac{|\langle \mathcal{D}_\Gamma f, \mathcal{B}_N f \rangle|^2}{\alpha^2 \beta^2} \le 1 - \cos^2\theta(\mathcal{D}_\Gamma f, \mathcal{B}_N f). \tag{4.84}$$

Substituting (4.81) and (4.84) into (4.80), we get

$$0 < \alpha^2 - 2\alpha\beta \cos\theta(\mathcal{D}_\Gamma f, \mathcal{B}_N f) + \beta^2 \le 1 - \cos^2\theta(\mathcal{D}_\Gamma f, \mathcal{B}_N f). \tag{4.85}$$

Now our goal is to get the maximum value of α. And we also take β as a constant. So the variables are α and $\cos\theta(\mathcal{D}_\Gamma f, \mathcal{B}_N f)$.

The first inequality of (4.85) is satisfied for any α and $\cos\theta(\mathcal{D}_\Gamma f, \mathcal{B}_N f)$, since the discriminant of $\alpha^2 - 2\alpha\beta \cos\theta(\mathcal{D}_\Gamma f, \mathcal{B}_N f) + \beta^2 = 0$ is $4\beta^2 [\cos^2\theta(\mathcal{D}_\Gamma f, \mathcal{B}_N f) - 1] \le 0$.

For the second inequality of (4.85), after making some changes, we get

$$[\alpha - \beta \cos\theta(\mathcal{D}_\Gamma f, \mathcal{B}_N f)]^2 \le (1 - \beta^2) \sin^2\theta(\mathcal{D}_\Gamma f, \mathcal{B}_N f). \tag{4.86}$$

As it has been proved in Theorem 4.7.4 that there exists a least angle θ_0 between the subspaces $\mathfrak{B}_N(\mathbb{S}^2, ds)$ and $\mathfrak{D}_\Gamma(\mathbb{S}^2, ds)$,

$$\theta_0 = \min_{f^{(N)} \in \mathfrak{B}_N} \inf_{g^{(\Gamma)} \in \mathfrak{D}_\Gamma} \theta(f^{(N)}, g^{(\Gamma)}) = \cos^{-1} \sqrt{\lambda_0^{(N)}} = \cos^{-1} \sqrt{\mu_0^{(\Gamma)}},$$

so we have $0 \le \sin \theta(\mathcal{D}_\Gamma f, \mathcal{B}_N f) \le 1$. Therefore, (4.86) changes into

$$|\alpha - \beta \cos \theta(\mathcal{D}_\Gamma f, \mathcal{B}_N f)| \le \sqrt{1 - \beta^2} \sin \theta(\mathcal{D}_\Gamma f, \mathcal{B}_N f), \qquad (4.88)$$

i.e.,

$$\beta \cos \theta(\mathcal{D}_\Gamma f, \mathcal{B}_N f) - \sqrt{1 - \beta^2} \sin \theta(\mathcal{D}_\Gamma f, \mathcal{B}_N f) \le \alpha$$
$$\le \beta \cos \theta(\mathcal{D}_\Gamma f, \mathcal{B}_N f) + \sqrt{1 - \beta^2} \sin \theta(\mathcal{D}_\Gamma f, \mathcal{B}_N f). \qquad (4.89)$$

As $0 < \beta < 1$, we take an angle $\theta_1 = \arccos^{-1} \beta$, so $\theta_1 \in [0, \pi/2]$. We also take $\theta = \theta(\mathcal{D}_\Gamma f, \mathcal{B}_N f)$ and $\theta \in [\theta_0, \pi]$. Then (4.89) becomes

$$\cos(\theta + \theta_1) \le \alpha \le \cos(\theta - \theta_1). \qquad (4.90)$$

Since our goal is to find the maximum value of α, we are only interested in the half part $\alpha \le \cos(\theta - \theta_1)$.

Let $f(\theta) = \cos(\theta - \theta_1)$. Then we only need to compare $0 < \alpha \le f(\theta)$. Let us look at Fig. 4.1.
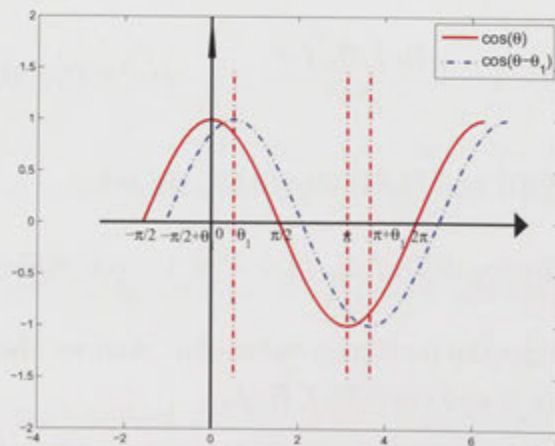
Figure 4.1: The variation of α and θ

If $0 < \theta_0 < \theta_1$, i.e., $0 < \beta < \sqrt{\lambda_0^{(N)}}$, as θ varies from θ_0 to π, then $f_{max} = 1$ when $\theta = \theta_1$ and $f_{min} = \cos(\pi - \theta_1) = -\sin(\theta) < 0$ when $\theta = \pi$. As it requires

$f(\theta) > 0$, therefore, we have $0 \leq f(\theta) \leq 1$, i.e., $\alpha_{max} = 1$ and $\alpha_{min} = 0$. And $\alpha_{max} = 1$ is obtained when $0 < \beta < \sqrt{\lambda_0^{(N)}}$. This is the spectral concentration for a spatial-limited signal case. However, in this section, as we have restricted $0 < \alpha < 1$, this situation will not happen.

If $\theta_1 \leq \theta_0 \leq \pi$, i.e., $\cos^{-1} \sqrt{\lambda_0^{(N)}} \leq \beta < 1$, as θ varies from θ_0 to π, $f_{max} = \cos(\theta_0 - \theta_1)$ when $\theta = \theta_0$ and $f_{min} = \cos(\pi - \theta_1) = -\sin(\theta) < 0$. Therefore, $\alpha_{max} = \cos(\theta_0 - \theta_1)$ and $\alpha_{min} = 0$. Therefore,

$$\alpha_{max} = \cos(\theta_0 - \theta_1) = \cos\left(\cos^{-1}\sqrt{\lambda_0^{(N)}} - \arccos\beta\right), \tag{4.91}$$

and as $\alpha \leq \alpha_{max}$, we have

$$\cos^{-1}\beta + \cos^{-1}\alpha \geq \cos^{-1}\sqrt{\lambda_0^{(N)}}. \tag{4.92}$$

The equality obtained as stated before is that $\langle \mathcal{D}_\Gamma f, \mathcal{B}_N f \rangle$ is real and

$$\cos\theta(\mathcal{D}_\Gamma f, \mathcal{B}_N f) = \cos\theta_0 = \sqrt{\lambda_0^{(N)}}, \tag{4.93a}$$

$$\mathcal{B}_N f = \beta f_0^{(N)}(\boldsymbol{x}), \tag{4.93b}$$

$$\mathcal{D}_\Gamma f = \frac{\alpha}{\sqrt{\lambda_0^{(N)}}}\mathcal{D}_\Gamma f_0^{(N)}(\boldsymbol{x}). \tag{4.93c}$$

Substituting (4.93a) into (4.79a) – (4.79c), we get

$$\lambda = \frac{1}{1 - \lambda_0^{(N)}} - \frac{\alpha_{max}}{\beta}\frac{\sqrt{\lambda_0^{(N)}}}{1 - \lambda_0^{(N)}}, \tag{4.94}$$

$$\mu = \frac{1}{1 - \lambda_0^{(N)}} - \frac{\beta}{\alpha_{max}}\frac{\sqrt{\lambda_0^{(N)}}}{1 - \lambda_0^{(N)}} \tag{4.95}$$

Changing (4.91) into

$$\beta = \alpha_{max}\sqrt{\lambda_0^{(N)}} + \sqrt{1 - \alpha_{max}^2}\sqrt{1 - \lambda_0^{(N)}}, \tag{4.96}$$

and substituting β into λ and μ, we obtain

$$p = \mu\beta = \frac{\sqrt{1 - \alpha_{max}^2}}{\sqrt{1 - \lambda_0^{(N)}}}, \tag{4.97}$$

$$q = \lambda \frac{\alpha_{max}}{\sqrt{\lambda_0^{(N)}}} = \frac{\alpha_{max}}{\sqrt{\lambda_0^{(N)}}} - \frac{\sqrt{1 - \alpha_{max}^2}}{\sqrt{1 - \lambda_0^{(N)}}}. \tag{4.98}$$

Therefore, the optimal function f which simultaneously achieves the most concentration both in the spatial domain and in the spectral domain is

$$f = p\mathcal{B}_N f_0^{(N)} + q\mathcal{D}_\Gamma f_0^{(N)}. \tag{4.99}$$

where p and q are given by (4.97) and (4.98).

4.9   Summary and Contributions

In this chapter, we introduced the infinite matrix representation for an operator defined on the unit sphere; a spatial kernel is solved by relating to the infinite matrix representation of the operator; then some quadratic functionals defined on the unit sphere are derived. Based on this work, some specific contributions are made:

1. A harmonic multiplication operation on the unit sphere is proposed, and its equivalence to the isotropic convolution is given [38]

2. Applying the harmonic multiplication weighting in the spectral domain, some spherical quadratic functionals are derived.

3. Franks general constrained variational framework is developed to the unit sphere [84];

4. General signal concentration problem on the unit sphere is solved by Franks framework and the quadratic functions [86].

Chapter 5

Spherical Basis Functions for Different Energy Concentration Measures On $\mathbb{S}^2$

The objective of this chapter is to find appropriate spherical basis functions to efficiently analyze and represent signals defined on the unit sphere. Motivated by the time duration and bandwidth moment weighting in the time-frequency domain, Section 5.2 proposes a global kth moment azimuthal measure (GMAM) and a local kth moment zenithal measure (LMZM) to a spectral-limited signal on the unit sphere. Two sets of spherical optimal eigenfunctions which consist of basis functions are obtained, respectively. Comparisons of these two sets of eigenfunctions and the spherical Slepian functions are made. Furthermore, a spatial-limited signal concentration problem based on a harmonic multiplication operation on the unit sphere is studied in Section 5.3.

5.1 Introduction

The problem of recovering or reconstructing an original signal defined on the sphere corrupted by noise, based on incompletely sampled data, has received attention lately, mainly in areas such as cosmic microwave background (CMB) radio analysis in astrophysics [43, 44, 49], surface representation in computer vision [12, 14, 87], and spectral estimation in geophysics [8, 11, 33]. The spherical filters, including analysis, smoothing and synthesis filters, are key tools for this operation. Therefore, designing a suitable filter by choosing a set of proper basis functions is a practical issue.

For the present research, most of the signals are assumed to be spectral-limited [13,

31, 33]. According to the Fourier transform (spherical harmonic transform), a spectral-limited signal occupies the whole sphere. However, in practice, only some part of the region on the unit sphere is available or of interest, that is, a spatial-limited signal is more common in reality. At present, a box window function is usually used to obtain a spatial function [43, 44], which causes infinite spherical harmonic coefficients in the spectral domain and therefore a truncation is needed for numerical simulation. Therefore, achieving the trade off between a finite spectrum and a finite spatial occupation is a practical problem.

In reality, due to the spatial features of the region of interest on the unit sphere, such as the melting of icecaps and surface displacement after large earthquakes [8], together with the numerical requirement of finite limitation of the spectral bandwidth, such a basis of simultaneously spatially and spectrally concentrated functions is needed for efficient data analysis and function representation on the unit sphere. Wavelets are often used as a localized filter to analyze the data for reconstruction, de-noising or de-convolution [47, 88–90]. However, the "dilation" of the wavelet on the unit sphere is hard to be reconciled on a spatially bounded region; further, the stereographic dilation needs a projection back procedure [21, 88].

On the other hand, the spherical Slepian functions are another good choice of basis functions due to their orthonormal property and being simultaneously spatially and spectrally concentrated in the spatial region and spectral bandwidth [31–33]. They have also been applied, for example, in analyzing data and representing functions on the unit sphere [8], spectral analysis [11, 91, 92], and spherical wavelet (a kind of spherical filter) design [49] for CMB power spectrum estimation, and the construction of invertible filter banks on the sphere [13].

However, researchers have shown, in the time-frequency domain, that the prolate spheroidal wave functions (PSWFs), which are the optimal band-limited functions of the Slepian concentration problem, have longer tails and lower decaying rates than the half sinusoids obtained by a second-moment weighting in the time domain [61] and optimal functions with a fourth-moment weighting in the time domain [34], [76]. Therefore, PSWFs are not good at offsetting potential interference between signals concentrated in different spectral regions.

Based on similar reasoning, it is necessary to investigate whether there exists other basis functions on the unit sphere, which have good limited spectral degree and good energy concentration in the spatial domain and also have better performance than the spherical Slepian functions in analyzing data, representing functions and reconstructing signals.

5.2 Spectral-limited Signal Concentration with Azimuthal Moment Weighting On $\mathbb{S}^2$

In this section, three different concentration measures are defined and the corresponding optimal functions are solved. Further, a comparison between these basis functions is made.

5.2.1 Measures for Spectral-limited Signal Concentration on $\mathbb{S}^2$

Assume $f(\boldsymbol{x}) \in L^2(\mathbb{S}^2, ds)$ is a spectral-limited signal of order N, i.e.,

$$f(\boldsymbol{x}) = \sum_{n=0}^{N} \sum_{m=-n}^{n} f_n^m Y_n^m(\boldsymbol{x}), \tag{5.1}$$

where $f_n^m = \langle f, Y_n^m \rangle$ are the spherical harmonic coefficients given by (2.20).

The spherical Slepian simultaneous energy concentration measure is defined by

$$\lambda_S \triangleq \frac{\int_\Gamma f^2(\boldsymbol{x})\, ds(\boldsymbol{x})}{\int_{\mathbb{S}^2} f^2(\boldsymbol{x})\, ds(\boldsymbol{x})} = \text{Maximum}, \tag{5.2}$$

and the optimal functions are the spherical Slepian functions which achieve the maximum energy in the spatial region $\Gamma \in \mathbb{S}^2$ [33].

By considering the entire sphere, a global kth moment azimuthal measure (GMAM) is defined as [93]

$$\lambda_G \triangleq \frac{\int_{\mathbb{S}^2} \theta^k f^2(\boldsymbol{x})\, ds(\boldsymbol{x})}{\int_{\mathbb{S}^2} f^2(\boldsymbol{x})\, ds(\boldsymbol{x})} = \text{Minimum}, \tag{5.3}$$

where $k = 1, 2, \cdots$.

The local kth moment zenithal measure (LMZM) λ_L is defined as [94]

$$\lambda_L \triangleq \frac{\int_\Gamma \theta^k f^2(\boldsymbol{x})\, ds(\boldsymbol{x})}{\int_{\mathbb{S}^2} f^2(\boldsymbol{x})\, ds(\boldsymbol{x})} = \text{Maximum}, \tag{5.4}$$

where $k = 0, 1, 2, \cdots$.

Comparing with these definitions, we find that:

- LMZM gives the simultaneous energy concentration measure (5.2) for $k = 0$ [33];

- the objective function of GMAM is to minimize λ_G, while that of LMZM is to maximize λ_L, though both GMAM and LMZM have the similar formulation (shown in the next section).

5.2.2 Problems Under Consideration

The objective in this chapter is to find such optimal functions in the specified region Γ that: 1) achieve the minimum azimuthally moment weighting measure on the whole sphere(GMZM), and 2) achieve the maximum zenithal moment weighting measure(LMZM), respectively. We take $k = 2, 4$ as examples. Our aim is to investigate whether these sets of the optimal functions with minimum global kth azimuthal measure and those with maximum local kth zenithal moment measure are good choices for spherical filter design.

5.2.3 Finite Dimensional Formulation for GMAM and LMZM

Suppose the region Γ is a cap with colatitude range $(0, \Theta)$. Looking at (5.3) and (5.4), we notice that:

- when $0 < \Theta < \pi$, the concentration measure λ corresponds to LMZM; when $\Theta = \pi$, λ corresponds to the GMAM;

- the formulations of these GMAM and LMZM are the same except the different extremization [93, 94].

Therefore, for calculational simplicity and also easy comparison with the spherical Slepian function [33], we use one formulation including both GMZM and LMZM and we also use real spherical harmonics [51]. However, we must understand that the "Global" minimization and "Local" maximization problems are completely different.

Following a similar procedure to [33], after substituting (5.1) into (5.4) and interchanging the orders of summation and integration, we obtain

$$\lambda = \frac{\sum_{n=0}^{N} \sum_{m=-n}^{n} f_n^m \sum_{q=0}^{N} \sum_{p=-q}^{q} f_q^p D_{nq}^{mp}}{\sum_{n=0}^{N} \sum_{m=-n}^{n} |f_n^m|^2} = \frac{\hat{\mathbf{f}}^T \mathbf{D} \hat{\mathbf{f}}}{\hat{\mathbf{f}}^T \hat{\mathbf{f}}}, \tag{5.5}$$

where $\mathbf{D}$ is a $(N+1)^2 \times (N+1)^2$ matrix with elements

$$D_{nq}^{mp} \triangleq \int_0^{2\pi} d\phi \int_0^{\Theta} \theta^k Y_n^m(\theta, \phi) Y_q^p(\theta, \phi) \sin \theta \, d\theta$$

$$= 2\pi \delta_{mp} \int_0^{\Theta} \theta^k X_n^{|m|}(\theta) X_q^{|p|}(\theta) \sin \theta \, d\theta$$

$$= \delta_{mp} \frac{(2n+1)^{\frac{1}{2}}(2q+1)^{\frac{1}{2}}}{2} \left[\frac{(n-|m|)!}{(n+|m|)!} \right]^{\frac{1}{2}}$$

$$\times \left[\frac{(q-|p|)!}{(q+|p|)!} \right]^{\frac{1}{2}} \int_0^{\Theta} \theta^k P_n^{|m|}(\cos \theta) P_q^{|p|}(\cos \theta) \sin \theta \, d\theta, \qquad (5.6)$$

and $\hat{\mathbf{f}}$ is the ordered column vector of spherical harmonic coefficients f_n^m,

$$\hat{\mathbf{f}} = (f_0^0, f_1^0, f_2^0, \cdots, f_N^0, f_1^{-1}, f_2^{-1}, \cdots, f_1^N, f_2^N, \cdots, f_N^N)^T. \qquad (5.7)$$

Note that $\mathbf{D}$ is a symmetric matrix and the Kronecker delta function δ_{mq} separates the matrix $\mathbf{D}$ into a block diagonal structure:

$$\mathbf{D} = \text{diag}(\mathbf{D}_0, \mathbf{D}_{-1}, \mathbf{D}_1, \cdots, \mathbf{D}_{-m}, \mathbf{D}_m, \cdots, \mathbf{D}_{-N}, \mathbf{D}_N)$$

and the sub-matrices satisfy

$$\mathbf{D}_{-m} = \mathbf{D}_m. \qquad (5.9)$$

The necessary condition for a stationary solution to (5.5) is the solution of the $(N+1)^2 \times (N+1)^2$ algebraic eigenvalue equation [33]

$$\mathbf{D}\hat{\mathbf{f}} = \lambda \hat{\mathbf{f}}. \qquad (5.10)$$

Following the same procedure to [33, 93], and using the intermediate condition $\mathbf{D}_{-m} = \mathbf{D}_m$, we only need to solve for a $(N-m+1) \times (N-m+1)$ matrix for fixed angular order m ($m \geq 0$),

$$\mathbf{D}_m \hat{\mathbf{f}}^{(m)} = \lambda \hat{\mathbf{f}}^{(m)} \qquad (5.11)$$

where

$$\mathbf{D}_m = \begin{bmatrix} D_{mm}^{mm} & D_{m(m+1)}^{mm} & \cdots & D_{mN}^{mm} \\ D_{(m+1)m}^{mm} & D_{(m+1)(m+1)}^{mm} & \cdots & D_{(m+1)N}^{mm} \\ \vdots & \vdots & \vdots & \vdots \\ D_{Nm}^{mm} & D_{N(m+1)}^{mm} & \cdots & D_{NN}^{mm} \end{bmatrix}.$$

Solving the eigenvalue equation (5.11), the eigenvectors $\{\hat{\mathbf{f}}_{(j)}^{(m)}\}$ are obtained where j is the index of the eigenvectors with $j = 1, 2, \cdots, (N-m+1)$. Then, the associated eigenfunctions can be found by (2.19) and (2.12),

$$f_{(j)}^{(m)}(\theta) = \sum_{n=m}^{N} \left(\hat{\mathbf{f}}_{(j)}^{(m)}\right)_n X_n^m(\theta), \tag{5.13}$$

where $\left(\hat{\mathbf{f}}_{(j)}^{(m)}\right)_n$ is the element of the eigenvector $\hat{\mathbf{f}}_{(j)}^{(m)}$. Finally the optimal spatial eigenfunction $f_j(\boldsymbol{x}) = f_j(\theta, \phi)$ for fixed m are given by

$$f_{(j)}^{(m)}(\theta, \phi) = \begin{cases} \sqrt{2} f_{(j)}^{(m)}(\theta) \sin(|m|\phi), & -N \leq m < 0; \\ f_{(j)}^{(m)}(\theta), & m = 0; \\ \sqrt{2} f_{(j)}^{(m)}(\theta) \cos(m\phi), & 0 < m \leq N. \end{cases} \tag{5.14}$$

5.2.4 Numerical Examples

As an example, we consider a maximum spectral degree $N = 18$ for the spectral-limited signal $f(\boldsymbol{x})$, which is also convenient for comparison with Simons' spherical Slepian function presented in [33].

Fig. 5.1 (a) depicts the optimal associated eigenfunctions $f_{(j)}^{(m)}(\theta)$ when $j = 1$ and $m = 0$ for $k = 2, 4$ with minimal eigenvalues for GMAM and Simons' spherical Slepian functions with maximal eigenvalues [33] in two caps $[0, 20°]$ and $[0, 40°]$. Here, "j" denotes the index of the function. This figure shows that the optimal functions for GMAM (5.3) compared with the spherical Slepian function (5.2): 1) tend to be more even as k increases, 2) concentrate between 0 and $40°$, 3) have a higher peak value in the original for $k = 2$ compared to those of $k = 4$ and Simons', and 4) approach the spherical Slepian function in the cap $[0, 20°]$ for $k = 4$. Fig. 5.1 (b) describes the optimal functions $f_{(1)}^{(1)}(\theta)$ of GMAM and Simons' method for $m = 1$, which is similar to Fig. 5.1 (a).

Fig. 5.2 shows the comparison of the optimal associated eigenfunctions for GMAM, LMZM and the spherical Slepian functions. In this figure, "$k = 0$, Simons" refers to the local 0-th moment zenithal measure, which is also Simons' spherical Slepian function with maximal energy concentration in the cap; "$k = 4$, GMAM" refers to the optimal functions obtained using the global 4th moment azimuthal measure (5.3). From the figure, it is easy to see that the optimal associated eigenfunction with LMZM has less energy in the cap than that with "$k = 4$, GMAM" and Simons' spherical Slepian function. A large portion of the energy for LMZM lies outside the colatitude $\theta = 20°$. Secondly, for LMZM, as k increases, the

(a)   (b)

Figure 5.1: Comparison of the optimal associated eigenfunctions $f_{(1)}^{(m)}(\theta)$ corresponding to GMAM (5.3) and Simons' spherical Splepian functions (5.2): (a) $m = 0$; (b) $m = 1$.

curve inclines to larger values in the main lobe and concentrate much more energy, from which we can deduce that the tail decays quicker. However, there seems no advantage for the optimal function of LMZM in the side-lobe's decaying comparing over Simons' Slepian function, which differs from the time-frequency case [34, 76].
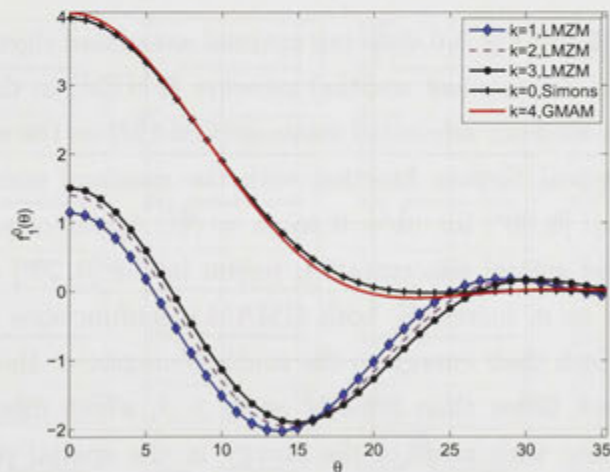
Figure 5.2: Comparison of the optimal associated eigenfunctions $f_{(1)}^{(0)}(\theta)$ corresponding to the kth ($k = 0, 1, 2, 3, 4$) moment zenithal measure (5.4) in the cap with $\Theta = 20°$, global 4th moment zenithal measure (5.3) and Simons' spherical Slepian concentration measure (5.2) in the cap with $\Theta = 20°$. $N = 18$.

The optimal associated eigenfunctions $f_1^0(\theta)$ of LMZM for $k = 4$ and Simons' spherical Slepian functions for different cap sizes are shown in Fig. 5.3. From these two figures, it is easy to see that the main-lobe of LMZM moves and the peak value

lies on the left-side to the cap edge as the cap colatitude increases. However, the spherical Slepian function shows better spatial concentration than LMZM, though roughly when $\Theta > 65°$ it tends to concentrate its energy away from the North pole [91]. For $k = 4$, the optimal function with minimum GMAM is shown in Fig. 5.2 with "$k = 4$, GMAM" and it is invariant by definition.
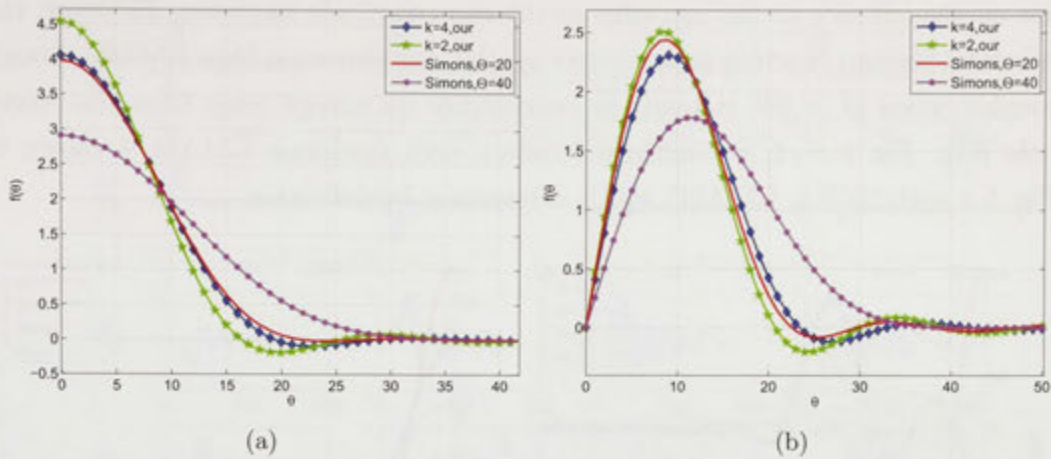

(a) (b)
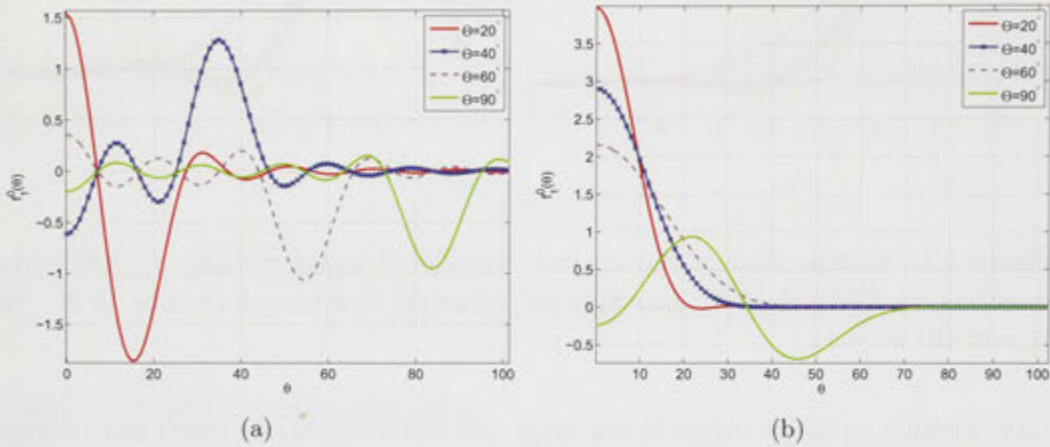
Figure 5.3: The optimal associated eigenfunctions $f_{(1)}^{(0)}(\theta)$ correspond to LMZM and Simons' spherical Slepian functions in the different cap. (a) LMZM and (b) spherical Slepian function. $N = 18$.

Fig. 5.4, Fig. 5.5 and Fig. 5.6 show our optimal associated eigenfunctions $f_{(1)}^{(m)}(\theta)$ with maximal local 4th moment zenithal measure (LMZM) in the cap $[0, 20°]$ and minimal global 4th moment azimuthal measure (GMAM) on the whole sphere along with Simons' spherical Slepian function with the maximal energy concentration measure in the cap $[0, 20°]$ for $m = 0$ to $m = N$. Apparently, the function for GMAM has a good spatial concentration region in the $[0, 20°]$ colatitude region. It also shows that as m increases, both GMAM eigenfunctions and the spherical Slepian functions leak their energy to the south hemisphere. However, the tails of GMAM decay much faster than Simons' as $m > 3$, which means the important eigenfunctions (those with most of the energy in the spatial region) of Simons' method are less than GMAM. Further, the optimal associated eigenfunction with LMZM has less energy concentration in the cap than that of GMAM and the spherical Slepian function; and it also has a similar side-lobe to Simons' Slepian function, both of which are worse than that of GMAM. Further, the side-lobes of both the function with LMZM and the spherical Slepian function decay more slowly than the optimal function with GMAM.

Finally, the first four optimal spatial functions $f_{(j)}^{(m)}(\theta, \phi)$ of the three measures considered for $m = 0, 1$ and $j = 1, 2, 3, 4$ on the unit sphere are shown in the

Our, k=4,Θ=20°, m=0-N
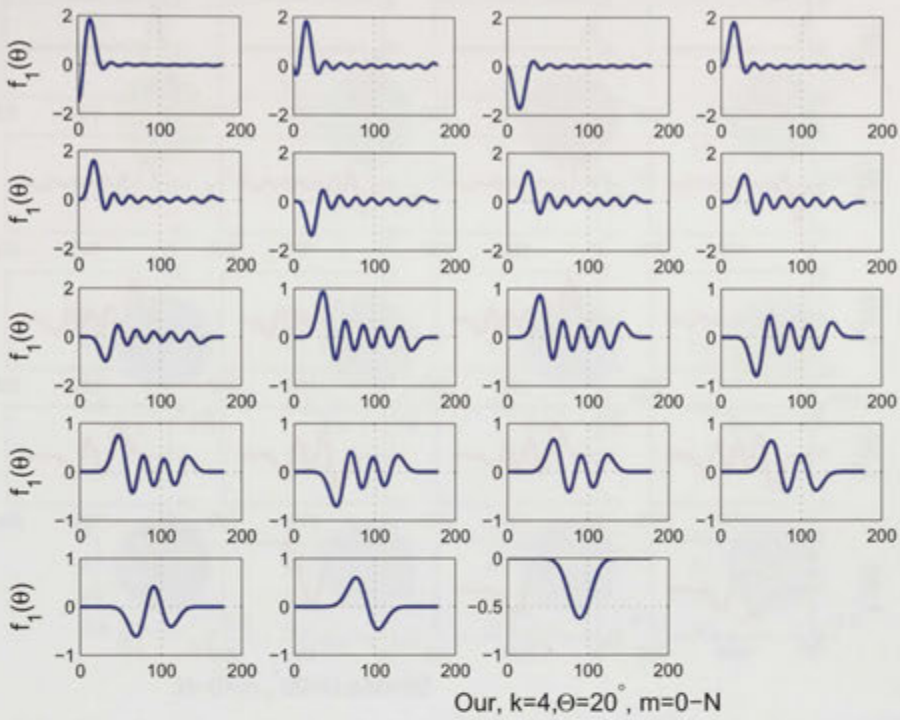
Figure 5.4: The optimal associated eigenfunctions $f_{(1)}^m(\theta)$ with the maximal local 4th moment zenithal measure (LMZM) (5.4) in the cap $[0, 20°]$. $N = 18$.

Our, k=4, m=0-N
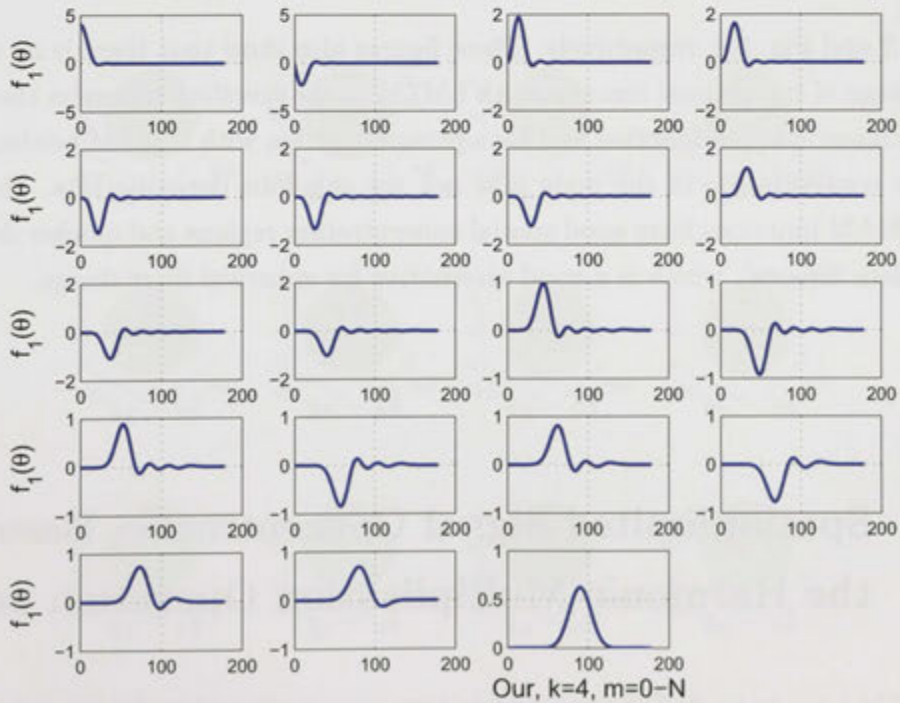
Figure 5.5: The optimal associated eigenfunctions $f_{(1)}^m(\theta)$ with the minimal global 4th moment azimuthal measure (GMAM) (5.3) on the whole sphere. $N = 18$.
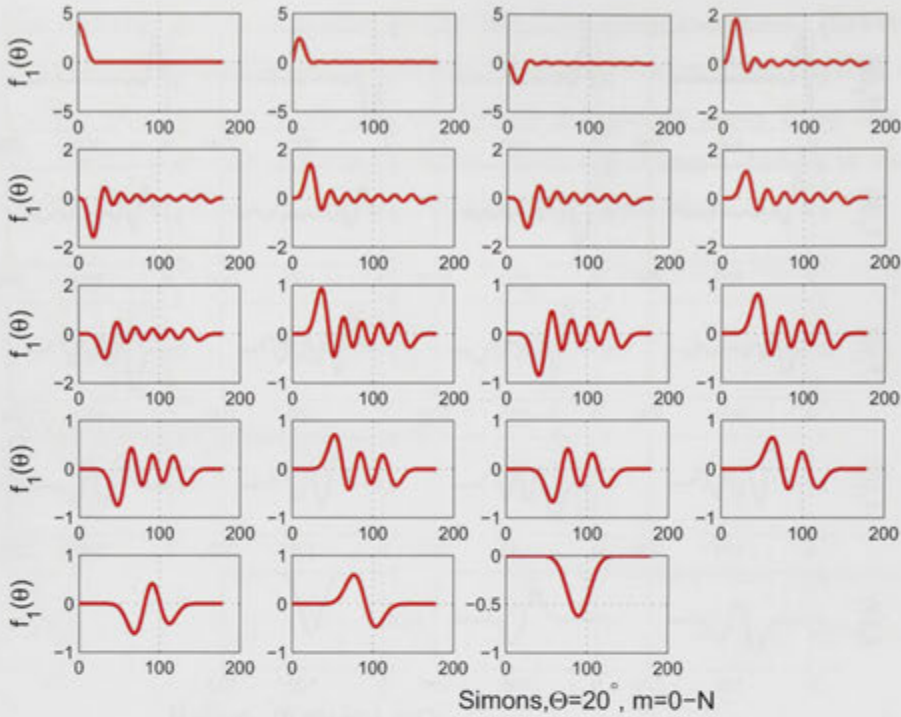
Figure 5.6: Simons' spherical Slepian functions $f_{(1)}^m(\theta)$ with the maximal energy concentration measure in the cap $[0, 20°]$. $N = 18$.

Fig. 5.7 and Fig. 5.8, respectively. These figures also show that there is no notable advantage of the optimal function with LMZM in the specified region on the sphere over Simons' Slepian function and the optimal function with GMAM neither in the energy concentration in the main lobe nor the side-lobe decaying rate. However, the GMAM functions have good spatial concentration regions and quicker decaying tails than Simons', which is a good alternative for spherical filter design.

5.3 Spatial-limited Signal Concentration Based on the Harmonic Multiplication Operation on $\mathbb{S}^2$

In this section, the focus is on the energy concentration of a spatial-limited signal f under a weighting function of v based on the harmonic multiplication operation given in the Section 4.3, Chapter 4.
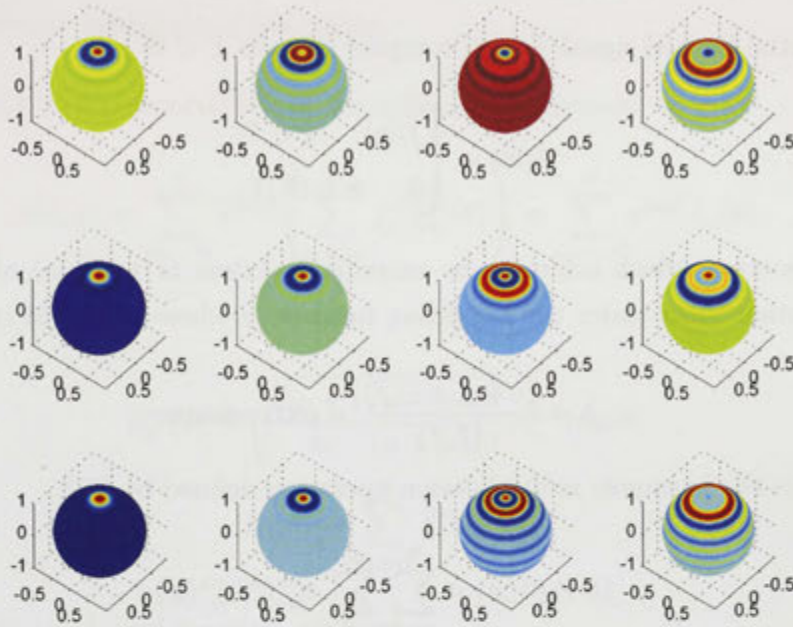
Figure 5.7: The first four Optimally spatial functions $f_{(i)}^{(m)}(\theta, \phi)$ of our LMZM and
GMAM when $k = 4$ and Simons' spherical Slepian function in the cap $[0, 20°]$ for
$m = 0$. The top row is our LMZM, the middle row is GMAM and the bottom is
Simons'.
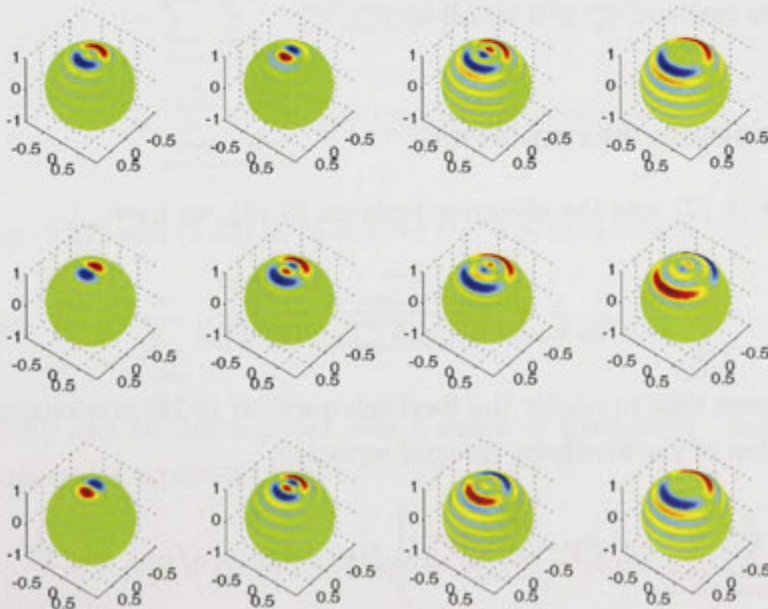
Figure 5.8: The first four Optimally spatial functions $f_{(i)}^{(m)}(\theta, \phi)$ of our LMZM and
GMAM when $k = 4$ and Simons' spherical Slepian function for $m = 1$ in the cap
$[0, 20°]$. The top row is our LMZM, the middle row is GMAM and the bottom is
Simons'.

5.3.1 Problem Statement

For a spatial-limited signal f with compact support $\Gamma \subset \mathbb{S}^2$,

$$f(\boldsymbol{x}) = \begin{cases} f(\boldsymbol{x}), & \boldsymbol{x} \in \Gamma; \\ 0, & \boldsymbol{x} \in \mathbb{S}^2/\Gamma, \end{cases} \tag{5.15}$$

we seek some f which achieves the extrema (maxima or minima) of the energy concentration ratio under the weighting function v whose spherical coeffients are positive,

$$\lambda = \frac{\langle v \odot f, v \odot f \rangle}{\langle f, f \rangle} = \textbf{extremum}, \tag{5.16}$$

where $\odot$ is the harmonic multiplication operation defined by [38],

$$(v \odot f)(\boldsymbol{x}) = \sum_{n=0}^{N} \sum_{m=-n}^{n} v_n^m f_n^m Y_n^m(\boldsymbol{x}). \tag{5.17}$$

Here, the spectral-limited function v is given by

$$v(\boldsymbol{x}) = \sum_{n=0}^{N} \sum_{m=-n}^{n} v_n^m Y_n^m(\boldsymbol{x}), \tag{5.18}$$

where v_n^m are real and $v_n^m \geq 0$ for all n, m.

5.3.2 Problem Formulation

Substituting (5.17) into the objective function (5.16), we have

$$\lambda = \frac{\sum_{n=0}^{N} \sum_{m=-n}^{n} |v_n^m f_n^m|^2}{\sum_{n=0}^{\infty} \sum_{m=-n}^{n} |f_n^m|^2}. \tag{5.19}$$

It is well known that to render the Rayleigh quotient (5.16) stationary, $f(\boldsymbol{x})$ must be the solution of the Fredholm integral equation,

$$\int_{\Gamma} \left[\sum_{n=0}^{N} \sum_{m=-n}^{n} |v_n^m|^2 Y_n^m(\boldsymbol{x}) \overline{Y_n^m(\boldsymbol{y})} \right] f(\boldsymbol{y}) \, ds(\boldsymbol{y}) = \lambda f(\boldsymbol{x}), \, \boldsymbol{x} \in \Gamma. \tag{5.20}$$

Denote the integral kernel as

$$D(\boldsymbol{x}, \boldsymbol{y}) = \sum_{n=0}^{N} \sum_{m=-n}^{n} |v_n^m|^2 Y_n^m(\boldsymbol{x}) \overline{Y_n^m(\boldsymbol{y})}. \tag{5.21}$$

For the simple calculation, we restrict the region to the polar cap $[0, \Theta]$, where Θ is the maximum colatitude of the region.

According to the separability of the spherical harmonics, we have

$$f(\theta, \phi) = \sum_{m=-N}^{N} e^{im\phi} \left(\sum_{n=|m|}^{N} f_n^m S_n^m(\theta) \right) = \sum_{m=-N}^{N} e^{im\phi} f_m(\theta), \tag{5.22}$$

where

$$S_n^m(\theta) = \sqrt{\frac{2n+1}{4\pi} \frac{(n-|m|)!}{(n+|m|)!}} \, P_n^{|m|}(\cos\theta), \tag{5.23}$$

$$f_m(\theta) = \sum_{n=|m|}^{N} f_n^m S_n^m(\theta). \tag{5.24}$$

Similarly, for the kernel function, we have

$$
\begin{aligned}
D(\boldsymbol{x}, \boldsymbol{y}) &= D(\theta, \phi, \theta', \phi') \\
&= \sum_{n=0}^{N} \sum_{m=-n}^{n} |v_n^m|^2 S_n^m(\theta) e^{im\phi} \overline{S_n^m(\theta')} e^{im\phi'} \\
&= \sum_{n=0}^{N} \sum_{m=-n}^{n} |v_n^m|^2 S_n^m(\theta) \overline{S_n^m(\theta')} e^{im\phi} e^{-im\phi'} \\
&= \sum_{m=-N}^{N} \sum_{n=|m|}^{N} |v_n^m|^2 S_n^m(\theta) \overline{S_n^m(\theta')} e^{im\phi} e^{-im\phi'}.
\end{aligned}
\tag{5.25}
$$

Substituting (5.22) and (5.25) in (5.20), for $0 \le \theta \le \Theta$, we have

$$\sum_{m=-N}^{N} e^{im\phi} \int_0^{\Theta} 2\pi \sum_{n=|m|}^{N} |v_n^m|^2 S_n^m(\theta) S_n^m(\theta') f_m(\theta') \sin\theta' \, d\theta' = \lambda \sum_{m=-N}^{N} e^{im\phi} f_m(\theta).$$

That is, (5.20) can be decomposed into a series of fixed-order, one-dimensional Fredholm eigenvalue equations [33],

$$\int_0^{\Theta} D(\theta, \theta') f_m(\theta') \sin\theta' \, d\theta' = \lambda f_m(\theta), \quad 0 \le \theta \le \Theta, \tag{5.27}$$

where $-N \le m \le N$ and the kernel

$$D(\theta, \theta') = 2\pi \sum_{n=|m|}^{N} |v_n^m|^2 S_n^m(\theta) S_n^m(\theta'). \tag{5.28}$$

Solving the integral equation (5.27), the optimally associated spatial-limited function $f_m(\theta)$ for fixed m is obtained,

$$f_m(\theta, \phi) = f_m(\theta)e^{im\phi}. \tag{5.29}$$

From here, we can conclude that the optimally spatial-limited function that maximizes the concentration ratio (5.16) is only related to the spectral degree n for fixed m. Therefore, only the variable n in the weighting coefficients v_n^m has some effect to the optimal eigenfunction $f_m(\theta)$. In the following, we take special values of v_n^m as examples to solve the corresponding optimal functions and discuss their properties.

5.3.3 $v_n^m = 1$ for all $0 \leq n \leq N$ and $-n \leq m \leq n$

This case has been well studied in [31–33], and the measure λ is the maximum energy concentrated in the spectral interval $[0, N]$ for a spatial-limited function f, that is,

$$\lambda = \frac{\sum_{n=0}^{N}\sum_{m=-n}^{n}|f_n^m|^2}{\sum_{n=0}^{\infty}\sum_{m=-n}^{n}|f_n^m|^2} = \textbf{maximum}. \tag{5.30}$$

The optimal signals are called the spherical prolate spheroidal wave functions (PSWFs), or the spherical Slepian functions.

5.3.4 $v_n^m = (\frac{n+1}{N+1})^k$ for all $0 \leq n \leq N$ and $-n \leq m \leq n$

Just like the bandwidth moment weighting in the frequency domain [34, 61, 76], we formulate the spectrum weighting on the unit sphere.

Take $v_n^m = (\frac{n+1}{N+1})^k, k = 1, 2, \cdots$. It should be noted that $k = 0$ is the special case of $v_n^m = 1$. The objective function in this case is changed into

$$\lambda = \frac{\sum_{n=0}^{N}\sum_{m=-n}^{n}(\frac{n+1}{N+1})^{2k}|f_n^m|^2}{\sum_{n=0}^{\infty}\sum_{m=-n}^{n}|f_n^m|^2} = \textbf{maximum}. \tag{5.31}$$

As we have proved before, it is equivalent to solve

$$\int_0^{\Theta} \left(2\pi \sum_{n=|m|}^{N} \left(\frac{n+1}{N+1}\right)^{2k} S_n^m(\theta)S_n^m(\theta')\right) f_m(\theta')\sin\theta'\,d\theta' = \lambda f_m(\theta). \tag{5.32}$$

We use Gaussian-legendre quadrature method [95] to solve the above integral equation and find the associated eigenfunctions.

5.3.5 Numerical Examples

Take $N = 18$ and $\Theta = 40°$ for convenient comparison with the spherical Slepian functions presented in [33]. We also take $k = 0, 1, 2$ as examples to study the properties of the optimal functions.

Fig. 5.9 shows the normalized eigenfunctions $f_m(\theta)$ with maximum concentration ratio λ for $m = 0$ and their corresponding squared spherical harmonic coefficients $(f_n^0)^2$. Fig. 5.9 shows that: 1) the optimal waveform of $f_0(\theta)$ does not vary much as k increases; 2) the peak value of the optimal functions moves to the right as k increases; 3) most of the energy of the optimal function concentrated in the first spectral degree $[0, 18]$ for all k; and 4) the spherical harmonic spectrum decays faster as k increases, but the decaying rate is much slower than that of the spherical Slepian function, which is a different result to the time-frequency case [34]. The non-zero value for $f_0(\theta)$ when $k \geq 1$ at the boundary $\Theta = 40$ also shows the limitation of the Gaussian-legendre quadrature method for inverse problems. A similar situation is shown in Fig. 5.10 for $m = 1$. However, the calculation error this time is much larger, for $f_1(40°) = -0.0495$ for $k = 1$ and $f_1(40°) = -0.0615$ for $k = 2$.

(a)   (b)
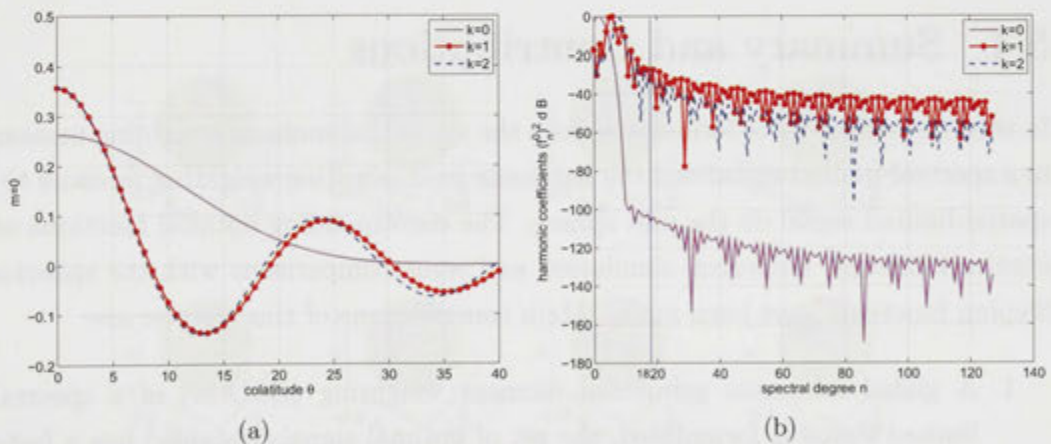
Figure 5.9: The normalized eigenfunctions $f_m(\theta)$ with the maximum concentration ratio $\lambda_k = 0.9999, 0.7155, 0.5802$ under different weighting $v_n^m = (\frac{n+1}{N+1})^k$ for varied $k = 0, 1, 2$. Here, $m = 0$. $k = 0$ corresponds to the spherical Slepian function.

Fig. 5.11 shows the corresponding normalized optimally associated spatial-limited functions $f_m(\theta, \phi)$ with the first four maximum concentration ratios λ for $m = 0$ and $m = 1$. Obviously, these figures show that the functions obtained from the v_n^m weighting have more side lobes than the spherical Slepian function and the increasing k has little effect on the spatial-limited signals. Fig. 5.12 shows the normalized optimally associated spatial-limited function $f_m(\theta, \phi)$ with the maximal concentration ratio under the weighting $v_n^m = (\frac{n+1}{N+1})^k$ for $k = 0, 1$ from $m = 0$ to
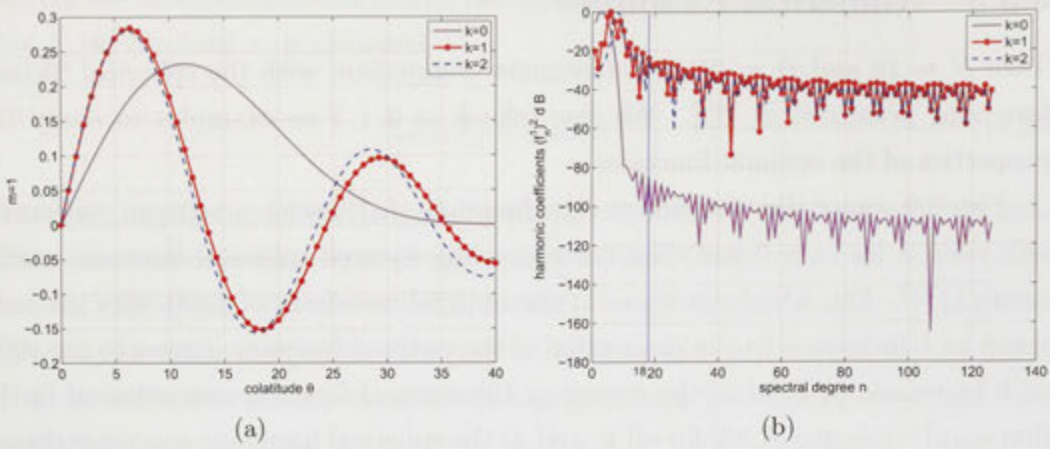
Figure 5.10: The normalized eigenfunctions $f_m(\theta)$ with the maximum concentration ratio $\lambda_k = 0.9999, 0.7023, 0.5836$ under different weighting $v_n^m = \left(\frac{n+1}{N+1}\right)^k$ for varied $k = 0, 1, 2$. Here, $m = 1$. $k = 0$ corresponds to the spherical Slepian function.

$m = 11$. It is easy to see that these two functions approach the same as m increases up to 7.

5.4 Summary and Contributions

In this chapter, we have formulated both the azimuthal moment weighting measure to a spectral-limited signal and the harmonic multiplication weighting measure to a spatial-limited signal on the unit sphere. The corresponding optimal functions are obtained through numerical simulation and some comparisons with the spherical Slepian functions have been made. Main contributions of this chapter are:

1. A global minimum azimuthal moment weighting (GMAM) of a spectral-limited signal is formulated; the set of optimal signals obtained has a faster decaying side lobe and good spatial concentration in comparison to the spherical Slepian functions [93];

2. A local minimum zenithal moment weighting (LMZM) of a spectral-limited signal is also formulated; in contrast to the optimal functions of GMAM and the spherical Slepian functions, the peak values or the main lobes of the optimal functions of LMZM are moving as the cap increases; other than that, no other obvious advantages are found [94];

3. An arbitrary spectral-limited function weighted to a spatial-limited function by the harmonic multiplication operation is formulated; simulation results

(a)

(b)
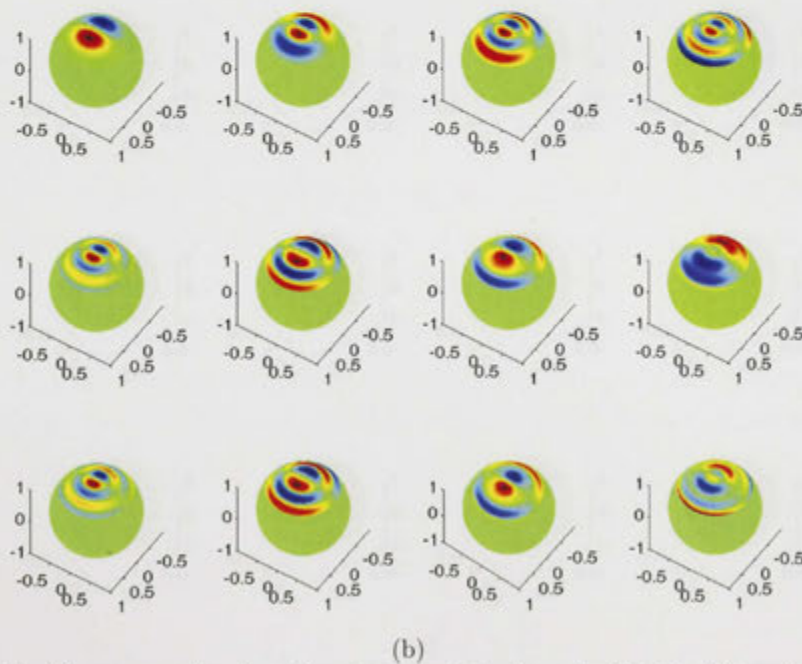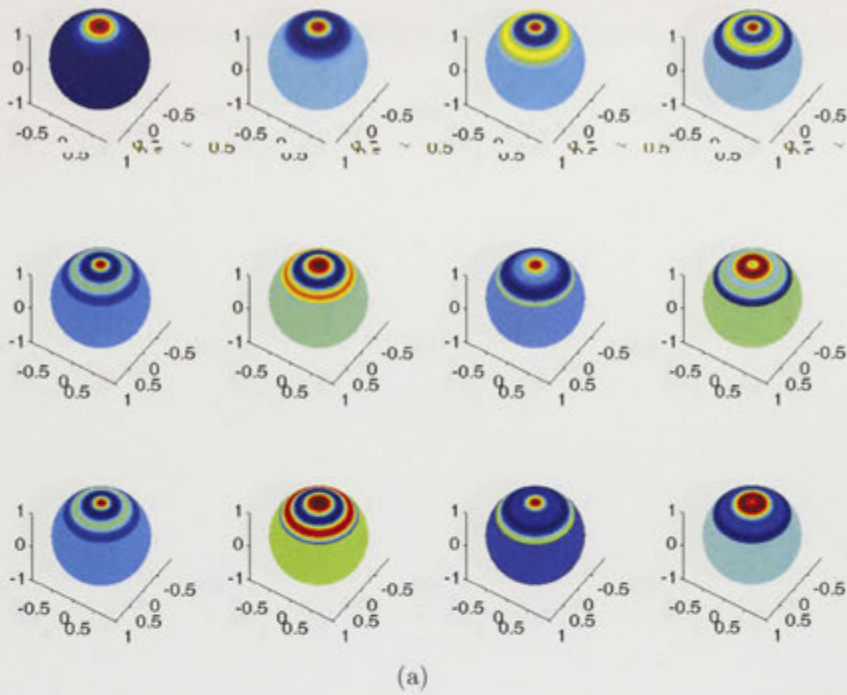
Figure 5.11: The normalized optimally associated spatial-limited functions $f_m(\theta, \phi)$ with the first four maximum concentration ratio under different weighting $v_n^m = (\frac{n+1}{N+1})^k$ for varied $k = 0, 1, 2$. $k = 0$ for the top line, $k = 1$ for the middle and $k = 2$ for the bottom. (a) $m = 0$ and (b) $m = 1$. $k = 0$ corresponds to the spherical Slepian function.
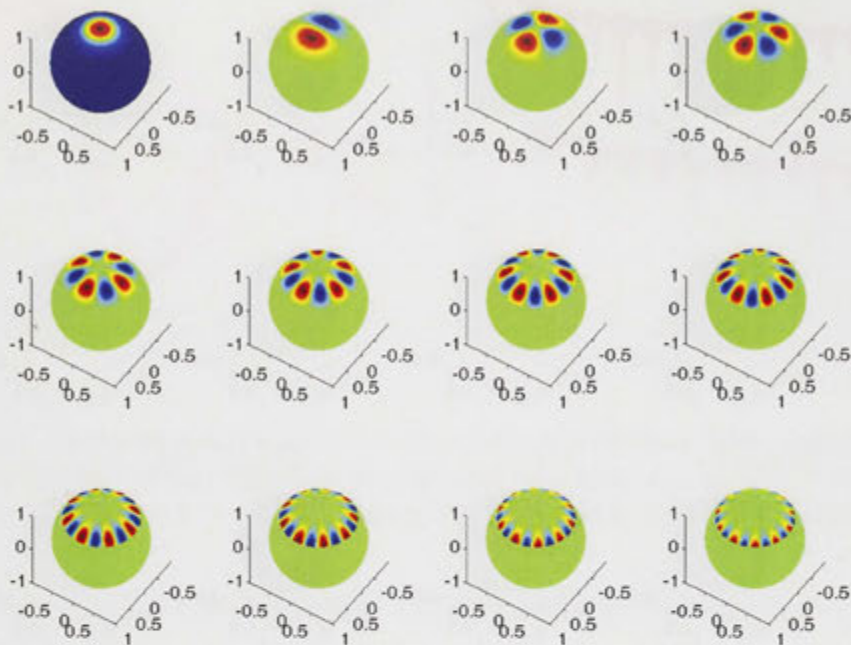
(a)
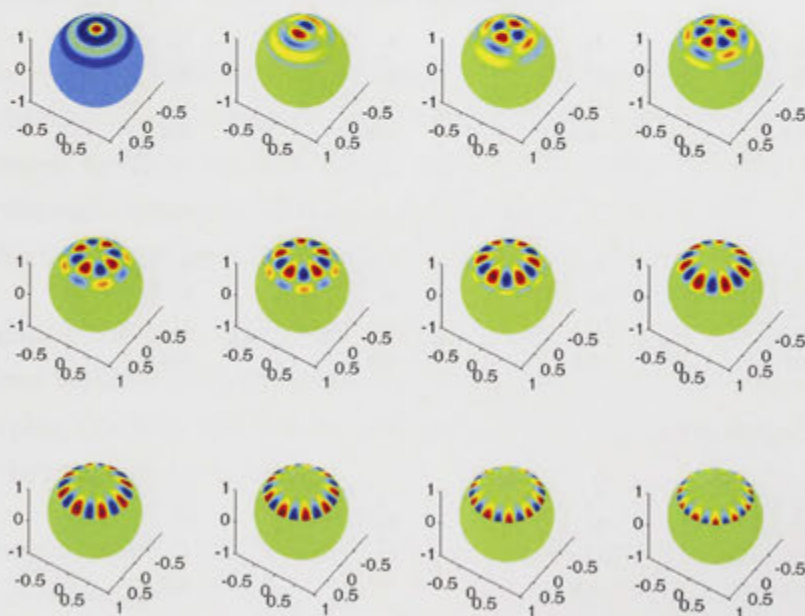
(b)

Figure 5.12: The normalized optimally associated spatial-limited functions $f_m(\theta, \phi)$ with the maximal concentration ratio for fixed m obtained from the weighting $v_n^m = \left(\frac{n+1}{N+1}\right)^k$ from $m = 0$ to $m = 11$. m increases from left to right and from top to bottom. (a) $k = 0$ and (b) $k = 1$. $k = 0$ corresponds to the spherical Slepian function.

show that the spherical spectrum of the obtained optimal function has slower decaying side lobe than that of the spherical spectrum of the spherical Slepian function [96], which is a totally different result to the time-frequency case [34].

Chapter 6

Spherical Convolution and Signal Reconstruction on $\mathbb{S}^2$

The present chapter develops results towards a systematic theory for signal processing on the unit sphere, including filtering, smoothing and estimation. In this chapter, one novel spherical convolution theorem based on a linear operator that combines tow rotations of the filter function defined on the unit sphere into a quadratic functional, which not only exhibits a well defined spherical harmonic characterization, but also specializes the isotropic convolution. Further, a simple reconstruction approach using the spherical harmonic multiplication is proposed, where a simple calculation method is shown comparing with the existing reconstruction algorithms.

Section 6.2 reviews the existing convolution theorem in the time-frequency domain. Section 6.3 recalls several existing spherical convolution formulations on the unit sphere. Further, the shortcomings of the corresponding spherical convolution formulations are pointed out. Section 6.4 proposes a spherical full isotropic convolution theorem based on a linear operator by a quadratic functional, which not only specializes isotropic convolution, but also relaxes some requirements of the spherical filters. Theoretical reconstruction algorithms by the existing spherical convolutions are discussed in Section 6.5. Finally, Section 6.6 reconstructs the original signal by the harmonic multiplication operation based on the analysis-synthesis filter idea.

6.1 Introduction

Unit sphere signal processing is an increasingly active area of research, such as smoothing and denoising in computer vision [13, 15, 97], spectral analysis in geophysics [11, 33], power spectrum estimation in cosmology [36, 40, 43, 44] and wireless

channel modeling and 3D beamforming/sensing [6, 79, 98]. Among these applications, linear convolution, corresponding to the filtering operation, is among the most fundamental operations. However, the convolution on the unit sphere is not consistently well defined.

In Euclidean space, for any two complex-valued functions f and g defined on the real line $\mathbb{R}$, the linear convolution is defined by

$$(f * g)(t) = \int_{\mathbb{R}} g(t - \tau) f(\tau) \, d\tau. \tag{6.1}$$

Convolution on the Euclidean space satisfies commutation, i.e., $f * g = g * f$. The convolution theorem states that convolution, or filtering, in the time domain corresponds to multiplication in the frequency domain. However, for functions defined on the unit sphere, the analogy of the frequency domain is to consider the spherical harmonic expansion. Therefore, multiplication in the spherical harmonic Fourier coefficients should also have the analogy of multiplication in the frequency domain. Further, translation in the time domain changes into rotation on the unit sphere.

At present, there exist three different approaches to define the spherical convolution: 1) isotropic convolution [36–38], 2) left convolution [35], and 3) spherical correlation [39]. These definitions are not consistently well defined compared with the linear convolution theorem in the Euclidean space. In addition, these definitions implicitly have some other extra requirements: isotropic convolution needs the filter axisymmetric, and spherical correlation, which strictly is not considered as a convolution due to the convolved values lying on the rotation group $SO(3)$, requires a rotation operation which needs high computation cost, and one projection back procedure. For the left convolution, though it has a simple spherical harmonic characterization which makes computation very easy, only the zonal part of spherical coefficients of the filter are used, that is to say, some non-zonal part information is lost.

In this chapter, we propose a novel spherical convolution theorem by defining a linear operator that combines two rotated functions from one fixed arbitrary filter function defined on the unit sphere, which specializes the isotropic convolution without axisymmetric requirement to the spherical filter. Comparing with the left convolution, our convolution theorem not only holds some of the same qualitative features with a in a non-trivial way difference, but also keeps all the information of the spherical filter. We also show the spherical harmonic multiplication operation can not be considered as a kind of isotropic convolution. Further, the spherical

harmonic multiplication operation is considered as a kind of anisotropic convolution and is used to reconstruct, or equalization, the original signal based on the analysis-synthesis filter method.

6.2 Convolution on Euclidean Space

Suppose f and g are complex-valued functions on $\mathbb{R}^d$, d-dimensional vector space over $\mathbb{R}$, then their convolution is given by

$$(f * g)(\boldsymbol{x}) = \int_{\mathbb{R}^d} f(\boldsymbol{y}) g(\boldsymbol{x} - \boldsymbol{y}) \, d\boldsymbol{y} \tag{6.2}$$

$$= \int_{\mathbb{R}^d} f(\boldsymbol{x} - \boldsymbol{y}) g(\boldsymbol{y}) \, d\boldsymbol{y}. \tag{6.3}$$

Here, $\boldsymbol{x} = (x_1, x_2, \cdots, x_d)$. Obviously, convolution satisfies the commutation property in the Euclidean space. Introduce an integral operator $\mathcal{G}$, then the convolution can be expressed as

$$(\mathcal{G}f)(\boldsymbol{x}) = (f * g)(\boldsymbol{x}) = \int_{\mathbb{R}^d} g(\boldsymbol{x} - \boldsymbol{y}) f(\boldsymbol{y}) \, d\boldsymbol{y}. \tag{6.4}$$

Obviously, the convolution kernel in the Euclidean space is $g(\boldsymbol{x} - \boldsymbol{y})$. We denote the Fourier transform of f by $\mathcal{F}(\cdot)$, which is defined by

$$F(\boldsymbol{\xi}) = (\mathcal{F}f)(\boldsymbol{x}) = \int_{\mathbb{R}^d} f(\boldsymbol{x}) e^{-i\boldsymbol{\xi} \cdot \boldsymbol{x}} \, d\boldsymbol{x}. \tag{6.5}$$

Theorem 6.2.1 *Convolution Theorem: For both $f, g \in \mathbb{R}^d$, the Fourier transform of the convolution is the **pointwise product** of the Fourier transforms:*

$$\mathcal{F}(f * g) = \mathcal{F}(f) \cdot \mathcal{F}(g). \tag{6.6}$$

6.3 Convolution on $\mathbb{S}^2$

6.3.1 Isotropic Convolution on $\mathbb{S}^2$

In Section 4.3.2 we have defined the isotropic convolution between function $f \in L^2(\mathbb{S}^2, ds)$ and an axisymmetric function $h \in \mathcal{F}^0(\mathbb{S}^2, ds)$ as

$$(\mathcal{K}_h f)(\boldsymbol{x}) = (h \circledast f)(\boldsymbol{x}) = \int_{\mathbb{S}^2} K_h(\boldsymbol{x} \cdot \boldsymbol{y}) f(\boldsymbol{y}) \, ds(\boldsymbol{y}),$$

where $K_h(\boldsymbol{x} \cdot \boldsymbol{y}) = \sum_{n=0}^{\infty} h_n^0 \sqrt{\frac{4\pi}{2n+1}} \sum_{m=-n}^{n} Y_n^m(\boldsymbol{x}) \overline{Y_n^m(\boldsymbol{y})}$. The isotropic convolution theorem is given by

$$\left(\widehat{h \circledast f}\right)_n^m = \sqrt{\frac{4\pi}{2n+1}} h_n^0 f_n^m,$$

where $h_n^0 = \langle h, Y_n^0 \rangle$ and $f_n^m = \langle f, Y_n^m \rangle$.

From this definition, we can observe that:

1. The filter function h must be axisymmetric, and the convolved function is also on the unit sphere.

2. Isotropic convolution does not satisfy the commutation property, i.e., $h \circledast f \neq f \circledast h$.

3. Isotropic convolution differs from the classical linear convolution theorem (6.6) due to the scaling factor $\sqrt{\frac{4\pi}{2n+1}}$.

6.3.2   Left Convolution on $\mathbb{S}^2$

The left convolution on the sphere is developed by Driscoll and Healy [35],

$$\left(\mathcal{R}_f h\right)(\boldsymbol{x}) = (f \star h)(\boldsymbol{x}) = \left(\int_{g \in SO(3)} f(g\eta) \mathcal{R}_g \, dg\right) h(\boldsymbol{x})$$

$$= \int_{g \in SO(3)} f(g\eta) h(g^{-1}\boldsymbol{x}) \, dg, \tag{6.9}$$

where $f, h \in L^2(\mathbb{S}^2, ds)$, η is the north pole, $\mathcal{R}$ is the rotation operator defined in Section 2.4.2 and g is a rotation element on the rotation group $SO(3)$.

Theorem 6.3.1 *Left Convolution Theorem on $\mathbb{S}^2$: For functions $h, f \in L^2(\mathbb{S}^2, ds)$, the Fourier transform of the left convolution is a pointwise product of the transforms:*

$$\left(\widehat{f \star h}\right)_n^m = 2\pi \sqrt{\frac{4\pi}{2n+1}} h_n^0 f_n^m, \tag{6.10}$$

where $f_n^m = \langle f, Y_n^m \rangle$ and $h_n^0 = \langle h, Y_n^0 \rangle$.

This definition shows that:

1. The left convolution integrated on $SO(3)$ can be understood to be analogous to the convolution on Euclidean space after substituting translation with

rotation,

$$(f \star h)(\boldsymbol{x}) = \int_{SO(3)} f(\rho \boldsymbol{\eta}) h(\rho^{-1} \boldsymbol{x}) \, d\rho$$

$$= \int_{SO(3)} [\mathcal{R}_{\rho^{-1}} f(\boldsymbol{\eta})] \, [\mathcal{R}_{\rho} h(\boldsymbol{x})] \, d\rho.$$

The above equation also equivalently shows that only the points of the function f at the north pole, $f(\boldsymbol{\eta})$, is considered in the integration on $SO(3)$. Due to the rotation invariant property at the north pole, all the spherical Fourier coefficients of f_n^m are kept without effect from the integration, while different situation happens to h_n^m, where only h_n^0 is rotation invariant. The 2π factor is from the all rotations.

2. The left convolution is not commutative, i.e., $h \star f \neq f \star h$.

3. Some part of the information, h_n^m with $m \neq 0$, is lost.

4. Except a scaling factor 2π, the left convolution theorem is same as the isotropic convolution theorem. Or more generally, the left convolution is equivalent to the isotropic convolution when both of the filters are axisymmetric [38,97].

6.3.3 Spherical Correlation on $\mathbb{S}^2$

The spherical correlation is proposed by Wandelt and Gorski who aimed to estimate the cosmic microwave background (CMB) power spectrum in astrophysics [39],

$$\langle f, \mathcal{R}_g h \rangle = \int_{\mathbb{S}^2} \overline{[\mathcal{R}_g h](\boldsymbol{x})} f(\boldsymbol{x}) \, d\boldsymbol{x} = \int_{\mathbb{S}^2} \overline{h(g^{-1}\boldsymbol{x})} f(\boldsymbol{x}) \, d\boldsymbol{x}$$

$$= \sum_{n=0}^{\infty} \sum_{m=-n}^{n} \sum_{m'=-n}^{n} \overline{D_{mm'}^n(g)} \, \overline{h_n^{m'}} f_n^m, \tag{6.11}$$

where $f, h \in L^2(\mathbb{S}^2, ds)$, and $D_{mm'}^n(g)$ is the Wigner-D function defined in Section 2.4.3. This definition sometimes is called the spherical convolution [13]. This definition shows that:

1. The spherical correlation is not consistent with the linear convolution theorem, where both of the functions in the convolution and the finally convolved function are in the same Euclidean space. The resulting function is in $SO(3)$, except when h is an axisymmetric function which can be explained to be on the unit sphere;

2. It has close correlation to the spherical wavelet transform and is popularly applied in physics and signal processing [21, 45, 99];

3. It requires a high calculation cost to reconstruct an original signal by a dilated and rotated wavelet [3].

6.4   Full Isotropic Convolution on $\mathbb{S}^2$

As discussed above, the existing convolution definitions have some shortcomings: 1) for the isotropic convolution, the spherical filter has to be axisymmetric and it also causes "parallel lines to be blurred into a single line" [100]; 2) for the left convolution, the function of interest must be centered on the north pole, which is not practical in applications due to the difficulty of implementation; 3) for the spherical correlation, the resulting function is on $SO(3)$, so an additional projection procedure is needed to project the intermediate function back to the sphere.

Therefore, it is desirable to set up a new definition for the spherical convolution, which applies to any function of interest and the spherical filter and in which the convolved function lies on the unit sphere. Motivated by the left convolution [35], the filter bank design idea [13] and the optimal filter design on the unit sphere [18, 42, 45, 101], a spherical full isotropic convolution theorem induced by a new operator is proposed, which 1) has no requirements to the functions participated in the operation, or simply, no extra rotation before the convolution is needed, 2) no information is lost.

6.4.1   Kernel Function

Without loss of generality, assume $h \in L^2(\mathbb{S}^2, ds)$ to be a spherical filter. Let $\mathcal{D}_h$ be an operator with kernel function $D_h(\boldsymbol{x}, \boldsymbol{y})$. Define

$$D_h(\boldsymbol{x}, \boldsymbol{y}) = \int_{SO(3)} \overline{h(\rho^{-1}\boldsymbol{y})} h(\rho^{-1}\boldsymbol{x}) \, d\rho. \tag{6.12}$$

Theorem 6.4.1

$$D_h(\boldsymbol{x}, \boldsymbol{y}) = \sum_{n=0}^{\infty} \sum_{m=-n}^{n} \sum_{m'=-n}^{n} \frac{8\pi^2}{2n+1} |h_n^m|^2 Y_n^{m'}(\boldsymbol{x}) \overline{Y_n^{m'}(\boldsymbol{y})} \tag{6.13}$$

$$= \sum_{n=0}^{\infty} \sum_{m=-n}^{n} 2\pi |h_n^m|^2 P_n(\boldsymbol{x} \cdot \boldsymbol{y}), \tag{6.14}$$

where $h_n^m = \langle h, Y_n^m \rangle$, and $P_n(\cdot)$ are the Legendre polynomials.

Proof

According to (2.28), we have

$$h(\rho^{-1}\boldsymbol{x}) = \sum_{q=0}^{\infty}\sum_{p=-q}^{q}\sum_{p'=-q}^{q} h_q^p D_{p'p}^q(\rho) Y_q^{p'}(\boldsymbol{x}),$$

$$h(\rho^{-1}\boldsymbol{y}) = \sum_{n=0}^{\infty}\sum_{m=-n}^{n}\sum_{m'=-n}^{n} h_n^m D_{m'm}^n(\rho) Y_n^{m'}(\boldsymbol{y}).$$

Substituting them into the definition of the kernel function (6.12), we have

$$D_h(\boldsymbol{x},\boldsymbol{y})$$

$$= \int_{SO(3)} \overline{\sum_{n=0}^{\infty}\sum_{m=-n}^{n}\sum_{m'=-n}^{n} h_n^m D_{m'm}^n(\rho) Y_n^{m'}(\boldsymbol{y})} \sum_{q=0}^{\infty}\sum_{p=-q}^{q}\sum_{p'=-q}^{q} h_q^p D_{p'p}^q(\rho) Y_q^{p'}(\boldsymbol{x}) \, d\rho$$

$$= \sum_{n=0}^{\infty}\sum_{m=-n}^{n}\sum_{m'=-n}^{n}\sum_{q=0}^{\infty}\sum_{p=-q}^{q}\sum_{p'=-q}^{q} \overline{h_n^m} h_q^p \overline{Y_n^{m'}(\boldsymbol{y})} Y_q^{p'}(\boldsymbol{x}) \int_{SO(3)} \overline{D_{m'm}^n(\rho)} D_{p'p}^q(\rho) \, d\rho.$$

By the Peter-Weyl theorem on compact groups that $D_{mm'}^n(\rho)$ forms an orthogonal basis on the Hilbert space $L^2(SO(3), d\rho)$ [13, 56, 57],

$$\int_{SO(3)} D_{m'm}^n(\rho)\overline{D_{p'p}^q(\rho)} \, d\rho = \frac{8\pi^2}{2n+1}\delta_{nq}\delta_{mp}\delta_{m'p'}, \tag{6.15}$$

Therefore,

$$D_h(\boldsymbol{x},\boldsymbol{y})$$

$$= \sum_{n=0}^{\infty}\sum_{m=-n}^{n}\sum_{m'=-n}^{n}\sum_{q=0}^{\infty}\sum_{p=-q}^{q}\sum_{p'=-q}^{q} \overline{h_n^m} h_q^p \overline{Y_n^{m'}(\boldsymbol{y})} Y_q^{p'}(\boldsymbol{x}) \frac{8\pi^2}{2n+1}\delta_{nq}\delta_{mp}\delta_{m'p'}$$

$$= \sum_{n=0}^{\infty}\sum_{m=-n}^{n}\sum_{m'=-n}^{n} \frac{8\pi^2}{2n+1}|h_n^m|^2 \overline{Y_n^{m'}(\boldsymbol{y})} Y_n^{m'}(\boldsymbol{x})$$

$$= \sum_{n=0}^{\infty}\sum_{m=-n}^{n} 2\pi |h_n^m|^2 P_n(\boldsymbol{x}\cdot\boldsymbol{y}),$$

where, in the last equation, we have used the addition theorem of the spherical harmonics,

$$\sum_{m=-n}^{n} Y_n^m(\boldsymbol{x})\overline{Y_n^m(\boldsymbol{y})} = \frac{2n+1}{4\pi}P_n(\boldsymbol{x}\cdot\boldsymbol{y}). \qquad \square$$

Comparing with the isotropic convolution kernel (6.17), if we let

$$\alpha_n = 2\pi \sum_{m=-n}^{n} |h_n^m|^2, \tag{6.17}$$

which is a function of the variable n, then

$$D_h(\boldsymbol{x}, \boldsymbol{y}) = \sum_{n=0}^{\infty} \alpha_n P_n(\boldsymbol{x} \cdot \boldsymbol{y}) \tag{6.18}$$

is an isotropic kernel function. Therefore, $D_h(\cdot)$ can be expressed in terms of a univariate function and

$$\alpha_n = \sqrt{\frac{2n+1}{4\pi}} \langle D_h, Y_n^0 \rangle. \tag{6.19}$$

The kernel function is also commutative: $D_h(\boldsymbol{x}, \boldsymbol{y}) = D_h(\boldsymbol{y}, \boldsymbol{x})$.

6.4.2 Spherical Full isotropic Convolution

The full isotropic convolution on the unit sphere is defined by

$$(\mathcal{D}_h f)(\boldsymbol{x}) = \int_{\mathbb{S}^2} D_h(\boldsymbol{x}, \boldsymbol{y}) f(\boldsymbol{y}) \, ds(\boldsymbol{y}). \tag{6.20}$$

Theorem 6.4.2 *Spherical Full isotropic Convolution Theorem: For any $f, h \in L^2(\mathbb{S}^2, ds)$, the Fourier transform of the full convolution on the unit sphere is:*

$$\widehat{(\mathcal{D}_h f)}_n^m = \sum_{m'=-n}^{n} \frac{8\pi^2}{2n+1} |h_n^{m'}|^2 f_n^m = \frac{4\pi}{2n+1} \alpha_n f_n^m, \tag{6.21}$$

where $\mathcal{D}_h$ is an operator with a kernel function (6.12) and $\alpha_n = 2\pi \sum_{m=-n}^{n} |h_n^m|^2$ given by (6.17).

Proof
Using the definition of convolution, this is

$$(\mathcal{D}_h f)(\boldsymbol{x}) = \int_{\mathbb{S}^2} D_h(\boldsymbol{x}, \boldsymbol{y}) f(\boldsymbol{y}) \, ds(\boldsymbol{y})$$

$$= \int_{\mathbb{S}^2} \left(\sum_{n=0}^{\infty} \sum_{m=-n}^{n} \sum_{m'=-n}^{n} \frac{8\pi^2}{2n+1} |h_n^m|^2 Y_n^{m'}(\boldsymbol{x}) \overline{Y_n^{m'}(\boldsymbol{y})} \right) \left(\sum_{q=0}^{\infty} \sum_{p=-q}^{q} f_q^p Y_q^p(\boldsymbol{y}) \right) ds(\boldsymbol{y})$$

$$= \sum_{n=0}^{\infty} \sum_{m=-n}^{n} \sum_{m'=-n}^{n} \sum_{q=0}^{\infty} \sum_{p=-q}^{q} \frac{8\pi^2}{2n+1} |h_n^m|^2 f_q^p Y_n^{m'}(\boldsymbol{x}) \int_{\mathbb{S}^2} \overline{Y_n^{m'}(\boldsymbol{y})} Y_q^p(\boldsymbol{y}) \, ds(\boldsymbol{y})$$

$$= \sum_{n=0}^{\infty} \sum_{m=-n}^{n} \sum_{m'=-n}^{n} \sum_{q=0}^{\infty} \sum_{p=-q}^{q} \frac{8\pi^2}{2n+1} |h_n^m|^2 f_q^p Y_n^{m'}(\boldsymbol{x}) \delta_{nq} \delta_{m'p}$$

$$= \sum_{n=0}^{\infty} \sum_{m=-n}^{n} \sum_{m'=-n}^{n} \frac{8\pi^2}{2n+1} |h_n^m|^2 f_n^{m'} Y_n^{m'}(\boldsymbol{x}).$$

According to the Fourier transform on the unit sphere (2.20), this is

$$\widehat{(\mathcal{D}_h f)}_n^{m'} = \sum_{m=-n}^{n} \frac{8\pi^2}{2n+1} |h_n^m|^2 f_n^{m'}.$$

After changing the notation of m' by m, there has no affect to the deduction. Let $\alpha_n = 2\pi \sum_{m=-n}^{n} |h_n^m|^2$, the proof is done. $\square$

Remark 6.1 *Comparing with the spherical diffusion smoothing which uses the left convolution theorem with a axisymmetric Gaussian kernel $z_n = e^{-n(n+1)kt}$ [15, 38], the bandwidth is controlled by a continuous spatial frequency kt, while the bandwidth of our full convolution is discrete due to α_n which is controlled by m.*

As the multiplication in the spectral spherical coefficients domain acts as an low pass filter, so when we use the full convolution in the practical applications, it is necessary to pay attention on the detailed values of the bandwidths of f and h. Suppose the allowable bandwidths of f and h are $[Bf_{min}, Bf_{max}]$ and $[Bh_{min}, Bh_{max}]$, respectively. According to the spherical full isotropic convolution theorem, for any spectral degree $0 \leq n \leq N$, the Fourier coefficients of the convolved function must satisfy

$$\max(Bf_{min}, Bh_{min}) \leq n \leq \min(Bf_{max}, Bh_{min}). \tag{6.23}$$

Corollary 6.4.1 *If the spherical filter function h is an axisymmetric function, then the full isotropic convolution is a kind of isotropic convolution.*

Proof

Since h is axisymmetric, $h(\boldsymbol{x}) = \sum_{n=0}^{\infty} h_n^0 Y_n^0(\boldsymbol{x})$ with $h_n^m = h_n^0 \delta_{m0}$. Therefore, the kernel function is isotropic,

$$D_h(\boldsymbol{x}, \boldsymbol{y}) = \sum_{n=0}^{\infty} 2\pi |h_n^0| P_n(\boldsymbol{x} \cdot \boldsymbol{y}). \tag{6.24}$$

And the full convolution is given by

$$(\mathcal{D}_h f)(\boldsymbol{x}) = \sum_{n=0}^{\infty} \sum_{m=-n}^{n} \frac{8\pi^2}{2n+1} |h_n^0|^2 f_n^m Y_n^m(\boldsymbol{x}). \tag{6.25}$$

$\square$

Remark 6.2 *Comparing with the isotropic convolution, the left convolution and the spherical harmonic multiplication, the full convolution has the following characteristics:*

1. *No special requirement for the spherical filter functions is needed.*

2. *No information is lost.*

3. *Does not conform to the classical convolution Theorem 6.2.1, where the full convolution is using the absolute square of the Fourier transform of the filters.*

4. *A special case of the isotropic convolution.*

6.5   Theoretical Reconstruction Based on Existing Spherical Convolution

Recovering or reconstructing original signals defined on the unit sphere based on sampled data is a practical problem in geophysics, cosmology and medical image processing. At present, most of the reconstructions are based on the outputs from the continuous spherical wavelet transform [88], left convolution [35] or isotropic convolution [49] between the function of interest and the spherical filter. However, for the left convolution, the function of interest has to be centered on the north pole; for the isotropic convolution, the spherical filter is axisymmetric; while for the spherical wavelet transform, the resulting function is on $SO(3)$, not on $\mathbb{S}^2$. Further, these reconstructions involve huge computation cost.

Actually, no matter what kind of convolution is used, the key point is whether this analysis filter can capture the full or at least most of the important information of the function of interest, such as component separation and feature detection, and further whether this convolution can provide an easy and exact reconstruction method to recover the original signal based on the convolved result. Of course, it still relates to the convenient realization of the spherical (analysis and synthesis) filters.

6.5.1   Reconstruction Based on Isotropic Convolution

The isotropic convolution is well defined on the unit sphere [36–38]. It is commonly used in astrophysics that convolves an axisymmetric beam function $h(\boldsymbol{x}) =$

$\sum_{n=0}^{\infty} h_n^0 Y_n^0(\boldsymbol{x})$ (h is regarded as an analysis filter) with the sky function f,

$$d = (h \circledast f)(\boldsymbol{x}) = \int_{\mathbb{S}^2} h(\boldsymbol{x} \cdot \boldsymbol{y}) f(\boldsymbol{y}) \, ds(\boldsymbol{y})$$

$$= \sum_{n=0}^{\infty} \sum_{m=-n}^{n} \sqrt{\frac{4\pi}{2n+1}} h_n^0 f_n^m Y_n^m(\boldsymbol{x}).$$

It is well known that the observed signal is contaminated with noise and the sampled data is discrete. Usually, a map-making procedure [48] based on the sampled data is operated to construct the sky map. Here, for simplicity, we consider the map-making is perfect and no noise is added, that is, d is the exact continuous intermediate analysis result. For the discrete reconstruction, it has been discussed in the paper [49].

Therefore, to recover the original signal f, a synthesis filter $\tilde{h}$ (azimuthal function) is used,

$$T = (\tilde{h} \circledast d)(\boldsymbol{x}) = \sum_{n=0}^{\infty} \sum_{m=-n}^{n} \sqrt{\frac{4\pi}{2n+1}} \tilde{h}_n^0 d_n^m Y_n^m(\boldsymbol{x})$$

$$= \sum_{n=0}^{\infty} \sum_{m=-n}^{n} \frac{4\pi}{2n+1} \tilde{h}_n^0 h_n^0 f_n^m Y_n^m(\boldsymbol{x}).$$

If the reconstruction is exact, that is, $T = f = \sum_{n=0}^{\infty} \sum_{m=-n}^{n} f_n^m Y_n^m$, it is only possible when

$$\frac{4\pi}{2n+1} \tilde{h}_n^0 h_n^0 = 1, \implies \tilde{h}_n^0 = \frac{2n+1}{4\pi} \frac{1}{h_n^0}. \tag{6.26}$$

Based on this definition, the calculation is simple. However, this method has a strict requirement of the spherical filter – axisymmetric about the north pole, which is very hard to be implement in practice. Therefore, some non-circular beam function or some isotropic assumption for the power spectrum of the function of interest is needed [40], which distorts the accuracy of the measurements and the computational cost is also increased.

6.5.2 Reconstruction Based on Left Convolution

It has been shown that there is only a scale factor 2π difference between the isotropic convolution and the left convolution. Therefore, the reconstruction is similar as the isotropic convolution. However, the shortcomings of this method, except the disadvantages given to the isotropic convolution, are that the function of interest f must be centered at the north pole and only the h_n^0 part is contributable.

6.5.3 Reconstruction Based on Spherical Correlation

According to (6.11), the spherical correlation between the function of interest and a rotated beam function b is given by

$$
\begin{aligned}
S(g) = \langle f, \mathcal{R}_g b \rangle &= \int_{\mathbb{S}^2} \overline{[\mathcal{R}_g b](\boldsymbol{x})} f(\boldsymbol{x})\, ds(\boldsymbol{x}) \\
&= \sum_{n=0}^{\infty} \sum_{m=-n}^{n} \sum_{m'=-n}^{n} \overline{D_{m'm}^n(g)\, \overline{b_n^m} f_n^{m'}},
\end{aligned}
\tag{6.27}
$$

As we have stated that this convolved result $S(g)$ lies on $SO(3)$, not on the unit sphere $\mathbb{S}^2$, therefore, a back projection procedure with conformal mapping is desired, where extra computation cost is added.

Suppose $\tilde{b}$ is a synthesis filter. Based on the inverse spherical convolution definition [13],

$$
\hat{f}(\boldsymbol{x}) = \int_{SO(3)} [\mathcal{R}_g \tilde{b}](\boldsymbol{x})\, S(g)\, dg = \sum_{n=0}^{\infty} \sum_{m=-n}^{n} \sum_{m'=-n}^{n} \frac{8\pi^2}{2n+1} b_n^{m'} \overline{\tilde{b}_n^{m'}} f_n^m Y_n^m(\boldsymbol{x}),
$$

the reconstruction is obtained if and only if

$$
\frac{8\pi^2}{2n+1} \sum_{m'=-n}^{n} b_n^{m'} \overline{\tilde{b}_n^{m'}} = 1.
\tag{6.28}
$$

Exact quadrature, including the equal-angular lat-lon grid sampling [35], Gauss-Legendre sky pixelization (GLESP) [102] and the generalized sampling theorem [13], exists for this method. However, the computation is complicated and the cost is high due to the rotation operation and the Wigner-D functions.

6.5.4 Reconstruction Based on Spherical Wavelet Transform

The spherical wavelet transform for the function of interest f and a rotated and dilated spherical wavelet Ψ is defined by [88]

$$
\begin{aligned}
W_\Psi^f(g, a)(\theta, \phi) &= \langle f, \mathcal{R}(g)\mathcal{D}(a)\Psi \rangle \\
&= \int_{\mathbb{S}^2} f(\theta, \phi), \overline{\Psi_{g,a}(\theta, \phi)} \sin\theta\, d\theta\, d\phi \\
&= \sum_{n=0}^{\infty} \sum_{m=-n}^{n} \sum_{m'=-n}^{n} f_n^m \overline{[\Psi_a]_n^{m'}}\, \overline{D_{mm'}^n(g)},
\end{aligned}
\tag{6.29}
$$

where $\mathcal{D}$ is the dilation operator [3,99] defined in Section 2.5.2 and Ψ_a is the dilated spherical wavelet

$$\Psi_a = \frac{1 + \tan^2\frac{\theta}{2}}{1 + (\frac{1}{a}\tan\frac{\theta}{2})^2} \times \frac{1}{a}\Psi\left(2\tan^{-1}(\frac{1}{a}\tan\frac{\theta}{2}), \phi\right).$$

The resulting function lies on $SO(3)$, though which could be considered on the unit sphere when Ψ is an axisymmetric function. Therefore, the equivalence between the harmonic multiplication theorem and the spherical correlation is only obtained when Ψ is axisymmetric.

The reconstruction of the original signal f is given by

$$f(\theta, \phi) = \int_{\mathbb{R}^+} d\mu(a) \int_{SO(3)} dg W_\Psi^f(g, a)[\mathcal{R}_g \mathcal{L}_\Psi \Psi_a](\theta, \phi), \qquad (6.31)$$

if and only if the admissibility condition is satisfied,

$$0 < C_\Psi^n = \frac{8\pi^2}{2n+1} \sum_{m=-n}^{n} \int_{\mathbb{R}^+} |(\Psi_a)_n^m|^2 \frac{da}{a^3} < \infty. \qquad (6.32)$$

Here, the operator $\mathcal{L}_\Psi$ is defined as $\mathcal{L}_\Psi f_n^m = f_n^m / C_\Psi^n$.

Using this definition, it is easy to detect some features or separate components of f through the rotation and dilation to a mother wavelet. However, looking at (6.32), though the theoretical reconstruction is ensured through the integration on the continuous dilation factor a, exact quadrature rules do not exist for it. Therefore, a discretization of the dilation factor is required [3]. Further, even using the kernel dilation method [3], where the reconstruction is exact, it is still relating to the integration where high calculation cost is required. This is why most of the papers at present are restricted to the case where the spherical wavelet is an axisymmetric functions [13, 49, 99].

6.6 Reconstruction Based on Harmonic Multiplication Operation on $\mathbb{S}^2$

Due to the difficulty in implementing the isotropic convolution and the high computational cost of the spherical correlation, it is desired to develop another reconstruction method with less computation and higher quantity recovery performance. In this section, since the harmonic multiplication can be regarded as a kind of anisotropic convolution from the operator concept. It is used to reconstruct the

original signal based on the sampled points. The analysis-synthesis filter bank concept [3, 13, 49] is used.

6.6.1   Theoretical Reconstruction Based on the Harmonic Multiplication Operation

We use the anisotropic property of the harmonic multiplication operation to analyze and synthesize the function of interest. Theoretical reconstruction based on the harmonic multiplication operation is verified. And the simplified calculation is also shown.

From the operator concept or the system theory, if we suppose h is an arbitrary asymmetric function, which is to be an analysis filter, f is the function of interest, such as the sky, then according to the harmonic multiplication operation, we have

$$I = h \odot f = \int_{S^2} K_h(\boldsymbol{x}, \boldsymbol{y}) f(\boldsymbol{y}) \, ds(\boldsymbol{y}) = \sum_{n=0}^{\infty} \sum_{m=-n}^{n} h_n^m f_n^m Y_n^m(\boldsymbol{x}).$$

It is well known that constructing an axisymmetric beam is hard and all of the practical beam in the measurements are non-axisymmetric or non-circular [39, 40]. In our scheme, h is asymmetric which is easily to be realized; further, the intermediate result I is still on the unit sphere, where no back projection procedure in the synthesis is required. Therefore, the calculation would be reduced.

To recover the original signal, we need to convolve the analysis result I with a spherical synthesis filter $\tilde{h}$. Of course, some intermediate procedures are needed, such as denoising and discrete sampling. However, for simplicity, we suppose there is no noise in the synthesis procedure. It is easy to realize the synthesis,

$$g = I \odot \tilde{h} = \sum_{n=0}^{\infty} \sum_{m=-n}^{n} I_n^m \tilde{h}_n^m Y_n^m = \sum_{n=0}^{\infty} \sum_{m=-n}^{n} h_n^m \tilde{h}_n^m f_n^m Y_n^m. \tag{6.34}$$

For the exact reconstruction, that is $g = f = \sum_{n=0}^{\infty} \sum_{m=-n}^{n} f_n^m Y_n^m$, we only need

$$h_n^m \tilde{h}_n^m = 1. \tag{6.35}$$

That is, $\tilde{h}_n^m = 1/h_n^m$. Therefore, we have

$$\tilde{h}(\boldsymbol{x}) = \sum_{n=0}^{\infty} \sum_{m=-n}^{n} \tilde{h}_n^m Y_n^m \boldsymbol{x} = \sum_{n=0}^{\infty} \sum_{m=-n}^{n} \frac{1}{h_n^m} Y_n^m \boldsymbol{x}. \tag{6.36}$$

In this method, it is only the multiplication of the spherical harmonic coefficients

between the function of interest and the spherical filter, no additional requirement is needed. Therefore, the calculation cost is greatly reduced in contrast with the isotropic convolution, the spherical correlation and the spherical wavelet transform methods.

6.6.2   Analysis Results

According to the spherical harmonic transform, a function on the unit sphere cannot simultaneously have finite support both in the spatial domain and the spectral domain. For a spatial-limited signal on the unit sphere, it occupies infinite spherical harmonic coefficients, which is impossible for the practical implementation and then a truncation procedure to finite spherical modes is always made. Therefore, a spectral-limited function is always used in the simulation.

In this section, we take some special functions of h to analyze the function of interest f. For simplicity, we assume that the maximum spectral degree of both f and h are $N = 5$. According to the harmonic multiplication definition, even the spectral degree of one of these two functions are larger than 5, its spherical harmonic coefficients would be truncated by another 0 spherical harmonic coefficients. We also assume that the spherical harmonic coefficients f_n^m are given by

$$f = \sum_{n=0}^{5} \sum_{m=-n}^{n} f_n^m Y_n^m,$$

where $f_0^0 = 1, f_1^{-1} = 2, f_1^0 = 3, f_1^1 = 4, \cdots, f_5^5 = 36$. Three special analysis filters are also assumed:

1. h is an axisymmetric function with $h_n^m = \delta_{m0}$,

$$h_1 = \sum_{n=0}^{5} Y_n^0. \tag{6.38}$$

2. h is not an axisymmetric function, but all of its elements equal to 1,

$$h_2 = \sum_{n=0}^{5} \sum_{m=-n}^{n} Y_n^m. \tag{6.39}$$

3. The spherical harmonic coefficients of h are $h_n^m = n + |m| + 1$,

$$h_3 = \sum_{n=0}^{5} \sum_{m=-n}^{n} (n + |m| + 1) Y_n^m. \tag{6.40}$$

According to the harmonic multiplication operation,

$$I = \sum_{n=0}^{5} \sum_{m=-n}^{n} h_n^m f_n^m Y_n^m,$$

we have

$$I_1 = \sum_{n=0}^{5} \sum_{m=-n}^{n} f_n^0 Y_n^0,$$

$$I_2 = \sum_{n=0}^{5} \sum_{m=-n}^{n} f_n^m Y_n^m = f,$$

$$I_3 = \sum_{n=0}^{5} \sum_{m=-n}^{n} (n + |m| + 1) f_n^m Y_n^m.$$

This shows that I_1 only contains part of the information of the original signal f, I_2 is exactly the original signal and I_3 is the weighted signal.

Simulation results are shown in Fig. 6.1. In each sub-figure, the left is the original function f, the middle is the analysis filter h_i for $i = 1, 2, 3$ and the right is the corresponding analysis result I_i. Fig. 6.1(a) shows the output is also axisymmetric; in Fig. 6.1(b), the output is precisely identical to the original image; and in Fig. 6.1 (c), the output is fairly similar to the original image, especially in the important features, which might be the perspective application for the harmonic multiplication theorem.

6.6.3 Synthesis Results

In this section, we do some synthesis experiments based on the analysis results. According to the theoretical reconstruction analysis in the subsection 6.6.1, we have known that only if the spherical harmonic coefficients of the synthesis filter reverse to those of the analysis filter, the reconstruction is achieved. That is, the synthesis filters are

$$\widetilde{h}_1 = \sum_{n=0}^{5} Y_n^0,$$

$$\widetilde{h}_2 = \sum_{n=0}^{5} \sum_{m=-n}^{n} Y_n^m,$$

$$\widetilde{h}_3 = \sum_{n=0}^{5} \sum_{m=-n}^{n} \frac{1}{n + |m| + 1} Y_n^m.$$

(a)

(b)

(c)

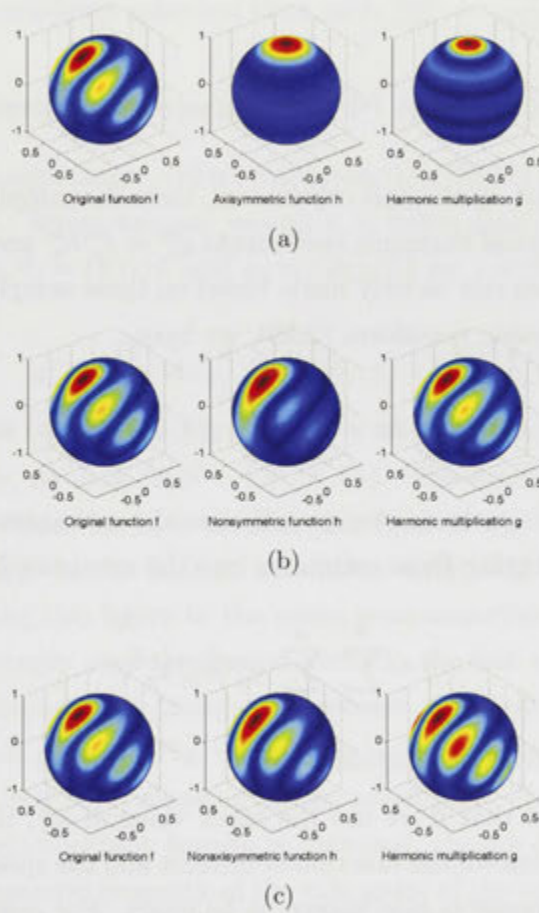Figure 6.1: (a) The original function f, the axisymmetric spherical filter h with $h_n^m = \delta_{m0}$ and the harmonic multiplication output $g = f \odot h$; (b) The original function f, the non-axisymmetric spherical filter h with $h_n^m = 1$ and the harmonic multiplication output $g = f \odot h$; (c) The original function f, the arbitrary spherical filter h with $h_n^m = n + |m| + 1$ and the harmonic multiplication output $g = f \odot h$.

Theoretical reconstruction in the subsection 6.6.1 does not need the sampling algorithms. However, in reality, we usually obtain some distributed data. Therefore, the reconstruction is discretized and some exact quadrature rules are need. In this chapter, we use three sampling algorithms: equidistant cylindrical projection (ECP) [99], equal-angular sampling method [35] and Gauss-Legendre sky pixelization (GLESP) [102]. The first method is only approximated and the later two are exact quadrature rules.

Reconstruction

As we have stated that, in the real experiment, only the sampling values of $g(\theta, \phi)$ are obtained, its spherical harmonic coefficients $g_n^m = f_n^m h_n^m$ are not known. Therefore, the reconstruction can be only made based on these sample points. According to the spherical harmonic transform (2.20), we have

$$g_n^m = \int_{\mathbb{S}^2} g(\boldsymbol{x})\overline{Y_n^m(\boldsymbol{x})}\,d\boldsymbol{x} = \int_0^{2\pi}\int_0^{\pi} g(\theta, \phi)\overline{Y_n^m(\theta, \phi)}\,\sin\theta\,d\theta\,d\phi.$$

And when we do the synthesis, we actually use the estimates of g_n^m. Denote the estimates $\hat{g}_n^m$. Substituting these estimates into the synthesis formula,

$$\hat{g} = \sum_{n=0}^{N}\sum_{m=-n}^{n} \hat{g}_n^m[\widetilde{h}]_n^m Y_n^m,$$

we obtain the reconstructed function.

It should be noted that if we use the exact value of g_n^m, the reconstruction is exact. Since we have known the function of interest and the spherical filters exactly, the actual synthesis result is also known to be exact. For comparison, the actual synthesis results are shown in Fig. 6.2. In the first example, we have deployed the axisymmetric function as the analysis filter which only captures the f_n^0 information of the original signal, so even if we use the right synthesis filter to the analysis filter, the synthesis result is $f_0 = \sum_{n=0}^{N} f_n^0 Y_n^0$, part of the original function, and completely different from the original signal. Therefore, we must avoid using an axisymmetric function as an analysis filter. The second and the third synthesis outputs are precisely identical to the original signal. The former is that we are using the filter with all the spherical harmonic coefficients 1, therefore, the analysis output and the synthesis output are both same as the original output. The latter is the exactly reconstructed function.
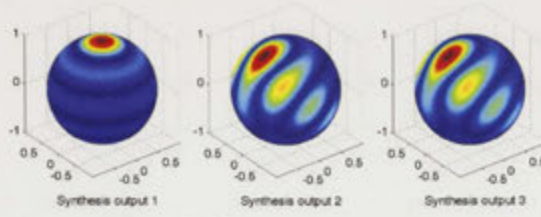
Figure 6.2: Synthesis output: (a) axisymmetric synthesis spherical filter with $[\widetilde{h}]_n^m = \delta_{m0}$; (b) non-axisymmetric synthesis spherical filter with $[\widetilde{h}]_n^m = 1$; (c) non-axisymmetric synthesis spherical filter with $[\widetilde{h}]_n^m = \frac{1}{n+|m|+1}$.

Equidistant Cylindrical Projection (ECP) Method for Reconstruction

Now we deploy the equidistant cylindrical projection (ECP) method [99] to recover the original signal. Equal angular sampling is taken and the number of sample points is L, that is, $\theta_j = (\pi j)/L$ and $\phi_j = (2\pi j/L)$ for $j = 0, 1, \cdots, L-1$, and

$$g_n^m \approx \frac{2\pi^2}{L^2} \sin(\frac{\pi}{L}) \sum_{j=0}^{L-1} g(\theta_j, \phi_j)\overline{Y_n^m(\theta_j, \phi_j)}. \tag{6.44}$$

Here, for simplicity, let $L = [2(N+1)]^2 = 144$. The synthesis results are shown in Fig. 6.3. Note that we have rotated this figure's view for easy comparison by "view([-65,65,60])" in the Matlab simulation code, but no other things have changed. Comparing this figure to the exact reconstruction result Fig. 6.2 (Here, though we have wrongly used the axisymmetric in the first example, we still think it is the exact reconstruction based on the exact spherical harmonic coefficients g_n^m), the result is not good. In Fig. 6.3 (a), the reconstructed function captures the important feature (red part) centered on the north pole. For Fig. 6.3 (b) and (c), the red part or the important feature is captured, though it has been expanded; further, the axisymmetric property of the side spots of the original function is lost. So the ECP method is quite inadequate in recovering the original signal.

Equal-angular in Lat-lon Grid Sampling for Reconstruction

The equal-angular in lat-lon grid sampling theorem [35] and the Gauss-Legendre sky pixelization (GLESP) [102] are claimed to be the exact reconstruction algorithms. In this section, we use them to recover the original signal and also verify these algorithm's performance. As the spectral degree of g is $N = 5$, to avoid the Nyquist restriction, at least $[2(N+1)]^2 = 144$ points need to be sampled to ensure the exact reconstruction. We take the number of samples $L = [2(N+1)]^2 = 144$.

For the equal-angular lat-lon grid method, according to Theorem 3 [35], the

Figure 6.3: Synthesis output based on the direct calculation: (a) axisymmetric synthesis spherical filter with $[\tilde{h}]_n^m = \delta_{m0}$; (b) non-axisymmetric synthesis spherical filter with $[\tilde{h}]_n^m = 1$; (c) non-axisymmetric synthesis spherical filter with $[\tilde{h}]_n^m = \frac{1}{n+|m|+1}$.

estimated spherical harmonic coefficients are

$$\hat{g}_n^m = \frac{\sqrt{2\pi}}{2(N+1)} \sum_{j=0}^{2N+1} \sum_{k=0}^{2N+1} a_j^{(N+1)} g(\theta_j, \phi_k) \overline{Y_n^m(\theta_j, \phi_k)}, \qquad (6.45)$$

for $n \leq N$ and $|m| \leq n$, $\theta_j = \pi j/(2(N+1))$, $\phi_k = \pi k/(2(N+1))$ and the weighting coefficients are

$$a_j^{(N+1)} = \frac{\sqrt{2}}{N+1} \sin\frac{\pi j}{2(N+1)} \sum_{l=0}^{N} \frac{1}{2l+1} \sin\frac{\pi[2l+1]j}{2(N+1)},$$

$$j = 0, 1, \cdots, 2N+1. \qquad (6.46)$$

This reconstruction is shown in Fig. 6.4. Comparing this figure to the exact reconstruction result Fig. 6.2, the result is quite good: in all of the three examples, the important information, including the red part and the axisymmetric property in Fig. 6.4 (b) and (c) is captured. However, Fig. 6.4 (a) exhibits some error, especially near the equator. Also the left bottom of the center part in both Fig. 6.4 (b) and Fig. 6.4 (c) has been elongated. Fig. 6.4 (b) shows better recovery than Fig. 6.4 (c), for the sizes of the side spot of Fig. 6.4 (c) have changed, from the originally large to small, into the small to larger presently. This might relate to the choice of the spherical filter, for we have restricted all the spherical harmonic coefficients of both the analysis and synthesis filter to 1 in the second example (Fig. 6.4 (b)), while the coefficients of the third example are nonlinear $(1+n+|m|$ and $1/(1+n+|m|)$ in Fig. 6.4 (c).
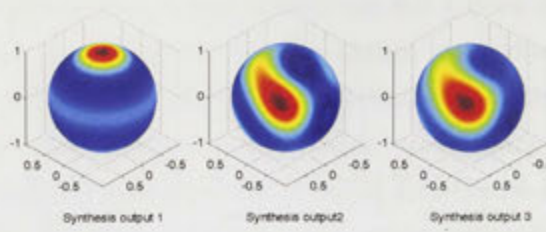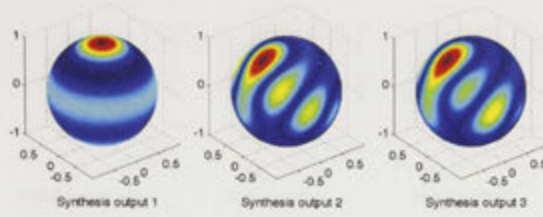
Figure 6.4: Synthesis output based on the direct calculation: (a) axisymmetric synthesis spherical filter with $[\widetilde{h}]_n^m = \delta_{m0}$; (b) non-axisymmetric synthesis spherical filter with $[\widetilde{h}]_n^m = 1$; (c) non-axisymmetric synthesis spherical filter with $[\widetilde{h}]_n^m = \frac{1}{n+|m|+1}$.

Gauss-Legendre Sky Pixelization (GLESP) for Reconstruction

For the Gauss-Legendre sky pixelization (GLESP) [102], according to

$$
\begin{aligned}
g_n^m &= \int_0^{2\pi} \int_0^{\pi} g(\theta,\phi)\overline{Y_n^m(\theta,\phi)}\sin\theta\, d\theta\, d\phi \\
&= \int_0^{2\pi} \left[\int_{-1}^{1} g(x,\phi)\overline{Y_n^m(x,\phi)}\, dx \right] d\phi \\
&= \int_0^{2\pi} \left[\sum_{j=1}^{M} w_j g(x_j,\phi)\overline{Y_n^m(x_j,\phi)} \right] d\phi \\
&\approx \frac{\pi}{M} \sum_{j=1}^{M} \sum_{k=1}^{2M} w_j g(x_j,\phi_k)\overline{Y_n^m(x_j,\phi_k)}.
\end{aligned}
\tag{6.47}
$$

In the above, we have made some operations: 1) $x_j = \cos\theta_j$; 2) the Gaussian-quadrature method [95] is used, w_j are the weighting coefficients and x_j are the net of roots of the Legendre polynomial $P_M(x_j) = 0$ where M is the maximum rank of the polynomial; 3) the Nyquist sampling theorem is also used that makes the sampling points $2M$ around the ϕ; 4) ϕ is equally sampled, $\phi_k = \pi k/M$ for $k = 1, 2, \cdots, 2M$; and 5) $M = 2(N+1)$.

According to the above operations, the number of sampling points of (θ, ϕ) are $2M^2 = [2(N+1)]^2 = 144$. But it should be noted that θ is not equally sampled. The synthesis result is shown in Fig. 6.5. Note that: in (a), the original function means the function that only contains $f_0 = \sum_{n=0}^{N} f_n^0 Y_n^0$. Comparing this figure to the exact reconstruction result in Fig. 6.2, we can see that both (a) and (b) are quite similar to the original function, which has better performance than the equal-angular sampling method; (c) does not compare well with the original function, which strangely enlarges the even side spots and also connects the first two side spots together and given them a higher value than the center spot.
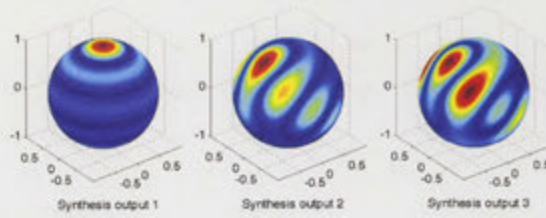
Figure 6.5: Synthesis output based on the direct calculation: (a) axisymmetric synthesis spherical filter with $[\widetilde{h}]_n^m = \delta_{m0}$; (b) non-axisymmetric synthesis spherical filter with $[\widetilde{h}]_n^m = 1$; (c) non-axisymmetric synthesis spherical filter with $[\widetilde{h}]_n^m = \frac{1}{n+|m|+1}$.

Summary

Among three sampling methods, we find the ECP sampling has the worst performance; the equal-angular lat-lon grid sampling theorem shows better performance if the spherical harmonic coefficients of the spherical filter, including the analysis and synthesis filter, are nonlinear or are functions of the spectral degree n and spectral order m; while the GLESP is better when the spherical harmonic coefficients of the spherical filter are constant. If the exact spherical coefficients of the analysis output are obtained, the exact reconstruction is realized.

6.7   Summary and Contributions

In this chapter, the classic convolution in the time-frequency is reviewed and the existing spherical convolutions are revisited; then the shortcomings of these definitions are discussed. Further, some theoretical reconstruction algorithms based on the current spherical convolutions are discussed. Based on these weak points, some specific contributions are made:

1. A novel spherical full isotropic convolution theorem based on a new operator is developed, which not only specializes the isotropic convolution, but also relaxes the requirement to the the spherical filter. Comparing with the left convolution, all the Fourier coefficients of the spherical filter are included, though the phase information is lost due to the quadratic formulation [103];

2. An simple reconstruction method based on the harmonic multiplication operation on the unit sphere is proposed by three different sampling methods [104].

Chapter 7

Conclusions and Future Research Directions

In this chapter we state the general conclusions drawn from this thesis. The summary of contributions can be found at the end of each chapter and are not repeated here. We also outline some future research directions arising from this work.

7.1   Conclusions

In this thesis, we firstly studied some further results concerning about the signal concentration in the time-frequency domain, including an orthonormal basis development and a general arbitrary signal concentration solution. Then, some analogous concentration properties, such as arbitrary moment weighting both in the special domain and in the spectral domain, were extended to the unit sphere. Furthermore, one spherical convolution theorem was developed. Finally, one simple reconstruction method on the unit sphere was proposed.

In Chapter 3, applying Franks general constrained variation method, we formulated a kth moment time-duration and bandwidth weighting measure in the time-frequency domain. A complete, orthonormal set of band-limited functions with minimum 4th moment time-duration concentration measure was obtained. Simulation results showed that this set of functions can be applied in radar system and representing any band-limited signals due to its higher energy concentration in the main lobe and fast decaying side lobes. Finally, an arbitrary signal with 2nd and 4th moment bandwidth measure were formulated and the corresponding optimal functions were obtained, which might be of use in practical waveform design.

In Chapter 4, we not only developed a harmonic multiplication operation on

the unit sphere, but also provided the equivalence with the isotropic convolution. Then some quadratic functional relating to an linear operator and its infinite matrix representation were made. Further, we also made an extension of the Franks general constrained variational method on the unit sphere. Finally, the general concentration problem on the unit sphere was solved based on the spherical Franks framework and the spherical Slepian functions.

Chapter 5 not only formulated the global azimuthal moment weighting but also the local zenithal moment weighting measures to a spectral-limited signal defined on the unit sphere. Two sets of optimal functions were obtained. Comparisons between these sets of optimal functions and the spherical Slepian functions were also made. Furthermore, the optimal solution to a spatial-limited signal with harmonic multiplication in the frequency weighting was studied.

Chapter 6 first reviewed the properties and shortcomings of the existing spherical convolutions, then proposed a new spherical full isotropic convolution, which specializes the isotropic convolution and relaxes the requirement of the spherical filter to the classical isotropic convolution and also keeps all the information. Further, the discussion to reconstruct an original signal was given. Finally, an exact reconstruction by the harmonic multiplication on the unit sphere was implemented by three different sampling methods.

7.2 Future Research Directions

In this section, we sketch out broad outlines of future research directions:

1. The prospective applications of our three set of basis functions obtained from the global minimum azimuthal moment measure on the whole sphere, the local maximum zenithal moment measure in one specified spatial region and the harmonic multiplication in the spectral weighting on one specified spatial region need to be explored, especially for the spatial filter design in geophysis [8], cosmology [49] and EEG/MEG [66] comparing with the spherical Slepian functions.

2. Surface representation and surface shape analysis can be based on the spherical basis functions in our thesis. Wavelets are the usually method to represent, denoise and smooth signal on the unit sphere [14, 97]. However, due to the sparse property and the heavy resulting calculation, it is necessary to find suitable basis functions and other methods.

3. Spherical filtering, smoothing and denoising by our spherical full isotropic convolution theorem is desirable comparing with the left convolution and the wavelet transform [90], especially the comparison to the spherical diffusion [15].

4. Using our spherical full isotropic convolution theorem, the optimal spherical filter design [19], detection some components embedded in the stochastic process [45] and estimation the power spectrum of the signal [11], is required in cosmology and geophysics.

5. Applying the uncertainty principle of minimum product of concentration measures into practical applications, a statistical reconstruction approach using a temporal-spatial model and wavelet analysis is promising from some discretely sampled data.

Appendix A

Appendices

A.1 General solution of the fourth-derivative equation

The goal is to solve the equation (3.23) with the boundary conditions $X(-W) = X(W) = 0$, $X'(-W) = X'(W) = 0$. The characteristic equation of (3.23) is

$$r^4 = \lambda. \tag{A.1}$$

As we point out that $X(f)$ is a real signal, so its fourth power is real, too, i.e., $\lambda \geq 0$. However, if $\lambda = 0$, the equation has the zero solution. Because the general solution is

$$X(f) = af^3 + bf^2 + cf + d,$$

where a, b, c and d are constants. Its first derivative is

$$X'(f) = 3af^2 + 2bf + c.$$

Substituting the boundary value $X(W) = 0$ and $X'(W) = 0$, we get $a = b = c = d = 0$. Obviously, the zero solution is not we want. So $\lambda > 0$.

For $\lambda > 0$, take $m^4 = \lambda$ and choose m positive. Then solving the characteristic equation (A.1), according to $(r - im)(r + im)(r - m)(r + m) = 0$, the general solution is

$$X(f) = A_1 e^{imf} + B_1 e^{-imf} + C_1 e^{mf} + D_1 e^{-mf},$$

where A_1, B_1, C_1 and D_1 are arbitrary constants. Due to $\cosh x = \frac{e^x + e^{-x}}{2}$, $\sinh x =$

$\frac{e^x - e^{-x}}{2}$, $\cos x = \frac{e^{ix} + e^{-ix}}{2}$ and $\sin x = \frac{e^{ix} - e^{-ix}}{2}$, the general solution can also be represented into

$$X(f) = A\cos(mf) + B\sin(mf) + E\cosh(mf) + F\sinh(mf), \quad |f| \le W,$$

where A, B, E and F are arbitrary constants. And its first derivative is

$$X'(f) = m[-A\sin(mf) + B\cos(mf) + E\sinh(mf) + F\cosh(mf)], \quad |f| \le W.$$

A.2 Special solution of the fourth-derivative equation

Based on the boundary values $X(-W) = X(W) = 0$, $X'(-W) = X'(W) = 0$ and the total energy of $I_3 = \langle x, x \rangle = \langle X, X \rangle = 1$, we get five equations:

$$X(-W) = A\cos(mW) - B\sin(mW) + E\cosh(mW) - F\sinh(mW) = 0 \quad \text{(A.5a)}$$
$$X(W) = A\cos(mW) + B\sin(mW) + E\cosh(mW) + F\sinh(mW) = 0 \quad \text{(A.5b)}$$
$$X'(-W) = m[A\sin(mW) + B\cos(mW) - E\sinh(mW) + F\cosh(mW)] = 0$$
$$\text{(A.5c)}$$
$$X'(W) = m[-A\sin(mW) + B\cos(mW) + E\sinh(mW) + F\cosh(mW)] = 0$$
$$\text{(A.5d)}$$
$$\langle X, X \rangle = \int_{-W}^{W} [A\cos(mf) + B\sin(mf) + E\cosh(mf) + F\sinh(mf)]^2 df = 1.$$
$$\text{(A.5e)}$$

We have pointed out that $m \ne 0$. Solving above equations (A.5a), (A.5b), (A.5c) and (A.5d), we get

$$A\cos(mW) + E\cosh(mW) = 0 \quad \text{(A.6a)}$$
$$B\sin(mW) + F\sinh(mW) = 0 \quad \text{(A.6b)}$$
$$A\sin(mW) - E\sinh(mW) = 0 \quad \text{(A.6c)}$$
$$B\cos(mW) + F\cosh(mW) = 0. \quad \text{(A.6d)}$$

As $\cosh(mW) \ne 0$, from equation (A.6d), we get

$$F = -B\cos(mW)/\cosh(mW).$$

Substituting F into equation (A.6b), we obtain

$$B \sin(mW) - B \cos(mW) \sinh(mW)/\cosh(mW) = 0.$$

Therefore,

$$B = 0$$

or

$$\sin(mW)\cosh(mW) - \cos(mW)\sinh(mW) = 0.$$

In sum,

- 1). When $B = 0$, from equation (A.6d), $F = 0$;

- 2). When $B \neq 0$, $\sin(mW)\cosh(mW) - \cos(mW)\sinh(mW) = 0$.

Similarly, from equations (A.6a) and (A.6c), we get:

- 1). When $A = 0$, from equation (A.6a), $E = 0$.

- 2). When $A \neq 0$, $\sin(mW)\cosh(mW) + \cos(mW)\sinh(mW) = 0$.

Therefore, when we take $B = F = 0$, due to the non-zero solution, $A \neq 0$ and $E \neq 0$ and $\sin(mW)\cosh(mW) + \cos(mW)\sinh(mW) = 0$. This case shows that $X(f)$ is an even function, i.e.,

$$X_e(f) = A\cos(mf) + E\cosh(mf).$$

When $B \neq 0$, $A = E = 0$ and $\sin(mW)\cosh(mW) - \cos(mW)\sinh(mW) = 0$. This case shows that $X(f)$ is an odd function, i.e.,

$$X_o(f) = B\sin(mf) + F\sinh(mf).$$

When $B \neq 0$ and $A \neq 0$, from $\sin(mW)\cosh(mW) + \cos(mW)\sinh(mW) = 0$ and $\sin(mW)\cosh(mW) - \cos(mW)\sinh(mW) = 0$, we get $\sin(mW) = 0$ and $\sinh(mW) = 0$. From equation (A.6a) and equation (A.6d), we get $E \neq 0$ and $F \neq 0$. Therefore, the solution for this case is the linear combination of the even solution $X_e(f) = A\cos(mf) + E\cosh(mf)$ and the odd solution $X_o(f) = B\sin(mf) + F\sinh(mf)$.

For the detailed value of A, B, C and D, substituting $X(f)$ into the equation (A.5e), we get

$$X_e(f) = A_e[\cos(mf) + \alpha\cosh(mf)],$$

where $A_e = 1/\sqrt{(1+\alpha^2)W}$, $\alpha = -\cos(mW)/\cosh(mW)$. And

$$X_o(f) = B_o[\sin(mf) + \beta \sinh(mf)],$$

where $B_o = 1/\sqrt{(1-\beta^2)W}$, $\beta = -\sin(mW)/\sinh(mW)$.

A.3 Distribution of m and m' (Theorem 3.2.1)

Proof

Let us consider the following three functions, firstly,

$$f_1(x) = \tan(x)$$
$$f_2(x) = -\tanh(x)$$
$$f_3(x) = \tanh(x).$$

As $0 \le \tanh(x) = \frac{\sinh(x)}{\cosh(x)} < 1$, for all $x \ge 0$, so the function $f_2(x)$ is a strictly monotonically increasing function with $f_2(\infty) \longrightarrow 1$; and $f_3(x)$ is a strictly monotonically decreasing function with $f_2(\infty) \longrightarrow -1$.

It is well known that: $\tan(x)$ is a periodical function with the period π, for any $k \in \mathbf{Z}$, $\tan(k\pi) = 0$, $\tan[(k\pi + \frac{\pi}{2})^-] \longrightarrow +\infty$ and $\tan[(k\pi + \frac{\pi}{2})^+] \longrightarrow -\infty$.

In a period, take $(k\pi - \frac{\pi}{2}, k\pi + \frac{\pi}{2})$, $k = 1, 2, 3, \ldots$ as an example, $\tan(x)$ monotonically increases from $-\infty$ to $+\infty$ as x increases from $k\pi - \frac{\pi}{2}$ to $k\pi + \frac{\pi}{2}$. So there must have and only have a crossing point x_{dk} with $-\tanh(x)$ in the down half of the plane. And it also has a unique crossing point x_{uk} with $\tanh(x)$ in the upper half of the plane. And the values of $x_{dk} < x_{uk}$.

Now it is necessary to show that there has no crossing point for $\tan(x)$ and $\tanh(x)$ in the interval $[0, \pi/2)$. Take another function $g(x) = f_1(x) - f_3(x) = \tan(x) - \tanh(x)$, for $x \in [0, \pi/2)$. Let take the first derivative of $g^{(1)}(x)$,

$$\begin{aligned}
g'(x) &= \frac{1}{\cos^2(x)} - \frac{1}{\cosh^2(x)} \\
&= \frac{\cosh^2(x) - \cos^2(x)}{\cosh^2(x)\cos^2(x)} \\
&= \frac{(\cosh(x) + \cos(x))(\cosh(x) - \cos(x))}{\cosh^2(x)\cos^2(x)} \\
&= \frac{\cosh(x) + \cos(x)}{\cosh^2(x)\cos^2(x)}(\cosh(x) - \cos(x)).
\end{aligned}$$

As $\cosh(x) = \frac{e^x + e^{-x}}{2} \ge 1$ for any $x \ge 0$; when $x \in [0, \pi/2)$, $0 < \cos(x) \le 1$.

Therefore,

$$g'(x) > 0.$$

So $g(x)$ is a strictly monotonically increasing function. And $g(0) = f_1(0) - f_3(0) = 0$, so in the interval $(0, \pi/2)$, $g(x) > 0$, i.e, $\tan(x) > \tanh(x)$, which means there is no crossing point between them. Fig. A.1 shows the relations between these three functions.
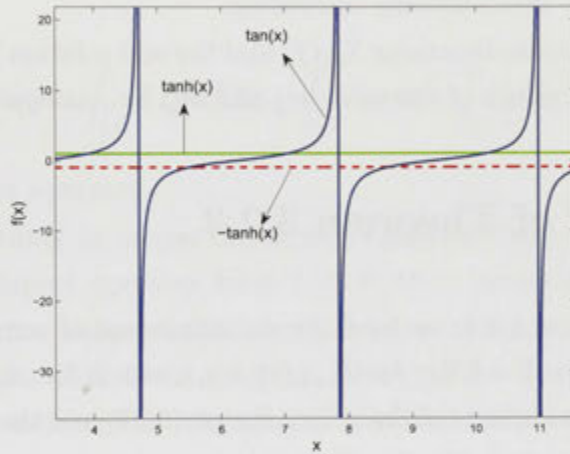
Figure A.1: The functions of $\tanh(x), -\tanh(x)$ and $\tan(x)$.

It has been proved above that in $(0, \pi/2)$, $\tan(x) > 0$, $-\tanh(x) < 0$ and $\tanh(x) > 0$ and there is no crossing point for the functions $\tan(x)$ and $\tanh(x)$. So the first crossing point x_1 is the crossing point x_{d1} of $\tan(x)$ and $-\tanh(x)$; the second crossing point x_2 is the crossing point x_{u1} of $\tan(x)$ and $-\tanh(x)$; the third crossing point x_3 is the crossing point x_{d2} of $\tan(x)$ and $-\tanh(x)$; the fourth crossing point x_4 is the crossing point x_{u2} of $\tan(x)$ and $-\tanh(x)$; and so on.

Now relating to our proof of the theorem, let us check the condition functions. For fixed W, the even condition function is

$$\cos(mW)\sinh(mW) + \sin(mW)\cosh(mW) = 0$$

and the odd condition function is

$$\cos(mW)\sinh(mW) - \sin(mW)\cosh(mW) = 0.$$

So if $\cos(mW) \neq 0$, i.e., $mW \neq (k\pi + \pi/2), k \in \mathbf{Z}$, the even condition is changed

into

$$\tan(mW) = -\tanh(mW)$$

and the odd condition is changed into

$$\tan(mW) = \tanh(mW).$$

From the above, the points $\{m_jW\}$ satisfying the even condition equation and the points $\{m_k'W\}$ satisfying the odd condition equation are interleaved, i.e, $m_1, m_1', m_2, m_2', m_3, m_3', ...$ and the values are monotonically increasing.

So the even solution functions $X_{ej}(f)$ and the odd solution functions $X_{ok}(f)$ can be ordered by the values of the value m_j and m_k', i.e., as equation (3.37) shown.$\square$

A.4   Proof of Theorem 3.2.2

Proof

From the subsection 3.2.4, we have got an infinite set of complete optimal band-limited functions $\{\psi_i\} = \{X_{ej}(f) \cup X_{ok}(f)\}, i, j, k = 1, 2, 3, ...$ in the frequency interval $[-W, W]$ which consists of the even solution (3.27) and the odd solution (3.29). The completeness is from the fact that based on the boundary conditions and the initial conditions, we have got all possible functions satisfying the fourth-order equation (3.23) by the general solution equation (3.25). Now we want to show that this set is orthonormal. The orthonormality in the frequency interval $[-W, W]$ can be obtained from two methods: 1). by direct calculation of the orthonormality between any two functions; 2). by functional analysis with spectrum theorem for the compact self-adjoint operator: the corresponding eigenfunctions for distinct eigenvalues are orthogonal.

For the eigenvalue equation (3.24), D^4 is a differential operator which is unbounded and its inverse operator does not exist. Therefore, we define another operator

$$L = D^4 + Id,$$

where Id is the identity operator. So the eigenvalue equation is changed into

$$LX = (1 + \lambda)X.$$

Now we will show that the new operator L is self-adjoint and its inverse operator L^{-1} exists.

As we have discussed before that eigenvalue equation (3.24) has a real solution if and only if $\lambda \geq 0$. And when $\lambda = 0$, the solution is zero function. Similarly, for the new eigenvalue equation (A.13), $LX = 0$ if and only if $X = 0$. So according to Theorem 4.5.2 in the book [83]: An operator L is invertible if and only if $Lu = 0$ implies $u = 0$. So L is invertible. Then its inverse operator L^{-1} exists.

Suppose $u, v \in \{\psi_i\}$, then

$$\langle Lu, v \rangle = \langle D^4 u + u, v \rangle = \int_{L^2} v(D^4 u) d\Omega + \int_{L^2} vu d\Omega = \int_{L^2} \left[u'' v'' + uv \right] d\Omega.$$

And

$$\langle v, Lu \rangle = \langle v, D^4 u + u \rangle = \int_{L^2} v(D^4 u) d\Omega + \int_{L^2} vu d\Omega = \int_{L^2} \left[u'' v'' + uv \right] d\Omega = (Lu, v).$$

So L is a self-adjoint operator.

Therefore, according to inverse differential operator Theorem 5.10.2 [83], L^{-1} is a self-adjoint compact operator from $L^2(-W, W)$. According to the Spectral theorem of self-adjoint compact operator, L^{-1} has a complete set of orthonormal eigenfunctions and its eigenvalues are real. Based on the Theorem 5.10.5 [83], L and L^{-1} have the same eigenfunctions and have the reciprocal eigenvalues. So L has an complete set of orthonormal eigenfunctions. As we also know that for distinct eigenvalues, their corresponding eigenfunctions are orthogonal.

From the Theorem 3.2.1, we have known that the values of m_j and m'_k are different. So the eigenvalues of L equaling to m^4 are different, too. Therefore, the eigenfunctions are orthogonal. As $X_e(f)$ and $X_o(f)$ are band-limited, unit energy signals, i.e., they are orthonormal. □

A.5   The Duality of Basis Functions between Two Operators

Proof

We use Grunbaum's **Lemma 1**. The assumptions about this lemma are that: suppose G is a topological group and $\hat{G}$ is its dual group; A is a compact subset of G, i.e., $A \subset G$; B is a compact subset of $\hat{G}$, i.e., $B \subset \hat{G}$; F is the Fourier transform and F^{-1} is its inverse Fourier transform; h is a function that has support on A, i.e., $Ah = h$. Then the Grunbaum's Lemma states:

Grunbaum's Lemma: If h is an eigenfunction of $AF^{-1}BFA$ with eigenvalue $\mu \neq 0$, then BFh is an eigenfunction of $BFAF^{-1}B$ with eigenvalue μ.

Now we take $A = \mathcal{D}_\Gamma$, $B = \mathcal{B}_N$, F is the spherical harmonics transform, F^{-1} is the inverse spherical harmonics transform and we have mixed F and F^{-1} into $\mathcal{D}_\Gamma$ and $\mathcal{B}_N$. Then the operator $AF^{-1}BFA$ becomes $\mathcal{D}_\Gamma\mathcal{B}_N\mathcal{D}_\Gamma$ and the operator $BFAF^{-1}B$ becomes $\mathcal{B}_N\mathcal{D}_\Gamma\mathcal{B}_N$. Then according to **Grunbaum's Lemma**, we have

$$\mathcal{D}_\Gamma\mathcal{B}_N\mathcal{D}_\Gamma h = \mu h, \tag{A.14}$$

$$\mathcal{B}_N\mathcal{D}_\Gamma\mathcal{B}_N(\mathcal{B}_N h) = \mu(\mathcal{B}_N h). \tag{A.15}$$

where h is a spatial-limited signal, i.e., $\mathcal{D}_\Gamma h = h$.

According to $\mathcal{D}_\Gamma$ definition (2.41) or (2.43) directly, we have

$$\mathcal{D}_\Gamma\mathcal{B}_N\mathcal{D}_\Gamma h = \int_\Gamma B_N(\boldsymbol{x}, \boldsymbol{y}) h(\boldsymbol{y}) \, ds(\boldsymbol{y}) = \mu h(\boldsymbol{x}), \quad \boldsymbol{x} \in \Gamma.$$

This eigenvalue equation is the same as (4.61). Therefore, $h = g_i^{(\Gamma)}(\boldsymbol{x}), i = 0, 1, \cdots,$ is the optimal spatial-function in the region Γ that achieves the maximum energy in the spectral interval $[0, N]$.

Let $f = \mathcal{B}_N h$, then f is a spectral-limited signal with maximum spectral degree N, i.e., $\mathcal{B}_N f = f$. According to (A.15), we have

$$\mathcal{B}_N\mathcal{D}_\Gamma\mathcal{B}_N f = \mu f. \tag{A.17}$$

And according to $\mathcal{B}_N$'s definition (2.38) or (2.44) directly, we get

$$
\begin{aligned}
&\mathcal{B}_N\mathcal{D}_\Gamma\mathcal{B}_N f \\
&= \int_{\mathbb{S}^2} B_N(\boldsymbol{x}, \boldsymbol{t}) \left[\chi_\Gamma(\boldsymbol{t}) \int_{\mathbb{S}^2} B_N(\boldsymbol{t}, \boldsymbol{y}) f(\boldsymbol{y}) \, ds(\boldsymbol{y}) \right] ds(\boldsymbol{t}) \\
&= \int_\Gamma B_N(\boldsymbol{x}, \boldsymbol{t}) \left[\int_{\mathbb{S}^2} B_N(\boldsymbol{t}, \boldsymbol{y}) f(\boldsymbol{y}) \, ds(\boldsymbol{y}) \right] ds(\boldsymbol{t}) \\
&= \int_{\mathbb{S}^2} \left[\int_\Gamma B_N(\boldsymbol{x}, \boldsymbol{t}) B_N(\boldsymbol{t}, \boldsymbol{y}) \, ds(\boldsymbol{t}) \right] f(\boldsymbol{y}) \, ds(\boldsymbol{y}). \tag{A.18}
\end{aligned}
$$

Using (2.39), we have

$$
\begin{aligned}
&B_N(\boldsymbol{x}, \boldsymbol{t}) B_N(\boldsymbol{t}, \boldsymbol{y}) \\
&= \sum_{n=0}^{N} \sum_{m=-n}^{n} Y_n^m(\boldsymbol{x}) \overline{Y_n^m(\boldsymbol{t})} \cdot \sum_{n'=0}^{N} \sum_{m'=-n'}^{n'} Y_{n'}^{m'}(\boldsymbol{t}) \overline{Y_{n'}^{m'}(\boldsymbol{y})} \\
&= \sum_{n=0}^{N} \sum_{m=-n}^{n} \sum_{n'=0}^{N} \sum_{m'=-n'}^{n'} \left(Y_n^m(\boldsymbol{x}) \overline{Y_{n'}^{m'}(\boldsymbol{y})} \right) \cdot \left(Y_{n'}^{m'}(\boldsymbol{t}) \overline{Y_n^m(\boldsymbol{t})} \right) \tag{A.19}
\end{aligned}
$$

Substituting (A.19) into (A.18), we have

$$
\mathcal{B}_N \mathcal{D}_\Gamma \mathcal{B}_N f
$$

$$
= \int_{\mathbb{S}^2} \sum_{n=0}^{N} \sum_{m=-n}^{n} \sum_{n'=0}^{N} \sum_{m'=-n'}^{n'} Y_n^m(\boldsymbol{x}) \overline{Y_{n'}^{m'}(\boldsymbol{y})} \left(\int_\Gamma Y_{n'}^{m'}(\boldsymbol{t}) \overline{Y_n^m(\boldsymbol{t})} \, ds(\boldsymbol{t}) \right) f(\boldsymbol{y}) \, ds(\boldsymbol{y})
$$

$$
= \sum_{n=0}^{N} \sum_{m=-n}^{n} \sum_{n'=0}^{N} \sum_{m'=-n'}^{n'} Y_n^m(\boldsymbol{x}) \left(\int_\Gamma Y_{n'}^{m'}(\boldsymbol{t}) \overline{Y_n^m(\boldsymbol{t})} \, ds(\boldsymbol{t}) \right) \int_{\mathbb{S}^2} f(\boldsymbol{y}) \overline{Y_{n'}^{m'}(\boldsymbol{y})} \, ds(\boldsymbol{y})
$$

$$
= \sum_{n=0}^{N} \sum_{m=-n}^{n} \sum_{n'=0}^{N} \sum_{m'=-n'}^{n'} Y_n^m(\boldsymbol{x}) \left(\int_\Gamma Y_{n'}^{m'}(\boldsymbol{t}) \overline{Y_n^m(\boldsymbol{t})} \, ds(\boldsymbol{t}) \right) f_{n'}^{m'}
$$

$$
= \sum_{n=0}^{N} \sum_{m=-n}^{n} \left(\sum_{n'=0}^{N} \sum_{m'=-n'}^{n'} f_{n'}^{m'} \int_\Gamma \overline{Y_n^m(\boldsymbol{t})} Y_{n'}^{m'}(\boldsymbol{t}) \, ds(\boldsymbol{t}) \right) Y_n^m(\boldsymbol{x})
$$

$$
= \mu f(\boldsymbol{x})
$$

$$
= \mu \sum_{n=0}^{N} \sum_{m=-n}^{n} f_n^m Y_n^m(\boldsymbol{x}). \tag{A.20}
$$

Then, we obtain

$$
\sum_{n'=0}^{N} \sum_{m'=-n'}^{n'} f_{n'}^{m'} \int_\Gamma \overline{Y_n^m(\boldsymbol{x})} Y_{n'}^{m'}(\boldsymbol{x}) \, ds(\boldsymbol{t}) = \mu f_n^m.
$$

Summing over all n from 0 to N and $-n \le m \le n$, we finally get

$$
\mathbf{D}_N \hat{\mathbf{f}} = \mu \hat{\mathbf{f}}. \tag{A.22}
$$

$\hat{\mathbf{f}}$ is the column vector containing the spherical harmonic coefficients of f. It proves that $\mathcal{B}_N \mathcal{D}_\Gamma \mathcal{B}_N f = \mu f$ is equivalent to $\mathbf{D}_N \hat{\mathbf{f}} = \mu \hat{\mathbf{f}}$ for $f = \mathcal{B}_N f$.

Comparing (A.22) with (4.52), it is obvious that

$$
\lambda = \mu.
$$

Since the eigenvectors $\{\hat{\mathbf{f}}_i^{(N)}\}$ and the associated eigenfunctions $\{f_i^{(N)}(\boldsymbol{x})\}$ of (4.52) are orthonormal, we also make a normalization to (A.22),

$$
\mathbf{D}_N \left(\frac{\hat{\mathbf{f}}}{\sqrt{\mu}} \right) = \mu \left(\frac{\hat{\mathbf{f}}}{\sqrt{\mu}} \right). \tag{A.24}
$$

This is equivalent to

$$\mathcal{B}_N \mathcal{D}_\Gamma \mathcal{B}_N \left(\frac{\mathcal{B}_N h}{\sqrt{\mu}} \right) = \mu \left(\frac{\mathcal{B}_N h}{\sqrt{\mu}} \right). \tag{A.25}$$

Now relating to the spectral concentration for a spatial-limited signal,

So when $h = g_i^{(\Gamma)}(\boldsymbol{x})$, we have

$$\lambda_i^{(N)} = \mu_i^{(\Gamma)}$$

and $\frac{\mathcal{B}_N h}{\sqrt{\mu}} = f_i^{(N)}(\boldsymbol{x})$, i.e.,

$$\left(\mathcal{B}_N g_i^{(\Gamma)} \right)(\boldsymbol{x}) = \sqrt{\lambda_i^{(N)}} f_i^{(N)}(\boldsymbol{x}).$$

Similarly, as we take $A = \mathcal{B}_N$, $B = \mathcal{D}_\Gamma$, F is the spherical harmonics transform, F^{-1} is the inverse spherical harmonics transform and we have mixed F and F^{-1} into $\mathcal{D}_\Gamma$ and $\mathcal{B}_N$. Then the operator $AF^{-1}BFA$ becomes $\mathcal{B}_N \mathcal{D}_\Gamma \mathcal{B}_N$ and the operator $BFAF^{-1}B$ becomes $\mathcal{D}_\Gamma \mathcal{B}_N \mathcal{D}_\Gamma$. Using the **Grunbaum's Lemma**, taking $h = \mathcal{B}_N h$ and following the same procedure, we get

$$\left(\mathcal{D}_\Gamma f_i^{(N)} \right)(\boldsymbol{x}) = \sqrt{\mu_i^{(\Gamma)}} g_i^{(\Gamma)}. \qquad \square$$

A.6   Least Angle between Two Subspaces

Proof

The proof is similar to the procedure in [23]. The difference is that we are dealing with the problem in the spatial-spectral domain, while the former was in the time-frequency domain.

Suppose $f^{(N)} \in \mathfrak{B}_N(\mathbb{S}^2, ds)$, $g^{(\Gamma)} \in \mathfrak{D}_\Gamma(\mathbb{S}^2, ds)$. According to the angle's definition (4.68), we have

$$\theta(f^{(N)}, g^{(\Gamma)}) = \cos^{-1} \frac{\Re\{\langle f^{(N)}, g^{(\Gamma)} \rangle\}}{\|f^{(N)}\| \cdot \|g^{(\Gamma)}\|}.$$

As cosine function is a monotonic decreasing function, to obtain the least angle $\theta(f^{(N)}, g^{(\Gamma)})$, it is equivalent to find the maximum value of

$$\frac{\Re\{\langle f^{(N)}, g^{(\Gamma)} \rangle\}}{\|f^{(N)}\| \cdot \|g^{(\Gamma)}\|}.$$

First, we fix $f^{(N)}$ to get the maximum value when $g^{(\Gamma)}$ varies. As $f^{(N)}$ is a spectral-limited function, according to the Fourier transform, $f^{(N)}$ occupies the whole sphere in the spatial domain. Therefore, $f^{(N)}$ can be decomposed into two parts: $\mathcal{D}_\Gamma f^{(N)}$ in the region Γ and $f^{(N)} - \mathcal{D}_\Gamma f^{(N)}$ in the region $\mathbb{S}^2/\Gamma$. And the two functions $\mathcal{D}_\Gamma f^{(N)}$ $f^{(N)} - \mathcal{D}_\Gamma f^{(N)}$ are orthogonal since the inner product $\langle \mathcal{D}_\Gamma f^{(N)}, f^{(N)} - \mathcal{D}_\Gamma f^{(N)} \rangle = 0$. Therefore, we have

$$
\begin{aligned}
\Re\{\langle f^{(N)}, g^{(\Gamma)} \rangle\} &= \Re\{\langle f^{(N)} - \mathcal{D}_\Gamma f^{(N)} + \mathcal{D}_\Gamma f^{(N)}, g^{(\Gamma)} \rangle\} \\
&= \Re\{\langle \mathcal{D}_\Gamma f^{(N)}, g^{(\Gamma)} \rangle\} \\
&= \|\mathcal{D}_\Gamma f^{(N)}\| \cdot \|g^{(\Gamma)}\| \cdot \cos\theta(\mathcal{D}_\Gamma f^{(N)}, g^{(\Gamma)}) \\
&\leq \|\mathcal{D}_\Gamma f^{(N)}\| \cdot \|g^{(\Gamma)}\|.
\end{aligned}
$$

The equality is obtained when $\cos\theta(\mathcal{D}_\Gamma f^{(N)}, g^{(\Gamma)}) = 1$. That is, $\mathcal{D}_\Gamma f^{(N)}$ is positively proportional to $g^{(\Gamma)}$, i.e.,

$$
g^{(\Gamma)} = k\mathcal{D}_\Gamma f^{(N)}, \tag{A.29}
$$

where k is an arbitrary positive constant.

Now we have

$$
\frac{\Re\{\langle f^{(N)}, g^{(\Gamma)} \rangle\}}{\|f^{(N)}\| \cdot \|g^{(\Gamma)}\|} \leq \frac{\|\mathcal{D}_\Gamma f^{(N)}\|}{\|f^{(N)}\|}.
$$

Our next step is to maximize $\frac{\|\mathcal{D}_\Gamma f^{(N)}\|}{\|f^{(N)}\|}$ when $f^{(N)}$ changes. According to Theorem 4.7.3 and (4.57), we have

$$
f^{(N)} = \sum_{i=0}^{(N+1)^2-1} a_i^{(N)} f_i^{(N)}(\boldsymbol{x}),
$$

with $a_i^{(N)} = \left\langle f^{(N)}, f_i^{(N)}(\boldsymbol{x}) \right\rangle$ for $i = 0, 1 \cdots, (N+1)^2 - 1$. According to Parseval's theorem 2.22 and the orthonormality of $\{f_i^{(N)}(\boldsymbol{x})\}$, we have

$$
\|f^{(N)}\|^2 = \sum_{i=0}^{(N+1)^2-1} |a_i^{(N)}|^2,
$$

$$
\|\mathcal{D}_\Gamma f^{(N)}\|^2 = \sum_{i=0}^{(N+1)^2-1} |a_i^{(N)}|^2 \lambda_i^{(N)}.
$$

As $1 > \lambda_0^{(N)} \geq \lambda_1^{(N)} \geq \lambda_2^{(N)} \ldots \geq \lambda_{(N+1)^2-1}^{(N)} > 0$,

$$
\frac{\|\mathcal{D}_\Gamma f^{(N)}\|^2}{\|f^{(N)}\|^2} = \frac{\sum_{i=0}^{(N+1)^2-1} |a_i^{(N)}|^2 \lambda_i^{(N)}}{\sum_{i=0}^{(N+1)^2-1} |a_i^{(N)}|^2} \leq \lambda_0^{(N)}.
$$

The equality is achieved when $a_0^{(N)} \neq 0$ and $a_i^{(N)} = 0$ for all $1 \leq i \leq (N+1)^2 - 1$, i.e.,

$$f^{(N)} = a_0^{(N)} f_0^{(N)}(\boldsymbol{x}). \tag{A.32}$$

Obviously, $a_0^{(N)}$ can be any nonzero number. We usually take $a_0^{(N)} = 1$.

In sum,

$$\frac{\Re\{\langle f^{(N)}, g^{(\Gamma)} \rangle\}}{\|f^{(N)}\| \cdot \|g^{(\Gamma)}\|} \leq \sqrt{\lambda_0^{(N)}} = \sqrt{\mu_0^{(\Gamma)}}.$$

where $\lambda_0^{(N)} = \mu_0^{(\Gamma)}$ has been proved in Theorem 4.7.3. The equality is obtained when (A.29) and (A.32) are both satisfied simultaneously, i.e.,

$$f^{(N)} = f_0^{(N)}(\boldsymbol{x}),$$
$$g^{(\Gamma)} = k\mathcal{D}_\Gamma f_0^{(N)}(\boldsymbol{x}).$$

with $k > 0$. Therefore, the least angle θ_0 equals to

$$\begin{aligned}
\theta_0 &= \min_{f^{(N)} \in \mathfrak{B}_N} \inf_{g^{(\Gamma)} \in \mathfrak{D}_\Gamma} \theta(f^{(N)}, g^{(\Gamma)}) \\
&= \cos^{-1} \sqrt{\lambda_0^{(N)}} \\
&= \cos^{-1} \sqrt{\mu_0^{(\Gamma)}}. \qquad \square
\end{aligned}$$

Bibliography

[1] L. E. Franks, *Signal theory*, Prentice Hall, Englewood Cliffs, N.J, 1969.

[2] D. N. Spergel and et.al, "Three-year Wilkinson microwave anisotropy probe (WMAP) observations: implications for cosmology," *Astrophys. J. Suppl.*, vol. 170, pp. 377, 2007.

[3] Y. Wiaux, J. D. McEwen, P. Vandergheynst, and O. Blanc, "Exact reconstruction with directional wavelets on the sphere," *Mon. Not. Roy. Ast. Soc.*, vol. 388, no. 2, pp. 770–788, mar 2008.

[4] T. S. Pollock, T. D. Abhayapala, and R. A. Kennedy, "Introducing space into MIMO capacity calculation," *Journal on Telecommunications Systems*, vol. 24, pp. 415–436, 23 Feb. - 1 Mar. 2003.

[5] T. D. Abhayapala, T. S. Pollock, and R. A. Kennedy, "Spatial decomposition of MIMO wireless channels," in *Proc. 7th International Symposium on Signal Processing and its Applications, ISSPA'03*, Paris, France, July 2003, vol. 1, pp. 309–312.

[6] R. A. Kennedy and T. D. Abhayapala, "Spatial concentration of wave-fields: Towards spatial information content in arbitrary multipath scattering," in *Proc. 4th Australian Communications Theory Workshop, AusCTW'2003*, Melbourne, Australia, February 2003, pp. 38–45.

[7] J. A. R. Blais and D. A. Provins, "Spherical harmonic analysis and synthesis for global multiresolution applications," *J. Geodesy*, vol. 76, no. 1, pp. 29–35, Jan. 2002.

[8] F. J. Simons, J. C. Hawthorne, and C. D. Beggan, "Efficient analysis and representation of geophysical processes using localized spherical basis functions," in *Proc. SPIE, Vol. 7446, Wavelets XIII, Aug 2-6 2009, San Diego, CA, USA*, 2009.

[9] G. A. Prieto, R. L. Parker, D. J. Thomson, F. L. Vernon, and R. L. Graham, "Reducing the bias of multitaper spectrum estimates," *Geophysical Journal International*, vol. 171, pp. 1269–1281, 2007.

[10] A. Amirbekyan, V. Michel, and F. J. Simons, "Parametrizing surface wave tomographic models with harmonic spherical splines," *Geophys. J. Int.*, vol. 174, pp. 617–628, 2008.

[11] F. A. Dahlen and F. J. Simons, "Spectral estimation on a sphere in geophysics and cosmology," *Geophysical Journal International*, vol. 174, pp. 774–807, Aug. 2008.

[12] P. Yu, P. E. Grant, Y. Qi, Xi Han, F. Segonne, R. Pienaar, E. Busa, J. Pacheco, N. Makris, R. L. Buckner, P. Golland, and B. Fischl, "Cortical surface shape analysis based on spherical wavelets," *IEEE Trans. Medical Imaging*, vol. 26, no. 4, pp. 582–597, Apr. 2007.

[13] B. T. T. Yeo, W. Ou, and P. Golland, "On the construction of invertible filter banks on the 2-sphere," *IEEE Trans. Image Process.*, vol. 17, no. 3, pp. 283–300, Mar. 2008.

[14] T. Bulow and K. Daniilidis, "Surface representations using spherical harmonics and gabor wavelets on the sphere," Tech. Rep. MS-CIS-01-37, University of Pennsylvania, 2001.

[15] T. Bulow, "Spherical diffusion for 3D surface smoothing," *IEEE Trans. Patt. Ana. Mach. Intel.*, vol. 26, no. 12, pp. 1650–1654, Dec. 2004.

[16] M. Kazhdan, T. Funkhouser, and S. Rusinkiewicz, "Rotation invariant spherical harmonic representation of 3*d* shape descriptors," in *Proc. of the 2003 Eurographics/ACM SIGGRAPH symposium on Geometry processing, vol.43, Aachen, Germany, 23-25 June 2003*, 2003, vol. 43, pp. 156–164.

[17] L. Cayon, J. L. Sanz, R. B. Barreiro, E. Martinlez, P. Vielva, L. Toffolatti, J. Silk, J. M. Diego, and F. Argueso, "Isotropic wavelets: a powerful tool to extract point sources from CMB maps," *Mon. Not. R. Astron. Soc*, vol. 315, pp. 757, 2000.

[18] J. L. Sanz, D. Herranz, and E. M. Gonzalez, "Optimal detection of sources on a homogeneous and isotropic background," *Astrophys. J.*, vol. 552, pp. 484–492, May 2001.

[19] R. B. Barreiro, P. Vielva, C. H. Monteagudo, and E. M. Gonzalez, "A linear filter to reconstruct the ISW effect from CMB and LSS observations," *IEEE Journal of Selected Topics in Signal processing*, vol. 2, pp. 747–754, Oct. 2008.

[20] R. A. Kennedy, W. Zhang, and T. D. Abhayapala, "Spherical harmonic analysis and model-limited extrapolation on the sphere: Integral equation formulation," in *Proc. International Conference on Signal Processing and Communication Systems, ICSPCS'2008, Gold Coast, Australia*, December 2008, p. 6.

[21] Y. Wiaux, L. Jacques, and P. Vandergheynst, "Correspondence principle between spherical and euclidean wavelets," *The Astrophysical Journal*, vol. 632, pp. 15–28, Oct. 2005.

[22] D. Slepian and H. O. Pollak, "Prolate spheroidal wave functions, Fourier analysis and uncertainty - I," *Bell System Tech. J*, vol. 40, pp. 43–63, Jan. 1961.

[23] H. J. Landau and H. O. Pollack, "Prolate spheroidal wave functions, Fourier analysis and uncertainty II," *Bell System Tech. J.*, vol. 40, no. 1, pp. 65–84, Jan. 1961.

[24] H. J. Landau and H. O. Pollak, "Prolate spheroidal wave functions, Fourier analysis and uncertainty - III: the dimension of the space of essentially time- and band-limited signals," *Bell System Tech. J*, vol. 41, pp. 1295–1336, July 1962.

[25] D. Slepian, "Prolate spheroidal wave functions, Fourier analysis and uncertainty - IV: Extensions to myan dimensions: Generalized prolate spheroidal functions," *Bell System Tech. J*, vol. 43, pp. 3009–3057, 1964.

[26] D. Slepian, "Prolate spheroidal wave functions, Fourier analysis, and uncertainty V- the discrete case," *Bell System Tech. J.*, vol. 57, no. 5, pp. 1371–1430, May-June 1978.

[27] G. Lachs, "Optimization of signal waveforms," *IEEE Trans. Inf. Theory*, vol. IT-9, pp. 95–97, Apr. 1963.

[28] A. Papoulis, "Minimum-bias windows for high-resolution spectral estimates," *IEEE Trans. Inf. Theory*, vol. IT-19, no. 1, pp. 9–12, Jan. 1973.

[29] J. F. Kaiser and R. W. Schafer, "On the use of the i_0-sinh window for spectrum analysis," *IEEE Trans. Acoust. Spee. Sign. Proc*, vol. ASSP-28, no. 1, pp. 105–107, Feb. 1980.

[30] Q. Jin, Z. Q. Luo, and K. M. Wong, "An optimum complete orthonormal basis for signal analysis and design," *IEEE Trans. Inf. Theory*, vol. 40, no. 3, pp. 732–742, May 1994.

[31] A. Albertella, F. Sanso, and N. Sneeuw, "Band-limited functions on a bounded spherical domain: the Slepian problem on the sphere," *Journal of Geodesy*, vol. 77, pp. 436–447, 1999.

[32] L. Miranian, "Slepian functions on the sphere, generalized gaussian quadrature rule," *Inverse Problems*, vol. 20, pp. 877–892, 2004.

[33] F. J. Simons, F. A. Dahlen, and M. A. Wieczorek, "Spatiospectral concentration on a sphere," *SIAM Review*, vol. 48, pp. 504–536, 2006.

[34] E. A. Fain and M. K. Varanasi, "Minimum bandwidth basis functions for the fourth-moment bandwidth measure," in *Proc. IEEE Int. Symp. Inf. Theory*, Sorrento, Italy, June 2000, p. 416.

[35] J. R. Driscoll and D. M. Healy Jr., "Computing Fourier transforms and convolutions on the 2-sphere," *Adv. Appl. Math*, vol. 15, pp. 202–250, June 1994.

[36] M. Tegmark, D. H. Hartmann, M. S. Briggs, and C. A. Meegan, "The angular power spectrum of BASTE 3B Gamma-ray bursts," *Astrophys. J*, vol. 468, pp. 214, Sept. 1996.

[37] K. Seon, "Smoothing of all-sky survey map with Fisher-von Mises function," *Journal of the Korean Physical Society*, vol. 48, pp. 331–334, Mar. 2006.

[38] R. A. Kennedy, T. A. Lamahewa, and L. Wei, "On azimuthally symmetric 2-sphere convolution," in *Proc. The 6th U.S./Australia Joint Workshop on Defence Applications of Signal Processing, DASP'2009*, Hawaii, USA, 26 - 30 Sep. 2009, p. 6.

[39] B. D. Wandelt and K. M. Gorski, "Fast convolution on the sphere," *Phys. Rev. D*, vol. 63, pp. 1230012(6), May 2001.

[40] S. Mitra, A. S. Sengupta, and T. Souradeep, "CMB power spectrum estimation using noncircular beams," *Phys. Rev. D*, vol. 70, pp. 103002, 2004.

[41] P. P. Mitra and H. Maniar, "Concentration maximization and local basis expansions (LBEX) for linear inverse problems," *IEEE Trans. Biomed. Eng.*, vol. 53, no. 9, pp. 1775–1782, Sept. 2006.

[42] D. Herranz, J. L. Sanz, R. B. Barreiro, and E. M. Gonzalez, "Scale-adaptive filters for the detection/separation of compact sources," *Astrophys. J.*, vol. 580, 2002.

[43] E. Hivon, K. M. Gorski, C. B. Netterfield, B. P. Crill, S. Prunet, and F. Hansen, "Master of the CMB anisotropy power spectrum: a fast method for statistical analysis of large and complex CMB data sets," *Astrophys. J.*, vol. 567, pp. 2–17, Mar. 2002.

[44] G. Fay, F. Guilloux, M. Betoule, J. F. Cardoso, J. Delabrouille, and M. L. Jeune, "CMB power spectrum estimation using wavelets," *Phys. Rev. D*, vol. 78, no. 8, pp. 20, 2008.

[45] J. D. McEwen, M. P. Hobson, and A. N. Lasenby, "Optimal filters on the sphere," *IEEE Trans. Signal Procss.*, vol. 56, no. 8, pp. 3813–3823, Aug. 2008.

[46] J. L. Starck, A. Bijaoui, B. Lopez, and C. Perrier, "Image reconstruction by the wavelet transform applied to aperture synthesis," *Astron. Astrophys.*, vol. 283, pp. 349–360, June 1994.

[47] J. L. Starck, Y. Moudden, P. Abrial, and M. Nguyen, "Wavelets, ridgelets and curvelets on the sphere," *Astronomy and Astrophysics*, vol. 446, no. 3, pp. 1191–1204, 2006.

[48] J. C. Hamilton, "CMB map-making and power spectrum estimation," *C. R. Physique*, vol. 4, no. 8, pp. 871–879, October 2003.

[49] F. Guilloux, G. Fay, and J. F. Cardoso, "Practical wavelet design on the sphere," *Appl. Comp. Harm. Anal.*, vol. 26, pp. 143–160, Mar. 2009.

[50] D. Colton and R. Kress, *Inverse Acoustic and electromagnetic scattering theory*, Springer-Verlag, Berlin, Germany, 1992.

[51] A. R. Edmonds, *Angular Momentum in Quantum Mechanics*, Princeton University Press, Princeton, NJ, 1996.

[52] C. H. Choi, J. Ivanic, M. S. Gordon, and K Ruedenberg, "Rapid and stable determination of ration matrices between spherical harmonics by direct recursion," *J. Chem. Phys.*, vol. 111, no. 19, pp. 8825–8831, 1999.

[53] T. Risbo, "Fourier transform summation of Legendre series and d-functions," *J. Geodesy*, vol. 70, no. 70, pp. 383–396, 1996.

[54] J. Ivanic and K. Ruedenberg, "Rotation matrices for real spherical harmonics: Direct determination by recursion," *J. Phys. Chem. A.*, vol. 100, no. 15, pp. 6342–6347, 1996.

[55] M. A. Blanco, M. Florez, and M. Bermejo, "Evaluation of the rotation matrices in the basis of real spherical harmonics," *J. Mol. Struct. (Theochem)*, vol. 419, pp. 19–27, 1997.

[56] Y. Wiaux, L. Jacques, P. Vielva, and P. Vandergheynst, "Fast directional correlation on the sphere with steerable filters," *The Astrophysical Journal*, vol. 652, pp. 820–832, Nov. 2006.

[57] D. A. Varshalovich, A. N. Moskalev, and V. K. Khersonskii, *Quantum theory of angular momentum*, World Scientific Publishing Company, 1988.

[58] D. Slepian, "On bandwidth," *Proceedings of the IEEE*, vol. 64, no. 3, pp. 292–300, Mar. 1976.

[59] A. Nuttall and F. Amoroso, "Minimum Gabor bandwidth of M orthogonal signals," *IEEE Trans. Inf. Theory*, vol. 14, no. 5, pp. 440–444, July 1965.

[60] A. Nuttall, "Minimum rms bandwidth of M time-limited signals with specified code or correlation matrix," *IEEE Trans. Inf. Theory*, vol. IT-14, no. 5, pp. 699–707, Sept. 1968.

[61] D. Gabor, "Theory of communication," *J. Inst. Elec. Eng.*, vol. 93, Part III, no. 26, pp. 429–457, Nov. 1946.

[62] L. C. Potter and K. S. Arun, "Energy concentration in band-limited extrapolation," *IEEE Trans. Acoust., Speech, Signal Processing*, vol. 37, no. 7, pp. 1027–1041, July 1989.

[63] A. Wyner and H. Landau, "Optimum waveform signal sets with amplitude and energy constraints," *IEEE Trans. Inf. Theory*, vol. IT-30, no. 4, pp. 615–622, July 1984.

[64] L. Xu, C. Bi, X. Chen, and J. Chen, "Resolution enhancement of nearfield acoustic holography by interpolation using band-limited signal restoration method," *Chinese Science Bulletin*, vol. 53, no. 20, pp. 3142–3150, Oct. 2008.

[65] A. Papoulis and M. Bertran, "Digital filtering and prolate functions," *IEEE Trans. Circuit Theory*, vol. CT-19, no. 6, pp. 674–681, Nov. 1972.

[66] Y. Xu, S. Haykin, and R. J. Racine, "Multiple window time-frequency distribution and coherence of EEG using slepian sequences and Hermite functions," *IEEE Trans. Biom. Eng.*, vol. 67, no. 7, pp. 861–866, July 1999.

[67] G. G. Walter and X. Shen, "Sampling with prolate spheroidal wave functions," *Sampling theory in signal and image processing*, vol. 2, no. 1, pp. 25–52, January 2003.

[68] G. G. Walter and X. Shen, "Wavelet based on prolate spheroida wave functions," *Journal of Fourier Analysis and Applications*, vol. 10, no. 1, pp. 1–26, 2004.

[69] G. G. Walter and X. Shen, "Periodic prolate spheroidal wavelets," *Journal of Functional Analysis and Optimization*, vol. 26, no. 7-8, pp. 953–976, 2005.

[70] X. Shen and G. G. Walter, "Construction of periodic prolate spheroidal wavelets using interpolation," *Numerical functional analysis and optimization*, vol. 28, no. 3-4, pp. 445–466, 2007.

[71] C. J. Bouwkamp, "On spheroidal wave fucntions of order zero," *J. Math. Phys.*, vol. 26, pp. 79–92, 1947.

[72] F. A. Grunbaum, "Eigenvectors of a Toeplitz matrix: discrete version of the prolate spheroidal wave functions," *SIAM J. Alg. Disc. Meth.*, vol. 2, no. 2, pp. 136–141, June 1981.

[73] H. Xiao, V. Rokhlin, and N. Yarvin, "Prolate spheroidal wavefunctions, quadrature and interpolation," *Inverse Problems*, vol. 17, no. 4, pp. 805–838, 2001.

[74] G. Beylkin and L. Monzon, "On generalized gaussian quadratures for exponentials and their applications," *Appl. Comp. Harm. Anal.*, vol. 12, no. 3, pp. 332–373, 2002.

[75] L. Wei and R. A. Kennedy, "Signal concentration on the unit sphere," in *Poster, ANU college of engineering and computer science, June 22, 2009.*

[76] L. Wei, R. A. Kennedy, and T. A. Lamahewa, "Band-limited signal concentration in time-frequency," in *Proc. Int. Conf. on Signal Processing and Communication Systems, ICSPCS'2009*, Omaha, Nebraska, USA, 28-30 Sep. 2009, pp. 1–6.

[77] L. Wei, R. A. Kennedy, and T. A. Lamahewa, "An optimal basis of band-limited functions for signal analysis and design," *IEEE Trans. Signal Processing*, vol. 58, pp. 12, Nov. 2010.

[78] L. Wei, R. A. Kennedy, and T. A. Lamahewa, "Further results on signal concentration in time-frequency," in *Proc. IEEE Int. Conf. Acoust., Speech, Signal Processing, ICASSP'2010*, Dallas, Texas, USA, 14-19 Mar 2010, pp. 4082–4085.

[79] R. A. Kennedy, P. Sadeghi, T. D. Abhayapala, and H. M. Jones, "Intrinsic limits of dimensionality and richness in random multipath fields," *IEEE Trans. Signal Process.*, vol. 55, no. 6, pp. 2542–2556, June 2007.

[80] E. N. Gilbert and D. Slepian, "Doubly orthogonal concentratied polynomials," *SIAM J. Math. Anal.*, vol. 8, no. 2, pp. 290–318, Apr. 1977.

[81] F. A. Grunbaum, L. Longhi, and M. Perlstadt, "Differential operators commuting with finite convolution integral operators: some non-Abelian examples," *SIAM J. Appl. Math.*, vol. 42, no. 5, pp. 941–955, Oct. 1982.

[82] P. Sadeghi, T. D. Abhayapala, and R. A. Kennedy, "Directional random scattering MIMO channels: entropy analysis and capacity optimization," in *Proc. IEEE International Conference on Communications, ICC'06, Vol.3, Istanbul, Turkey, June 2006, pp.1331-1336*, 2006.

[83] L. Debnath and P. Mikusinski, *Introduction to Hilbert Spaces with Applications*, Academic Press, San Diego, CA, 1990.

[84] L. Wei, R. A. Kennedy, and T. A. Lamahewa, "Quadratic variational framework for signal design on the 2-sphere," *summitted to IEEE Trans. Signal Processing*.

[85] R. Pail, G. Plank, and W. D. Schuh, "Spatially restricted data distributions on the sphere: the method of orthonormalized functions and applications," *Journal of Geodesy*, vol. 75, pp. 44–56, 2001.

[86] L. Wei and R. A. Kennedy, "General concentration on the unit sphere," *to be submitted to IEEE Transactions on Signal Processing*.

[87] T. Bulow, "Multiscale image processing on the sphere," *Proc. 24th DAGM Symp. Patt. Rec.*, vol. 2449, pp. 609–617, 2002.

[88] J. P. Antoine and P. Vandergheynst, "Wavelets on the 2-sphere: a group-theoretical approach," *Appl. Comput. Harmon. Anal.*, vol. 7, pp. 262–291, 1999.

[89] R. Vio, J. G. Nagy, L. Tenorio, P. Andreani, C. Baccigalupi, and W. Wamsteker, "Digital deblurring CMB maps: performance and efficient implementation," *Astron. Astrophys*, vol. 401, pp. 389, Jan. 2003.

[90] J. L. Starck, E. J. Candes, and D. L. Donoho, "The curvelet transform for image denoising," *IEEE Trans. Image process.*, vol. 11, no. 6, pp. 670–684, June 2002.

[91] M. A. Wieczorek and F. J. Simons, "Localized spectral analysis on the sphere," *Geophys. J. Int.*, vol. 162, pp. 655–675, 2005.

[92] M. A. Wieczorek and F. J. Simons, "Minimum-variance multitaper spectral estimation on the sphere," *J. Four. Anal. Appl.*, vol. 13, pp. 665–692, 2007.

[93] L. Wei, R. A. Kennedy, and T. A. Lamahewa, "Signal concentration on unit sphere: An azimuthally moment weighting approach," in *Proc. IEEE Int. Conf. Acoust., Speech, Signal Processing, ICASSP'2010*, Dallas, Texas, USA, 14-19 Mar 2010, pp. 3698–3701.

[94] L. Wei, R. A. Kennedy, and T. A. Lamahewa, "Signal concentration on unit sphere: A local k-th moment zenithal energy concentration measure," in *Proc. 11th Australian Communications Theory Workshop, AusCTW'2010*, Canberra, Australia, Feb. 2010, pp. 97–101.

[95] W. H. Press, S. A. Teukolsky, W. T. Vetterling, and B. P. Flannery, *Numerical recipes in C: The art of scientific computing*, Cambridge University Press New York, 1988.

[96] L. Wei and R. A. Kennedy, "On spectral concentration of signals on the 2-sphere under a generalized moment weighting criterion," in *Proc. European Signal Processing Conference, EUSIPCO'2010*, Aalborg, Denmark, Aug. 2010, p. 4.

[97] T. Bulow, "Spherical diffusion for surface smoothing and denoising," Technical Report (CIS), University of Pennsylvania Department of Computer and Information Science, 2001.

[98] A. S. Y. Poon, R. W. Broderson, and D. N. C. Tse, "Degrees of freedom in multiple-antenna channels: A signal space approach," *IEEE Trans. Inf. Theory*, vol. 51, no. 2, pp. 523–536, Feb. 2005.

[99] J. D. McEwen, M. P. Hobson, D. J. Mortlock, and A. N. Lasenby, "Fast directional continuous spherical wavelet transform algorithms," *IEEE Trans. signal process.*, vol. 55, pp. 520–529, Feb. 2007.

[100] J. M. Geusebroek, A. W. M. Smeulders, and J. V. D. Weijer, "Fast anisotropic gauss filtering," *IEEE Trans. Image. Proc.*, vol. 12, no. 8, pp. 938–943, Aug. 2003.

[101] K. Ng, "Full-sky correlation functions for CMB experiments with asymmetric window functions," *Phys. Rev. D*, vol. 71, pp. 083009, Apr. 2005.

[102] A. G. Doroshkevich, Naselsky P. D., O. V. Verkhodanov, D. I. Novikov, V. I. Turchaninov, I. D. Novikov, P. R. Christensen, and L. Y. Chiang, "Gauss-Legendre sky pixelization GLESP for CMB maps," *Int. J. Mod. Phys. D.*, vol. 14, pp. 275, May 2005.

[103] L. Wei and R. A. Kennedy, "A norvel spherical convolution on the 2-sphere," *submitted to IEEE Signal Processing Letter*.

[104] L. Wei and R. A. Kennedy, "Exact reconstruction based on the harmonic multiplication operation on the unit sphere," *to be submitted to IEEE Transactions on Signal Processing*.